NASA TN D-1634

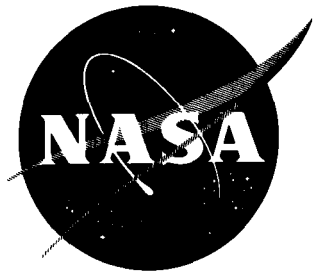

TECHNICAL NOTE

D-1634

WING AND FLAP LOADS OBTAINED FROM A WIND-TUNNEL INVESTIGATION OF A LARGE-SCALE V/STOL MODEL

By Robert J. Huston, John F. Ward,
and Matthew M. Winston

Langley Research Center
Langley Station, Hampton, Va.

NATIONAL AERONAUTICS AND SPACE ADMINISTRATION

WASHINGTON

April 1963

NATIONAL AERONAUTICS AND SPACE ADMINISTRATION

TECHNICAL NOTE D-1634

WING AND FLAP LOADS OBTAINED FROM A WIND-TUNNEL INVESTIGATION OF A LARGE-SCALE V/STOL MODEL

By Robert J. Huston, John F. Ward,
and Matthew M. Winston

SUMMARY

Wing and flap loads on tilt-wing, tilt-wing-with-slat, and deflected-slipstream configurations, obtained during tests of a large-scale model in the Langley full-scale wind tunnel, are presented for an angle-of-attack range corresponding to transition flight of a vertical or short take-off and landing (V/STOL) aircraft. Included are wing root moments and shears, flap forces and moments, and partial-span wing pressure distributions for a range of flap deflections and lift-drag conditions corresponding to longitudinal acceleration and deceleration.

The relationship between angle of attack and normal or chordwise bending moments at the root was found to be basically a cosine or sine function, respectively, but became modified significantly by the flow condition on the wing and by the balance of longitudinal forces. Normal and chordwise bending moments were relatively unaffected by deflection of the 30-percent-chord flaps; in contrast, the wing torsion was substantially affected by flap deflection and by the balance of longitudinal forces. Local areas of flow separation, principally behind upward traveling propeller blades, caused erratic movements in the spanwise centers of pressure. The addition of a 19-percent-chord partial-span slat to the tilt-wing configuration, in combination with 30° of flap deflection, resulted in the elimination of buffet caused by local areas of flow separation for the range of conditions covered.

INTRODUCTION

The structural loading characteristics of aircraft intended for V/STOL operation have not yet been adequately defined for the designer. Part of the reason for this inadequacy is attributable to the small model sizes used in most of the earlier investigations, which prevented detailed information to be obtained on the distribution of aerodynamic loading over the wing.

The present investigation with a large-scale model was conducted to provide information on the wing and flap loads applicable to both tilt-wing and deflected-slipstream configurations. The model was tested in the Langley full-scale tunnel where wing-root and flap structural loads and partial-span pressure distributions were measured by means of strain-gage bridges and pressure orifices installed on the wing and flaps.

The results of a static-thrust investigation with this model are presented in references 1 and 2. A sample of the initial results of the structural loads investigation of the present report was included as a part of reference 3.

The present investigation provides results on the wing loads for a wing angle-of-attack range corresponding to conditions from near hovering to conventional airplane flight. Also included are results obtained for a limited range of longitudinal accelerations and decelerations. The analysis and results presented are intended as an aid in planning the structural design of V/STOL aircraft and, as such, are not restricted to the configuration investigated.

SYMBOLS

The positive sense of forces, moments, and angles are indicated in figure 1.

b wing span, ft

b' span of instrumented wing panel, ft

b_f flap span, ft

c wing chord, ft

$\bar{c}_f$ root-mean-square chord of flap rearward of hinge line, ft

$\bar{c}_c$ mean value of section-chord-force coefficient on segment of wing span behind propeller, $\dfrac{\int_{-0.867}^{0.750} \frac{\text{Section chord pressure force}}{qc} \, d\left(y_p/R\right)}{\int_{-0.867}^{0.750} d\left(y_p/R\right)}$

$\bar{c}_n$ mean value of section normal-force coefficient on wing span segment behind propeller, $\dfrac{\int_{-0.867}^{0.750} \frac{\text{Section normal pressure force}}{qc} \, d\left(y_p/R\right)}{\int_{-0.867}^{0.750} d\left(y_p/R\right)}$

$F_{c,f}$ flap chord force, lb

C_C flap-chord-force coefficient, $\frac{F_{c,f}}{qS_f}$

C_D drag coefficient, $\frac{D}{qS}$

C_N flap normal-force coefficient, $\frac{N_f}{qS_f}$

C_H flap hinge-moment coefficient, $\frac{H_f}{qS_f\bar{c}_f}$

C_L lift coefficient, $\frac{L}{qS}$

D net drag of model, including components of propeller forces, lb

H_f flap hinge moment, ft-lb

i_w wing incidence, deg

L net lift of model, including components of propeller forces, lb

M_c wing-root chordwise bending moment, ft-lb

M_n wing-root normal bending moment, ft-lb

M_t total wing torsional moment about 0.35c, ft-lb

M_y pitching moment of model about 0.35c, ft-lb

N_f flap normal force, lb

q free-stream dynamic pressure, lb/sq ft

R propeller radius, ft

S wing area, sq ft

S_f flap area rearward of hinge line, $b_f\bar{c}_f$, sq ft

T_c' effective thrust coefficient,
$\sin\alpha\left(C_{L_{\text{power on}}} - C_{L_{\text{power off}}}\right) - \cos\alpha\left(C_{D_{\text{power on}}} - C_{D_{\text{power off}}}\right)$

V free-stream velocity, ft/sec

V_c wing root normal shear load, lb

V_n wing root normal shear load, lb

y distance from airplane center line along span

y^* distance from airplane center line ratioed to wing semispan, $\frac{y}{b/2}$

y_p distance from midspan-propeller center of rotation along wing span, positive in region behind upward turning propeller blade, ft

α free-stream angle of attack measured from wing chord line, deg

α_{fus} free-stream angle of attack measured from fuselage center line, deg

δ jet-boundary correction factor

δ_f flap deflection, deg

δ_s slat deflection, deg

χ wake skew angle, angle between tunnel vertical and wake center line, positive rearward, deg

Subscripts:

D due to drag

f,30 30-percent-chord flap

f,55 55-percent-chord flap

L due to lift

u horizontal interference

w vertical interference

y condition at position y

fus fuselage

root condition at wing root

tip condition at wing tip

MODEL, APPARATUS, AND TESTS

Model Description

Photographs of the tilt-wing and deflected-slipstream configurations of the model installed in the 30 × 60 foot test section of the Langley full-scale tunnel are shown in figure 2. A three-view drawing of the model is presented in figure 3. The model was tested without a horizontal stabilizer. The geometric characteristics of the model are listed in the following table:

Propeller:	
Diameter, ft	5.0
Solidity (thrust basis)	0.1935
Airfoil section	NACA 64-0XX
Wing:	
Span, ft	35.0
Span, instrumented panel, ft	14.08
Chord, ft	4.375
Area, sq ft	153.125
Airfoil section	NACA 63_2A215
Pivot, percent c	35
Flaps:	
Span, total each wing, ft	15.46
Span, instrumented section, ft	5.02
Chord, projection of both, percent c	55
Chord, projection of rear, percent c	30
Chord rearward of hinge line (rear), ft	1.03
Chord rearward of hinge line (both), ft	1.94
Slat:	
Span, center segment, ft	8.83
Span, outboard segments, ft	4.58
Chord, percent c	19
Vertical stabilizer:	
Span, ft	6.0
Chord, ft	3.5
Area, sq ft	21.0
Airfoil section	NACA 0012

The contours of the two slotted flaps, 55- and 30-percent wing chord, are shown in figure 4. The flaps were mounted on external brackets (fig. 5), manually adjustable, and locked in place by pins inserted in the brackets. During tests of the tilt-wing configuration, the slot of the front flap was sealed.

In a few tests, a fixed-incidence slat was attached to the wing between the propeller drive shaft nacelles as shown in figure 5. The slat was constructed by rolling a section of sheet metal to the contour of the first 19 percent of the upper surface of the wing section. The lower lip of the slat followed the

contour of the first 5 percent of the lower surface of the wing. Deflection of the slat was measured as the relative angle between the wing chord line and the slat chord line.

Configurations

Three model configurations were tested. The first, designated as "tilt-wing," was the basic model on which a single 30-percent-chord slotted flap was used. This configuration was tested with flap deflection varying from 0° to 50° in 10° increments. The second configuration, designated as "tilt wing with slat" (fig. 5) was tested with the 30-percent-chord flap both undeflected and deflected 30°. The third configuration, designated as "deflected slipstream," was the basic model with a double-slotted flap (55- and 30-percent wing chord). This configuration was tested with two combinations of flap deflections; first with the front flap section deflected 20° and the rear flap section deflected 40° and then with the front flap section deflected 40° and the rear flap section deflected 50°.

Model Instrumentation

Wing-root-loads instrumentation.- The wing structural loads were measured near the right wing root (41 inches from airplane center line) with strain-gage bridges (fig. 1(b)). The strain-gage bridges were installed and calibrated according to the procedure outlined in reference 4, except that the wing torsion was measured through a separate strain-gage balance installed on the end of the wing-position actuator. All strain-gage bridges were installed in duplicate to allow a choice of bridge outputs which would give the least probable error. The calibration procedure of reference 4 was extended to include a wing incidence range from zero to 90°. The wing loads measured included wing torsion and wing bending moments and shears in the normal and chordwise directions.

The accuracy of the loads data presented, as estimated from the scatter and repeatability of the data along with the probable error calculated by the method of reference 4, is presented in the following table for a model lift of 3,500 pounds:

	Estimated accuracy
Wing-root-loads instrumentation:	
Total wing torsion ratio, M_t/Lc	±0.003
Wing normal bending-moment ratio, M_n/Lb'	±0.005
Wing chordwise bending-moment ratio, M_c/Lb'	±0.010
Wing normal load center of pressure, percent b'	$\pm 2\frac{1}{2}$
Wing chordwise load center of pressure, percent b'	±5

The output of all strain-gage bridges was recorded on a recording oscillograph and visually read from a dial-type instrument. The wing steady loads were computed, principally, from visual readings of the dial-type instrument that

successfully damped out high-frequency periodic and random variations in the strain-gage-bridge output.

Flap-loads instrumentation.- The front and rear flaps behind the center propeller of the left-hand wing panel were supported by strain-gage balances. The forward balance, attached to the primary wing structure, measured the total flap loads. The balance attached behind the front flap measured the rear-flap loads. No attempt was made to determine any rolling tendency of the flaps. The accuracy of the flap loads, as estimated from the scatter and repeatability of the data along with repeatability of the calibrations, is presented in the following table for a model lift of 3,500 pounds:

	Estimated accuracy
Flap-loads instrumentation:	
30-percent-chord flap:	
Chord-force-coefficient ratio, $\frac{C_{C(f,30)}}{C_L}$	±0.02
Normal-force-coefficient ratio, $\frac{C_{N(f,30)}}{C_L}$	±0.02
Hinge-moment-coefficient ratio, $\frac{C_{H(f,30)}}{C_L}$	±0.02
55-percent-chord flap:	
Chord-force-coefficient ratio, $\frac{C_{C(f,55)}}{C_L}$	±0.04
Normal-force-coefficient ratio, $\frac{C_{N(f,55)}}{C_L}$	±0.02
Hinge-moment-coefficient ratio, $\frac{C_{H(f,55)}}{C_L}$	±0.02

Static-pressure instrumentation.- The wing and flaps behind the center propeller of the right-hand wing panel were fitted with static-pressure orifices. The chordwise and spanwise locations of these orifices are given in figure 6. The pressures were indicated on a fluid manometer display, which was photographically recorded.

Test Procedure and Corrections

Test procedure.- The model lift, drag, pitching moment, and wing and flap loads were measured over a range of wing-propeller angles of attack corresponding to transition of a V/STOL aircraft. The angle-of-attack variation was obtained by varying the wing incidence at 10° increments with the fuselage angle of attack at zero degrees. At each wing incidence, the propeller rotational speed (at fixed blade pitch) and the tunnel airspeed were varied to obtain approximately 3,500 pounds of lift and a zero net drag. Then, at each incidence, the entire model was varied through an angle range from -15° to 16° from the level-fuselage

attitude. This procedure was used to simulate a complete transition of a 3,500-pound V/STOL aircraft from hovering to conventional forward flight, with a level fuselage attitude for the unaccelerated transition conditions. Conditions corresponding to longitudinal acceleration and deceleration of the model had, respectively, a nose-down and nose-up fuselage attitude.

With the propellers removed, total aerodynamic and wing and flap loads were measured over an angle-of-attack range from -8.5° to beyond the stall with the wing incidence fixed at zero. These measurements were made at a dynamic pressure of approximately 16 pounds per square foot and a Reynolds number (based on wing chord) of 3.22×10^6.

Prior to each test, the structural inertia loads were measured through the complete range of wing incidence and fuselage attitudes to be investigated. These inertia loads were subsequently subtracted from the loads measured during the tests to obtain the aerodynamic increments to the wing and flap loads. The wing-root loads include the contribution of the propellers.

Corrections.- The model force data (C_L and D/L) and angles of attack have been corrected for airstream misalinement, for buoyancy, and for mean jet-boundary effects. The jet-boundary corrections were applied by using the procedure outlined in appendix C of reference 5 and the jet-boundary interference factors presented in figure 7. The horizontal interference factors of figure 7 are adjusted to account for the jet-boundary effects on the wind-tunnel velocity measurement device, which was located at the entrance to the tunnel test section, according to the instructions of reference 5.

The theory of reference 5, which was used to correct the data also indicates a large lateral correction to angle of attack and dynamic pressure. The maximum lateral variation in flow is presented in figure 8 as the difference in the jet-boundary interference factors between the wing root and the wing tip. The result of applying these interference factors is an effective aerodynamic washout and a lateral variation in the free-stream dynamic pressure. Typical effective aerodynamic washout and lateral dynamic pressure variations are presented in figure 9 as a function of lift coefficient, and in figure 10, at constant lift coefficient, as a function of the wing semispan. No corrections were made to the wing-root loads for these lateral variations in flow, however, because of the lack of a suitable method of correction.

One additional comment on the jet-boundary corrections should be noted on the basis of experience gained in applying the theory of reference 5 to the data. The magnitude and lateral variations of jet-boundary interference velocities encountered in this investigation, and the increased probability of systematic variations in the measured aerodynamic forces on the entire model, indicate that the use of ratios of model to wind-tunnel sizes as large as that of the investigation are undesirable and should be avoided.

PRESENTATION OF RESULTS

The loads data from this investigation include wing and flap loads for the powered model (propellers on) and wing loads for the model with the propellers removed. In order to adjust for small variations in the lift of the powered model which occurred as the angle of attack was varied from the initially trimmed condition ($L \approx 3{,}500$ lb), the wing bending moments are nondimensionalized by dividing by the product of lift and the instrumented panel span. An analysis in appendix A indicates that this results in an appropriate nondimensional ratio for this investigation. For the same reason, the wing torsional moments are nondimensionalized by dividing by the product of lift and the wing chord length. In addition, the wing bending moments are divided by the wing shears to obtain spanwise center-of-pressure locations. Conditions corresponding to a longitudinal balance of forces are identified by the label "D/L = 0." Conditions corresponding to positive longitudinal accelerations (or positive rate of climb) are identified by "D/L = -0.1" and "D/L = -0.2." Longitudinal decelerations (or negative rate of climb) are identified by "D/L = 0.1" and "D/L = 0.2."

The aerodynamic characteristics included in this paper with the wing-root loads are identified as "corrected data" and "uncorrected data." The notation "corrected data" indicates that the model force data includes the jet-boundary corrections determined from figure 7. Lift and drag values used throughout this paper, except those specifically labeled "uncorrected data" in the figures of aerodynamic characteristics, are "corrected data."

The normal-force and chord-force loading distributions, obtained by integration of the chordwise pressure distributions, are divided by the associated component of the total model force acting in the wing normal or chordwise directions.

For the propellers-off condition, the wing shears are nondimensionalized by dividing by the product of wing area and free-stream dynamic pressure, and the wing bending moments are nondimensionalized by dividing by the product of wing area, wing panel span, and free-stream dynamic pressure.

The results of this investigation are presented as outlined in the following table:

	Figure
Aerodynamic and wing-loads characteristics of unpowered model (propellers removed)	11
Tilt-wing configuration:	
Wing-root loads	12 to 18
Pressure loading	19 to 21
Flap loads	22 to 28
Tilt wing with slat ($\delta_s = -30^\circ$):	
Wing-root loads	29 to 30
Vibratory-loads time history	31
Deflected slipstream:	
Wing-root loads	32 to 33
Flap loads	34 to 35

DISCUSSION

Tilt-Wing Configuration

Wing-root loads.- The results of the wing-root-loads measurements for a tilt-wing V/STOL configuration are presented in figures 12 to 17 for a range of flap deflections from 0° to 50°. A summary of the results of flap deflection at a steady level-flight condition (D/L = 0) is given in figure 18.

The data indicate that at constant lift, the maximum normal bending moments occur in the angle-of-attack range corresponding to that for conventional aircraft flight. The maximum chordwise bending moments occur at angles of attack and lift coefficients approaching hovering flight. Between the two extremes of conventional flight and hovering, the relationship between angle of attack and normal bending moments or chordwise bending moments is seen to be basically a cosine and a sine function, respectively, but is modified significantly by the flow condition on the wing (flow separated or unseparated and the attendant loading distribution) and by the balance of longitudinal forces.

In the mid angle-of-attack range, where the combination of normal and chordwise moments is at its maximum, an erratic variation of these moments occurs with angle of attack. Comparing figures 12 to 17 with figure 18 indicates that at a constant angle of attack, small changes from steady level flight to accelerating flight (D/L negative) or decelerating flight (D/L positive) result in equal or greater changes in normal and chordwise bending moments than are obtained by deflection of the flap from 0° to 50°. A simple analysis of the normal and chordwise loads on a wing panel (appendix A) confirms the strong dependence of the root moments on the longitudinal balance of forces; that is, changes in the longitudinal balance of forces from the trim condition result in an overall shift in the normal and chordwise bending-moment variation with angle of attack. The erratic variation of the moments with angle of attack and longitudinal balance of forces, in the mid angle-of-attack range, are therefore attributed to the variations in the wing air load distribution when these conditions are changed. The possibility of erratic variations of the propeller forces and moments with angle of attack is discounted.

Visual observations of tufts on the wing for this mid angle-of-attack range indicated the presence of flow separation starting near the leading edge, principally behind upward turning propeller blades. This flow condition was aggravated by deceleration (D/L positive) and relieved by acceleration (D/L negative). In addition, deflection of the 30-percent-chord flap, which allowed a lower wing angle of attack for longitudinal trim at a specified velocity, tended to relieve local wing separation up to the point of flow separation on the flap. The correlation of these visual observations of the flow over the wing with the trends observed in the loads measurements indicates that slipstream-induced flow separation was the primary cause of the erratic variation of moments with angle of attack.

One additional factor appears to affect the magnitude of the combined normal and chordwise moments in the mid angle-of-attack range. Calculations made by use of the experimental results of this investigation and the analysis of

appendix A indicate that the drag center of pressure is located on the panel outboard of the 50-percent wing-panel span through much of the angle-of-attack range. This result can be expected, as is shown in appendix B, whenever the span loading becomes more uniform than the elliptic lift distribution; that is, the spanwise center of pressure of induced drag on the semispan approaches the wing tip as the lift distribution becomes more uniformly distributed. This result is important in the mid angle-of-attack range because the outboard position of the drag center of pressure will add to the root normal bending moment and tend to sustain the normal moments at the values obtained at low angles of attack. Methods of determining the spanwise distribution of induced drag are available in the published literature, for instance, in reference 6.

The wing torsional moments (figs. 12 to 17), consisting of wing and propeller aerodynamic pitching moments plus thrust moment due to propeller-centerline offset, appear smooth throughout the angle-of-attack range. Substantial variations in torsional moment appear as the result of acceleration (D/L negative) and deceleration (D/L positive) at constant angle of attack; however, the largest increments in torsional moment appear as the result of flap deflection from 0° to 50° in steady level flight (fig. 18).

A critical loading condition on the wing root cannot be stated in general form, as this loading would be a function of the structural design of the wing and flap programing with angle of attack. However, it appears from the results presented that a wide range of conditions will normally require analysis in a design study.

Pressure distribution.- In the previous section a strong correlation was noted between the occurrence of local areas of separation on the wing and erratic wing-root moments. An examination of the load distribution on the wing therefore appeared in order. The available measurements of pressure distribution are limited to a segment of the wing panel behind a single propeller (fig. 6); however, the measurements are adequate for surveying the general nature of the effect of the slipstream on the distribution of air loads.

The mean pressure forces and effective thrust are given as a function of wing angles of attack in figure 19 for the tilt-wing configuration with zero flap deflection. The data presented are for approximately zero longitudinal acceleration and correspond to the normalized loading plots given in figure 20. The normalized loading plots were obtained by dividing the normal and chord pressure forces by the appropriate component of the total resultant force on the model. This procedure yields a nondimensional factor indicative of the magnitude of the pressure load contributions to the total model forces. Before the results presented are discussed, it should be emphasized that the pressure distributions presented do not include the contributions of induced drag, skin friction, and rotational losses to the total aerodynamic drag.

Angle of attack: The normalized loadings presented in figure 20 for steady level flight ($D/L \approx 0$) indicate that the effect of the slipstream on spanwise distribution of forces at angles of attack below normal wing stall ($\alpha = 14.4^\circ$ and 14.5°) and slightly above stall ($\alpha = 19.4^\circ$) is negligible. As pointed out in reference 2, an insignificant variation in span loading exists over this same interval with the propellers removed. At intermediate angles of attack

(α = 29.4° and 40.4°) the slipstream caused a nearly symmetrical loading bulge behind the propeller, somewhat similar to the loading predicted in reference 7 and found experimentally in reference 8 with a uniform circular jet. When wing angles of attack were increased above 40°, the span loading became rapidly unsymmetrical with the peak loads occurring outboard of the propeller center line in the region of the wing acted upon by the slipstream flow from the upward traveling propeller blades. If the loading on the wing behind all three propellers is assumed similar to that behind the midspan propeller (with wing-tip and fuselage effects neglected and the direction of rotation of each propeller considered), it is apparent that the spanwise center of pressure of the normal force moves with increasing angle of attack from a nearly central position toward the most outboard propeller. From the lift and drag components of the resulting pressure force the spanwise center of pressure of the pressure drag on the panel may also be inferred to move toward the wing tip. This change is in addition to the previously discussed outward movement of the induced-drag center of pressure. This experimental evidence supports the conclusions in the previous section which were obtained from an analysis of the measured root moments and shears.

Acceleration and deceleration: The effect of longitudinal acceleration (negative D/L) or deceleration (positive D/L) on the normalized loading is shown in figure 21. Correlation of the pressure measurements with visual observation of tufts indicated that flow separation and decreased loading occurred on the wing in the region of upward traveling propeller blades $\left(\text{positive } y_p/R\right)$ for both the "trimmed" and decelerating conditions at angles of attack of approximately 30° and 40°. An appreciable increase in the loading behind the upward traveling propeller blades occurred at an accelerating condition. Inasmuch as the propeller thrust and rotational speed increase with changes in the ratio D/L from positive values to negative values (at constant angle of attack), it appears that slipstream rotation, sometimes causing flow separation, can grossly affect the wing loading and the resulting root bending moments.

As wing angles of attack approach hovering, where the principal flow over the wing is due to the propeller slipstream, visual observation of tufts indicated that local areas of stall ceased to be present with variations in the ratio D/L. It is shown in figure 21 that at a wing incidence of 70°, the spanwise distribution of loading is appreciably less affected by acceleration or deceleration than at lower angles of wing incidence.

Flap loads.- The effects of longitudinal acceleration (D/L negative) and deceleration (D/L positive) on flap loads through the angle-of-attack range, for a range of flap deflection from 0° to 50°, are presented in figures 22 to 28. Throughout the flap-deflection and angle-of-attack range, the flap loads for accelerating flight (D/L negative) and steady level flight (D/L = 0) were smooth and without abrupt discontinuities. A discontinuity begins to appear in the mid-transition region with increasing flap deflection (figs. 25, 26, and 27) for a decelerating condition. Inasmuch as the flow over the flaps was separated throughout the angle-of-attack range for flap deflections of 30° or greater, and the ratios of flap loads to lift exhibited the discontinuity only at decelerating conditions, the discontinuity is believed to be due to separation and reattachment of the flow on the forward portion of the wing. As previously noted, flow separation was present near the leading edge of the wing behind upward-turning

propeller blades at wing angles of attack from 30° to 50°. This flow separation was also noted to be aggravated at decelerating conditions (positive D/L) and to cause erratic wing bending moments and spanwise center-of-pressure movement. The fact that flap deflection, as a means for relieving these conditions, is limited to flap deflections of about 30° indicates a need for other approaches to slipstream flow problems in this range (decelerating) of transitional flight. The results of one such approach are now discussed.

Tilt-Wing Configuration With Slat

During tests of the tilt-wing configuration, it was apparent that local areas of flow separation at certain conditions were causing severe buffeting and vibration of the model. Visual observation of tufts indicated that separation was occurring abruptly over a triangular area of the wing with the apex of the triangle near the leading edge and centered between the two outboard propellers. This area was subjected to slipstream flow developed from the passage of upward traveling propeller blades. Since it was apparent that the rotational components of the slipstream were causing local stall, an attempt to alleviate this local stalling by adding a slat between the two outboard propeller nacelles was made. In addition, a slat was installed across the fuselage between the inner nacelles (fig. 5) in an attempt to eliminate root separation due to the combination of the upward flow from the propeller and the fuselage-wing junction. The resulting flow conditions were considerably improved as is discussed in the next section.

Effect of slat on flow separation.- Visual observations of tufts on the wing and flaps indicated that the slat was extremely effective in delaying flow separation on the outward portion of the wing and in reducing the area of flow separation near the wing root. The slat was able to delay flow separation to angles of attack as much as 16° higher than was possible with the slat-off configuration (both configurations at flap deflection of 30°) at a constant propeller rotational speed. Prior to the installation of the slat, the wing segment behind the upturning propeller blades stalled at an angle as much as 8° less than that of the wing segment behind the downturning propeller blades. After the slat was installed, the wing segment behind the upturning propeller blades stalled at an angle as much as 8° more than that of the wing segment behind the downturning propeller blades. This result indicates that a more optimum slat design would involve variable incidence or variable geometry compatible with the local flow conditions as suggested by reference 2.

Wing-root loads.- The wing-root loads for the tilt-wing-with-slat configuration are presented in figures 29 and 30. It is apparent that the combination of the slat with a flap deflection of 30° gives the most uniform variation of wing-root bending moments and spanwise centers of pressure for the two slat-flap combinations. The favorable effect of the flap was previously shown in figure 15. The effect of the slat on the wing loads is evidenced principally by an outward movement of the chord-force spanwise center of pressure and a substantial increase in the wing torsional moment.

Vibratory loads.- The addition of the slats to the wing, in addition to delaying flow separation, caused almost complete elimination of buffeting of the model through the range of conditions covered. A time history of the vibratory

loads encountered with and without the slat is presented in figure 31. Aside from some high-frequency vibration at the rotational frequency of the propeller, the principal low-frequency, large-amplitude vibrations are either substantially reduced or eliminated. The tabulated values of steady-state load and vibratory load shown in figure 31 indicate the outboard shift in the chordwise center of pressure and the simultaneous reduction in the magnitudes of the vibratory loads as a result of adding the slat.

Flight tests of a tilt-wing aircraft, reported in reference 9, have shown that the usable flight envelope can be restricted by buffeting so that controllability is unacceptable. During these flight tests, controllability was considerably improved by adding a permanently drooped leading edge to the wing. The present results indicate that the use of a partial-span slat, retracting for conventional flight, would be a more effective solution to the problem of extending the controllable flight envelope.

Deflected-Slipstream Configuration

Wing-root loads.- Wing-root loads for the deflected-slipstream configuration, with two combinations of deflection of the double-slotted flaps, are presented in figures 32 and 33. Chord-force spanwise centers of pressure have been omitted because the small magnitude of the chordwise shears made an accurate determination of the spanwise centers of pressure impossible. The normal bending moments with both combinations of flap deflection were larger than those measured for the tilt-wing configuration. For the largest flap deflection (fig. 33) the normal bending moments decreased with increasing angle of attack. In addition, the spanwise center of pressure of the normal forces moved inboard with increasing angle of attack for both flap combinations. The variations in moments and center-of-pressure location with angle of attack were smooth and indicated the absence of any appreciable flow problems for the deflected-slipstream wing. It was noted, during the tests with the deflected-slipstream configuration, that there was little tendency toward model buffeting or vibration. Records from the oscillograph, however, indicated that vibrations were of greater amplitude with this configuration than with the tilt-wing-with-slat configuration (fig. 31(b)) but were of lesser amplitude than those obtained without the slat (fig. 31(a)).

Visual observation of tufts on the wing and flaps indicated that separation was present on the rear flaps throughout the angle-of-attack range, that separation was present on the front flaps only at large positive values of the ratio D/L, and that the forward portion of the wing was always free of separated flow.

Flap loads.- The loads presented in figures 34 and 35 for the front flap are the total loads restrained by the brackets holding the front flap. The loads on both flaps are presented as normal and parallel to the chord line of the surface forward of the flap. (See fig. 1.)

CONCLUSIONS

The results of an investigation of the structural loads on a large-scale general research V/STOL model indicate the following:

1. The relationship between angle of attack and normal or chordwise bending moments at the root was found to be basically a simple cosine and sine function, respectively, but was modified significantly by the flow condition on the wing and by the balance of longitudinal forces. Normal and chordwise bending moments were relatively unaffected by deflection of the 30-percent-chord flaps; in contrast, the wing torsion was substantially affected by flap deflection and by the balance of longitudinal forces.

2. Local areas of flow separation, principally behind upward traveling propeller blades, caused erratic movements in the spanwise centers of pressure. The addition of a 19-percent-chord partial-span slat to the tilt-wing configuration, in combination with a flap deflection of 30°, resulted in the elimination of buffet caused by local areas of flow separation for the range of conditions covered.

3. The magnitude and lateral variations of jet-boundary-interference velocities encountered in this investigation and the subsequent increased probability of systematic variations in the measured aerodynamic forces on the entire model indicate that the use of ratios of model to wind-tunnel sizes as large as that of this investigation are undesirable and should be avoided.

Langley Research Center,
National Aeronautics and Space Administration,
Langley Station, Hampton, Va., January 23, 1963.

APPENDIX A

DEVELOPMENT OF EQUATIONS FOR NORMAL AND CHORDWISE BENDING MOMENTS

Additional Symbols

In addition to the previously defined symbols, the following symbols are used exclusively in this appendix.

a	yawing-moment multiplying factor (integer), value and sign depending upon number of propellers per semispan and their direction of rotation
D_w	drag of wing semispan, excluding all propeller forces, lb
$D_{w,p}$	drag of wing semispan, including all propeller forces, lb
L_w	lift of wing semispan, excluding all propeller forces, lb
$L_{w,p}$	lift of wing semispan, including all propeller forces, lb
n	number of propellers per semispan
N	normal force per propeller, lb
y_n	spanwise center of propeller normal forces on semispan, measured from wing root, ft
y_T	spanwise center of propeller thrust forces on semispan, measured from wing root, ft
T	thrust per propeller, lb
$M_{Z,p}$	propeller yawing moment, ft-lb
β	spanwise center of lift L_w on wing semispan, measured from wing root, ft
γ	spanwise center of drag D_w on wing semispan, measured from wing root, ft

Normal Bending Moment

The aerodynamic forces and moments acting on the wing to produce a normal bending moment at the wing root are the wing normal force, the propeller normal force, and a normal couple. The normal couple is included to account for a normal-force distribution producing a moment but having no contribution to the

total normal force. An example of conditions producing this moment is obtained when the wing is acted upon by a propeller slipstream causing an asymmetrical loading about the propeller axis on the wing segment behind the propeller, but when the net normal force on the wing segment is zero. An additional factor contributing to the normal couple will be the propeller shaft torque. The existence, magnitude, and direction of this couple depends on the number of propellers and mode of rotation of the propellers on the wing. The calculated input of the shaft torque for this model, at the most extreme conditions of large angle of attack near hovering, was approximately 290 foot-pounds. At the desired lift of 3,500 pounds, this input results in an increase in M_n/Lb' of 0.006 as compared with an estimated measurement accuracy of ±0.005.

The normal bending moment may be written as

$$M_n = \text{Normal-force center of pressure} \times \text{Normal force} + \text{Normal couple} \qquad (A1)$$

or in terms of propeller and wing aerodynamic forces and their associated centers of pressure

$$M_n = y_n nN + \beta L_w \cos \alpha + \gamma D_w \sin \alpha + \text{Normal couple} \qquad (A2)$$

However, it is desirable to express the normal bending moment as a function of the overall lift and drag of the semispan panel $L_{w,p}$ and $D_{w,p}$ as these more nearly represent the operating conditions of the airplane. Note that

$$L_w = L_{w,p} - nN \cos \alpha - nT \sin \alpha \qquad (A3)$$

and

$$D_w = D_{w,p} - nN \sin \alpha + nT \cos \alpha \qquad (A4)$$

Substituting equations (A3) and (A4) into equation (A2), introducing the wing semispan and the "center of pressure" of the propeller thrust on the panel as appropriate variables, and rearranging terms to obtain a nondimensional ratio results in:

$$\frac{M_n}{L_{w,p}b/2} = \frac{\beta}{b/2}\left(\cos \alpha + \frac{\gamma}{\beta}\frac{D_{w,p}}{L_{w,p}} \sin \alpha\right) + \frac{y_n}{b/2}\frac{nN}{L_{w,p}}\left[1 - \left(\frac{\gamma}{y_n} \sin^2\alpha + \frac{\beta}{y_n} \cos^2\alpha\right)\right]$$

$$+ \frac{y_T}{b/2}\frac{nT}{L_{w,p}}\left(\frac{\gamma}{y_T} - \frac{\beta}{y_T}\right)\frac{\sin 2\alpha}{2} + \frac{\text{Normal couple}}{L_{w,p}b/2} \qquad (A5)$$

Chordwise Bending Moment

The aerodynamic forces and moments acting on the wing to produce a chordwise bending moment at the wing root are the wing chord force, propeller thrust, propeller yawing moment, and chordwise wing couple. The existence, magnitude, and direction of the propeller yawing-moment contribution depends on the number of propellers and mode of rotation of the propellers on the wing. The chordwise bending moment may be written as:

$$M_c = (\text{Chord-force center of pressure}) \times (\text{Chord forces}) + (\text{Chordwise couple}) + (\text{Propeller yawing moment}) \tag{A6}$$

or in terms of propeller and wing aerodynamic forces and their associated centers of pressure:

$$M_c = y_T nT + \beta L_w \sin\alpha - \gamma D_w \cos\alpha + aM_{Z,p} + \text{Chordwise couple} \tag{A7}$$

Substituting equations (A3) and (A4) into equation (A7), introducing the panel span and the "center of pressure" of the propeller normal force on the panel as appropriate variables, and rearranging terms to obtain a nondimensional ratio results in:

$$\frac{M_c}{L_{w,p}b/2} = \frac{\beta}{b/2}\left(\sin\alpha - \frac{\gamma}{\beta}\frac{D_{w,p}}{L_{w,p}}\cos\alpha\right) + \frac{y_n}{b/2}\frac{nN}{L_{w,p}}\left(\frac{\gamma}{y_n} - \frac{\beta}{y_n}\right)\frac{\sin 2\alpha}{2} + \frac{y_T}{b/2}\frac{nT}{L_{w,p}}\left[1 - \left(\frac{\beta}{y_T}\sin^2\alpha + \frac{\gamma}{y_T}\cos^2\alpha\right)\right] + a\frac{Y}{L_{w,p}b/2} + \frac{\text{Chordwise couple}}{L_{w,p}b/2} \tag{A8}$$

Significance of Results of Analysis

The importance of the equations developed in this appendix is not in predicting the root moments but in showing the trends in moments due to changes in certain parameters. For instance, it can be seen that increasing the D/L ratio causes increased normal bending moments but causes decreased chordwise bending moments. $\left(\text{Note that } \frac{D}{L} \approx \frac{D_{w,p}}{L_{w,p}}, \quad \frac{M_c}{Lb'} \approx \frac{1}{2}\frac{M_c}{L_{w,p}b/2}, \text{ and } \frac{M_n}{Lb'} \approx \frac{1}{2}\frac{M_n}{L_{w,p}b/2}.\right)$ In addition, an increase in the ratio D/L, without other corresponding changes, causes the greatest increase in normal moments at angles of attack approaching

90° but causes the greatest decrease in chordwise bending moments at angles of attack approaching 0°.

In addition, the importance of differences in the spanwise location of the panel centers of lift and drag at constant D/L can be assessed. Calculations made by using equations (A5) and (A8), assuming a reasonable location of the lift center of pressure and typical propeller aerodynamic characteristics, indicate that an outboard location of the drag-force center of pressure causes the greatest increase in normal bending moment at an angle of attack of about 50°, and the greatest decrease in chordwise bending moment at an angle of attack of about 30°. It was also noted, from the calculations, that lift and drag center-of-pressure changes with angle of attack, corresponding to those expected with flow separation occurring within the propeller slipstream, can cause reversals in the slope of the chordwise bending-moment variation with angle of attack, at angles of attack of about 30° to 50°. However, the same center-of-pressure changes cause a nearly constant normal bending moment in the same angle-of-attack range.

With movement of lift and drag centers of pressure simultaneous with changes in the ratio D/L, the separate effects of both are amplified. In addition, the angle-of-attack range affected by these changes is extended.

The trends predicted by equations (A5) and (A8) are in general agreement with the experimental results presented.

APPENDIX B

SEMISPAN LOCATION OF INDUCED-DRAG CENTER OF PRESSURE

The simplest type of trailing vortex system occurs with a uniform loading where the circulation Γ is constant across the span. It is shown in reference 10 (pp. 134-138) that the downwash distribution and induced drag can be represented as:

$$\frac{w}{V} = \frac{C_L}{2\pi A} \frac{(b/2)^2}{(b/2)^2 - y^2} \tag{B1}$$

$$\frac{dD_i}{dy} = \rho w \Gamma \tag{B2}$$

where

A	wing aspect ratio
D_i	induced drag, lb
w	downwash velocity, ft/sec
y	wing station, ft
Γ	circulation, sq ft/sec
ρ	mass density of air, slugs/cu ft

Substituting equation (B1) into equation (B2) results in

$$\frac{dD_i}{dy} = \rho V \Gamma \frac{C_L}{2\pi A} \frac{(b/2)^2}{(b/2)^2 - y^2} \tag{B3}$$

The spanwise center of pressure of the induced drag on the semispan is

$$\text{Induced-drag center of pressure} = \frac{\int_0^{b/2} y \, dD_i}{\int_0^{b/2} dD_i} \tag{B4}$$

Substituting equation (B3) into equation (B4) and simplifying results in

$$\text{Induced-drag center of pressure} = \frac{\int_0^{b/2} \frac{y\,dy}{(b/2)^2 - y^2}}{\int_0^{b/2} \frac{dy}{(b/2)^2 - y^2}} \tag{B5}$$

In the limit as y approaches $b/2$, integration of equation (B5) results in

$$\text{Induced-drag center of pressure} = \frac{b}{2} \tag{B6}$$

It is seen, therefore, that the center of pressure of induced drag on the semispan of a uniformly loaded wing is at the tip of the semispan. This result, while only of academic interest in itself, indicates a general trend; that is, as the loading on a wing becomes more uniform, the center of pressure of induced drag on a semispan of the wing approaches the wing tip.

REFERENCES

1. Huston, Robert J., and Winston, Matthew M.: Data from a Static-Thrust Investigation of a Large-Scale General Research VTOL-STOL Model in Ground Effect. NASA TN D-397, 1960.

2. Winston, Matthew M., and Huston, Robert J.: Propeller Slipstream Effects as Determined From Wing Pressure Distribution on a Large-Scale Six-Propeller VTOL Model at Static Thrust. NASA TN D-1509, 1962.

3. Ward, John F.: Structural-Loads Surveys on Two Tilt-Wing VTOL Configurations. NASA TN D-729, 1961.

4. Skopinski, T. H., Aiken, William S., Jr., and Huston, Wilber B.: Calibration of Strain-Gage Installations in Aircraft Structures for the Measurement of Flight Loads. NACA Rep. 1178, 1954. (Supersedes NACA TN 2993.)

5. Heyson, Harry H.: Linearized Theory of Wind-Tunnel Jet-Boundary Corrections and Ground Effects for VTOL-STOL Aircraft. NASA TR R-124, 1962.

6. Pearson, H. A.: Span Load Distribution for Tapered Wings With Partial-Span Flaps. NACA Rep. 585, 1937.

7. Rethorst, Scott, Royce, Winston, and Wu, T. Yao-tsu: Lift Characteristics of Wings Extending Through Propeller Slipstreams. Rep. No. 1 (Contract No. Nonr 2388(00)), Vehicle Res. Corp. (Pasadena, Calif.), Sept. 1958.

8. Snedecker, Richard S.: Experimental Determination of Spanwise Lift Effects on a Wing of Infinite Aspect Ratio Spanning a Circular Jet. Rep. No. 525 (Contracts Nonr 1858(14) and Nonr 1858(01)), Dept. Aero. Eng., Princeton Univ., Feb. 1961.

9. Pegg, Robert J.: Summary of Flight-Test Results of the VZ-2 Tilt-Wing Aircraft. NASA TN D-989, 1962.

10. Glauert, H.: The Elements of Aerofoil and Airscrew Theory. Second ed., Cambridge Univ. Press, 1948.

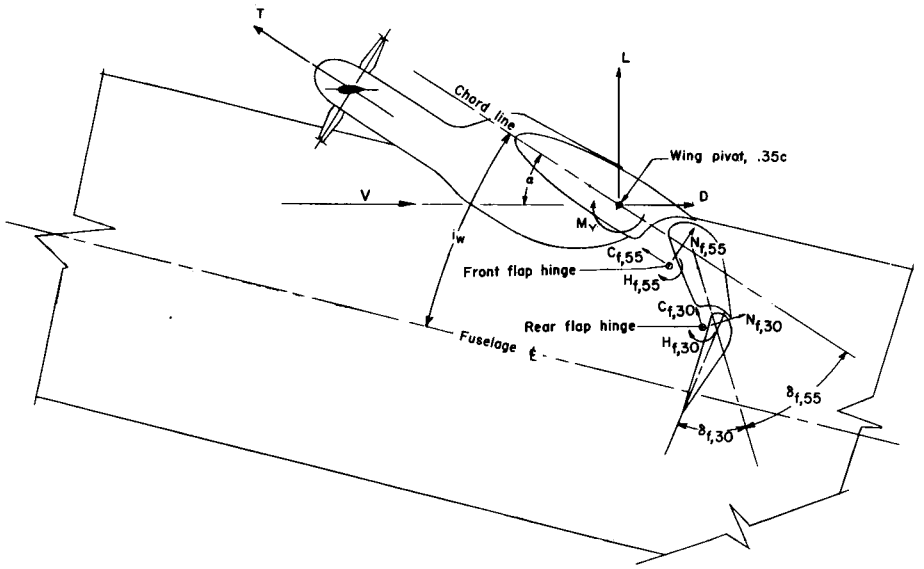

(a) Aerodynamic forces and flap-loads sign convention.

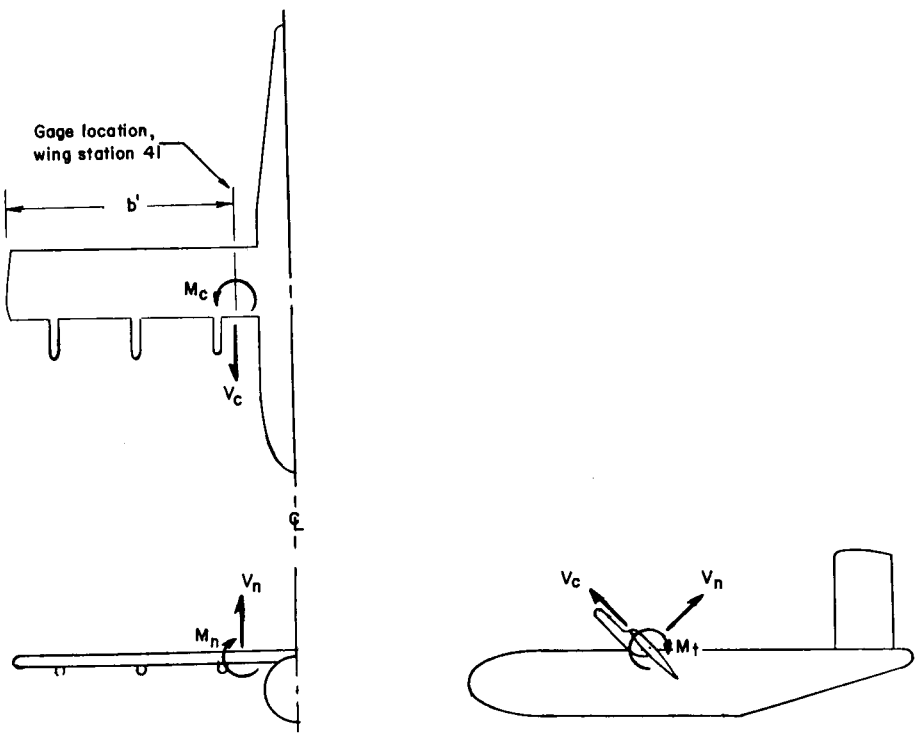

(b) Wing-loads sign convention.

Figure 1.- Conventions used to define positive senses of forces, moments, and angles.

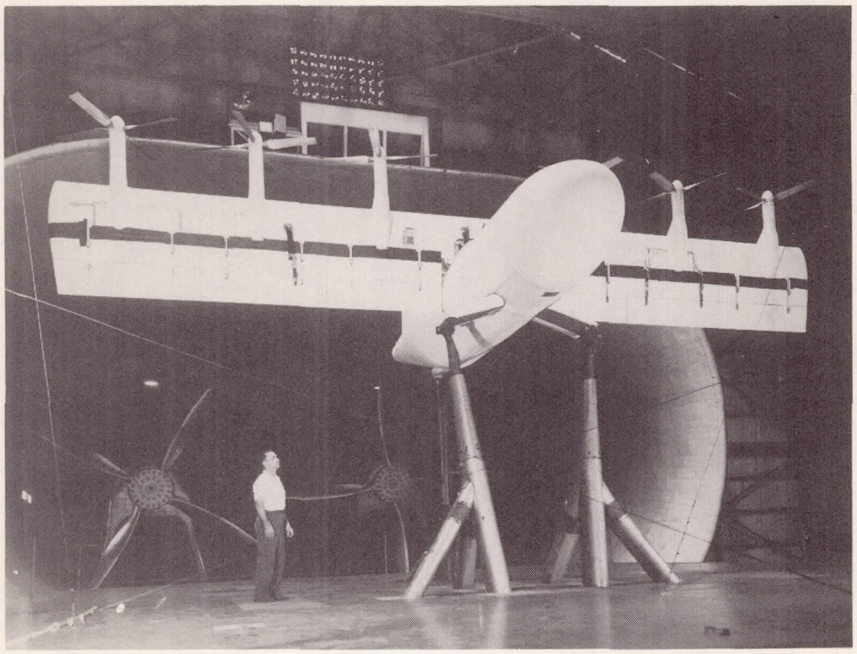

(a) Tilt-wing configuration. L-60-3155

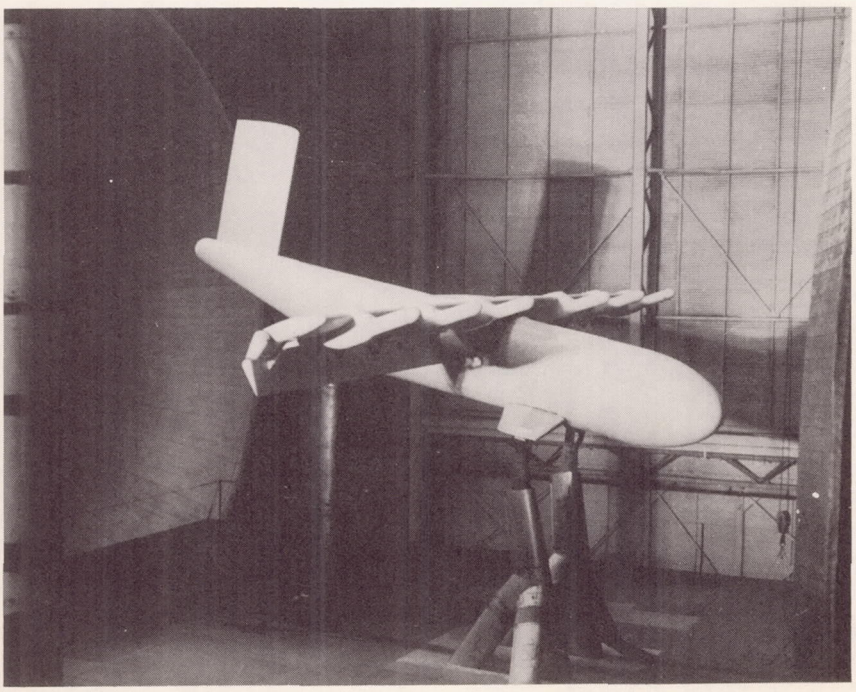

(b) Deflected-slipstream configuration. L-62-3218

Figure 2.- Model used in investigation.

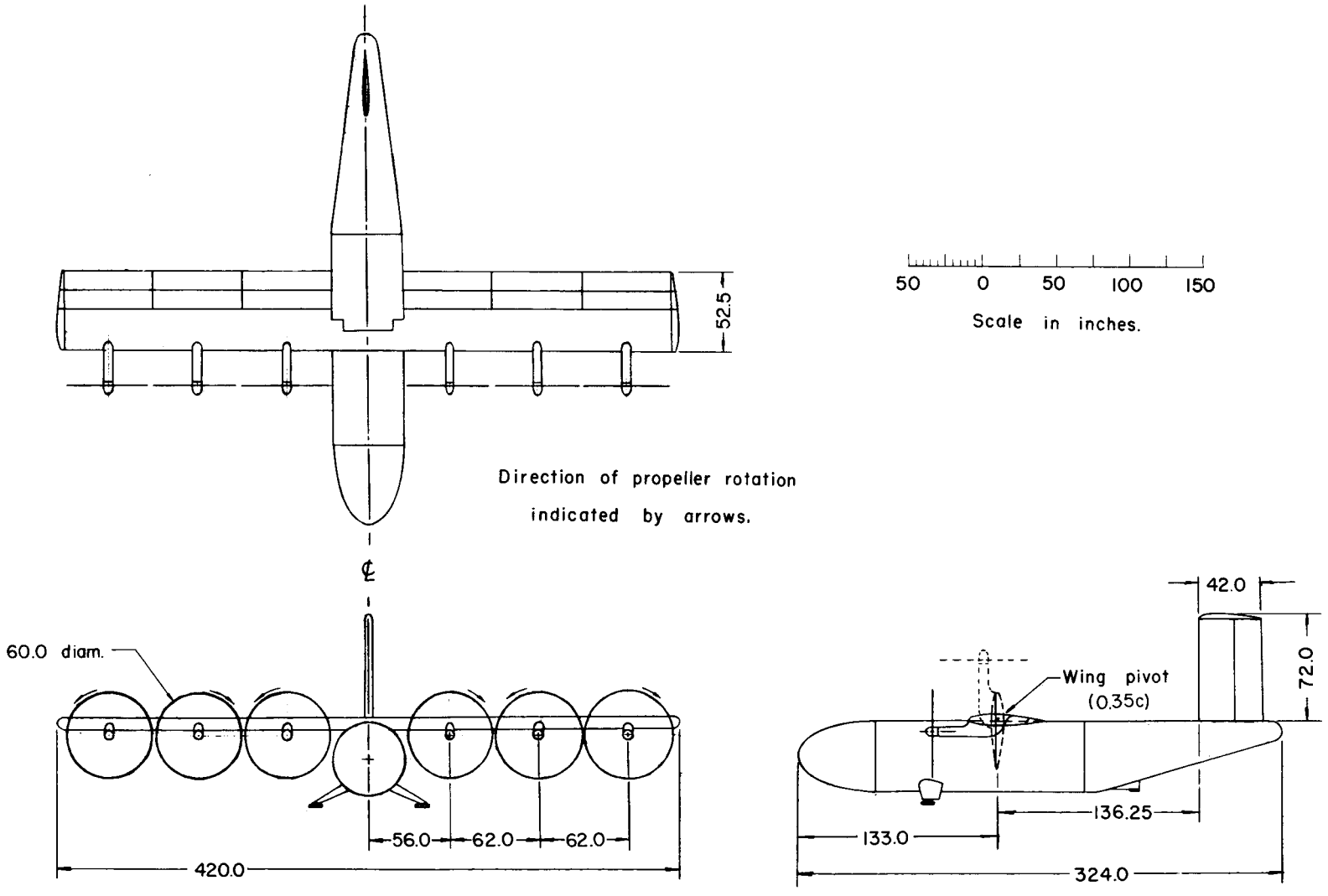

Figure 3.- Three-view sketch of model. All dimensions are in inches.

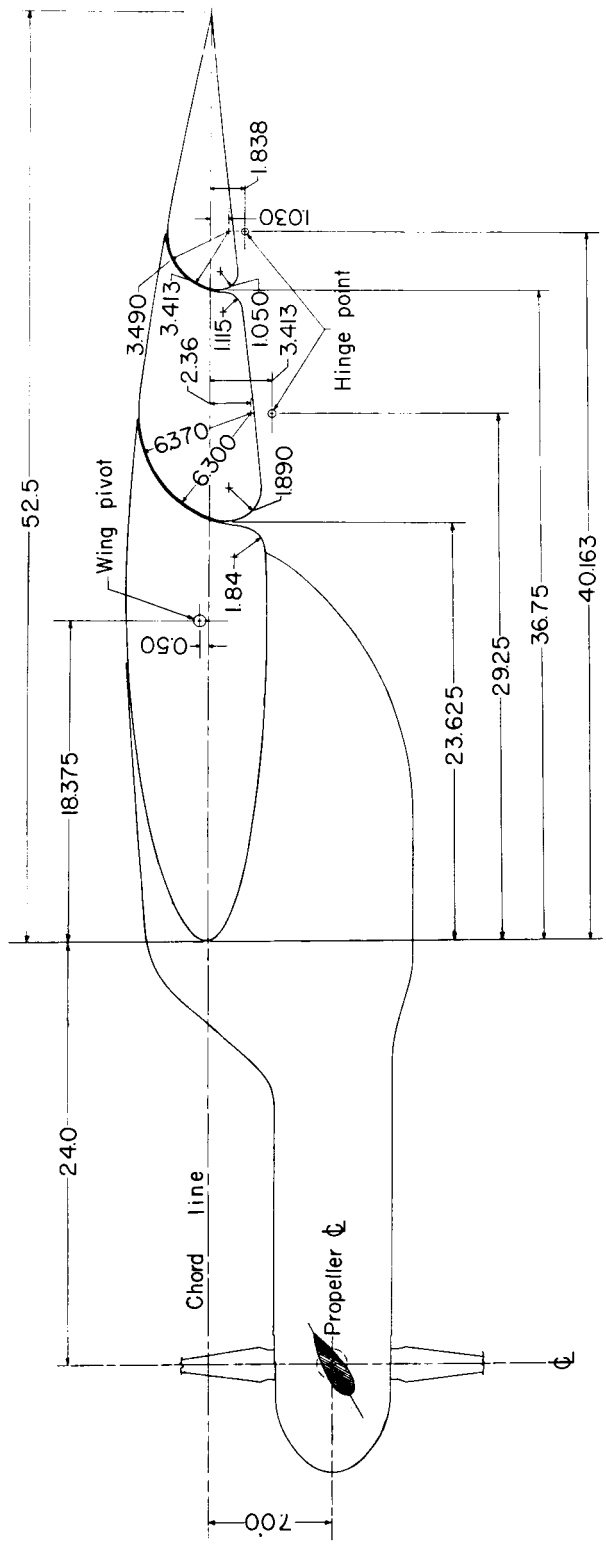

Figure 4.- Geometric characteristics of wing section. All dimensions are in inches.

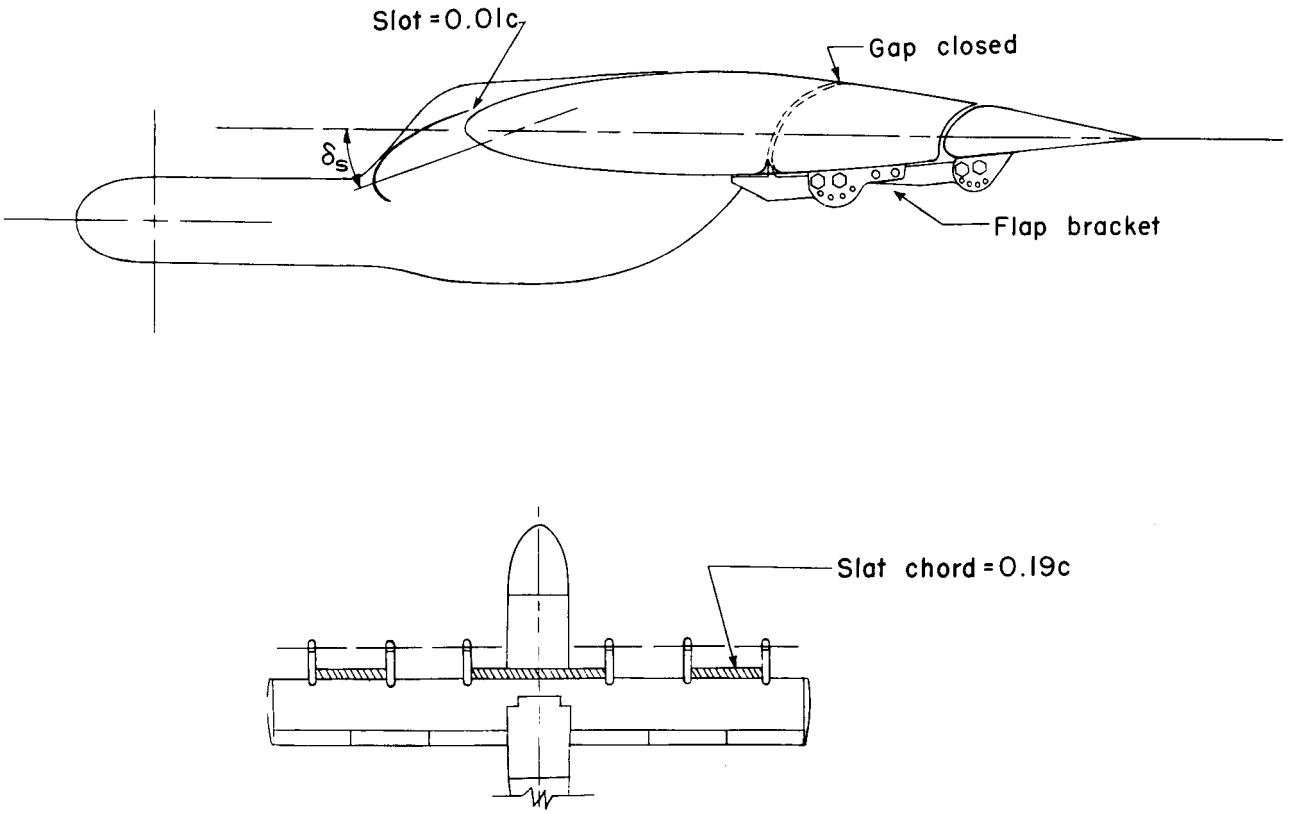

Figure 5.- Slat location and geometry.

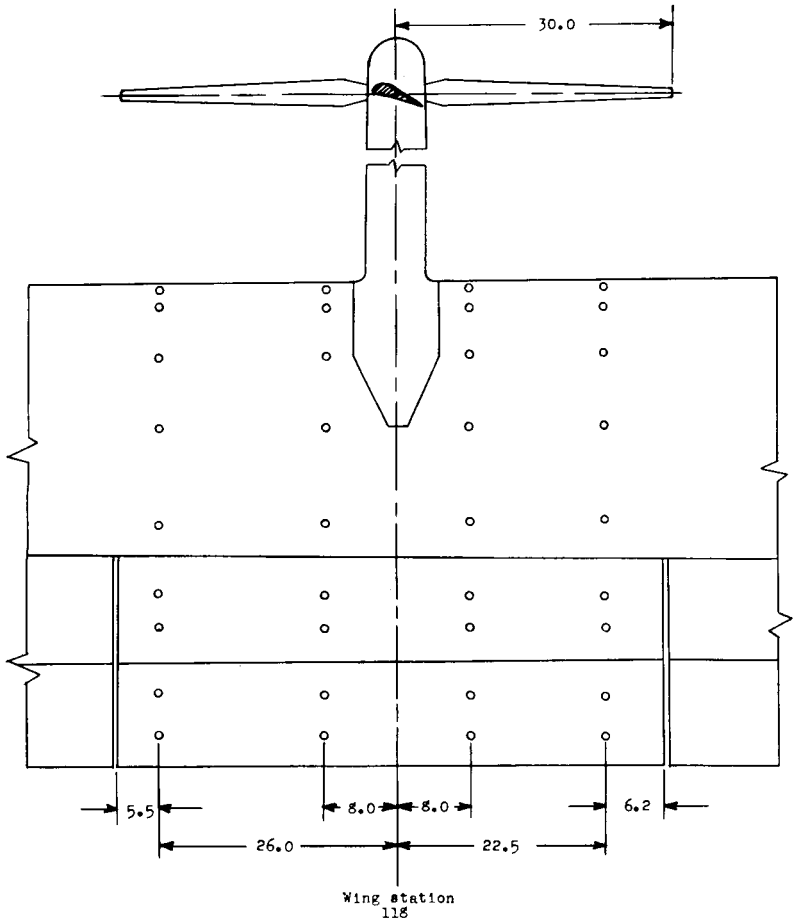

Orifice Locations		
Tube	Station, percent chord	Ordinate, percent chord
1	0	0
2	1.5	2.23
3	5.0	3.96
4	15.0	6.76
5	30.0	8.53
6	50.0	8.19
7	1.5	-1.77
8	5.0	-3.18
9	15.0	-5.14
10	30.0	-6.25
11	45.0	-2.59
12	46.6	1.75
13	50.0	5.41
14	45.0	-2.03
15	50.0	5.26
16	55.0	7.33
17	65.0	6.42
18	71.5	5.41
19	48.3	-5.52
20	55.0	-5.05
21	65.0	-3.92
22	69.9	-0.90
23	73.4	2.50
24	70.0	-0.95
25	72.6	3.26
26	76.5	4.48
27	84.9	3.01
28	93.3	1.37
29	78.6	-2.19
30	89.5	-1.07

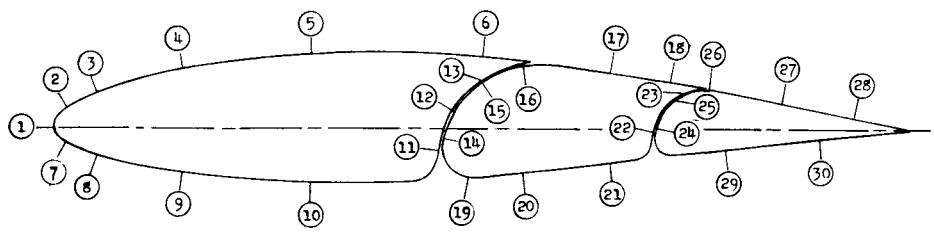

Figure 6.- Orifice locations on wing and flaps. All dimensions are in inches.

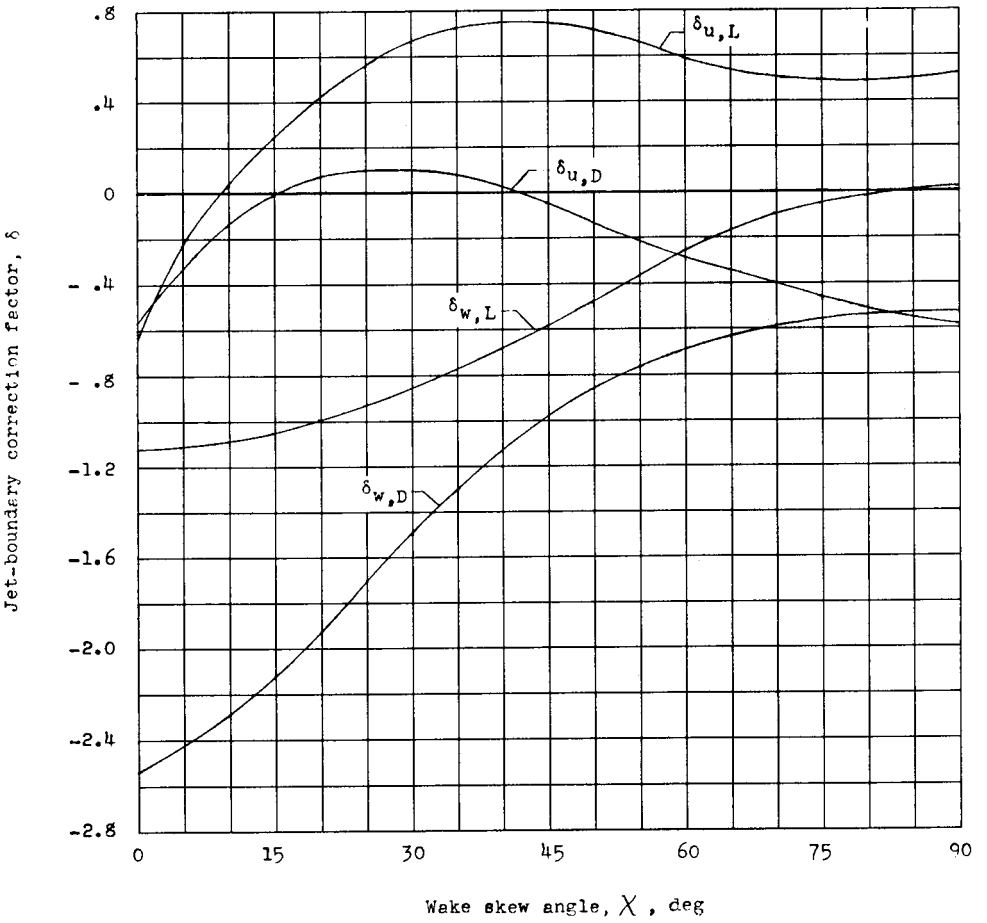

Figure 7.- Mean correction factors used in applying jet-boundary corrections.

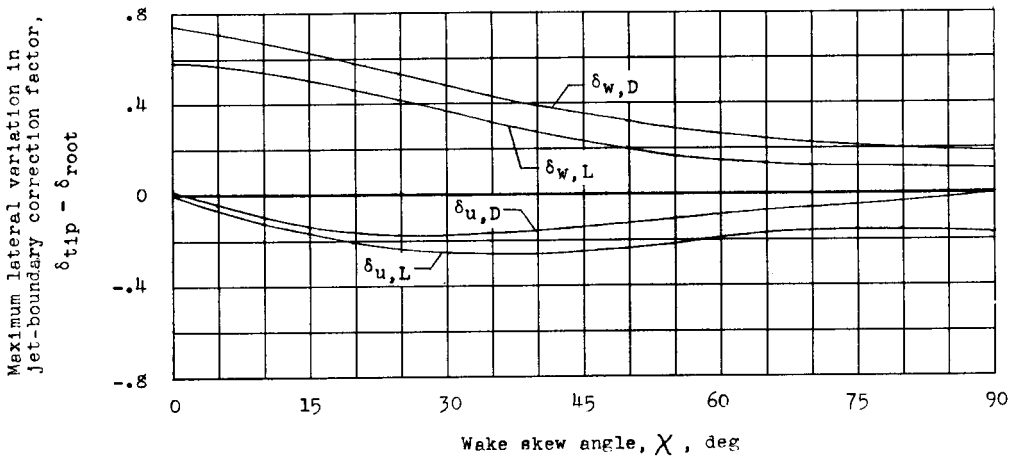

Figure 8.- Maximum lateral variation in jet-boundary correction factors.

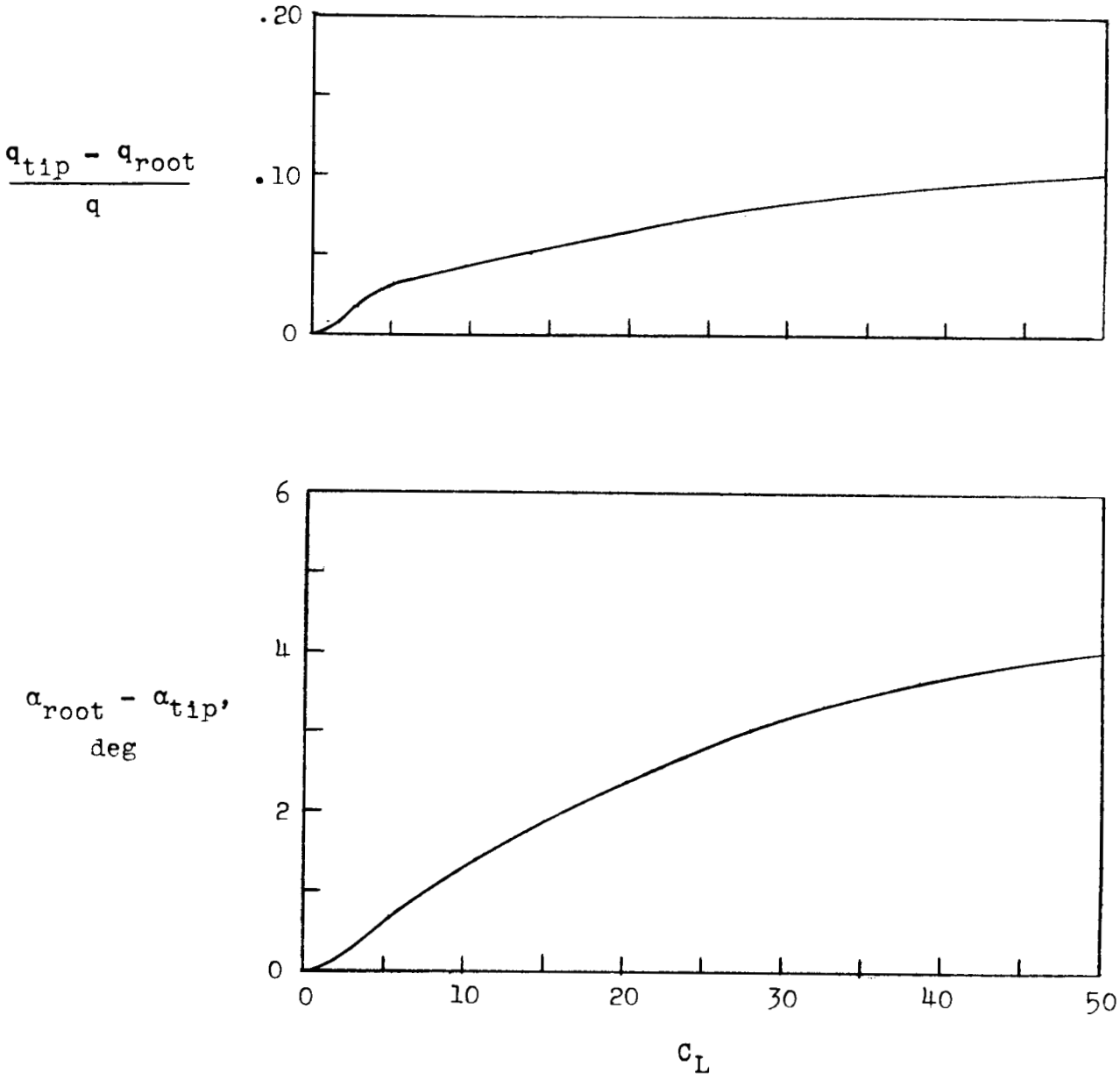

Figure 9.- Aerodynamic washout and lateral variation in dynamic pressure due to lateral variation in jet-boundary interference velocities. Tilt-wing configuration; $\delta_{f,30} = 0^{\circ}$; D/L = 0.

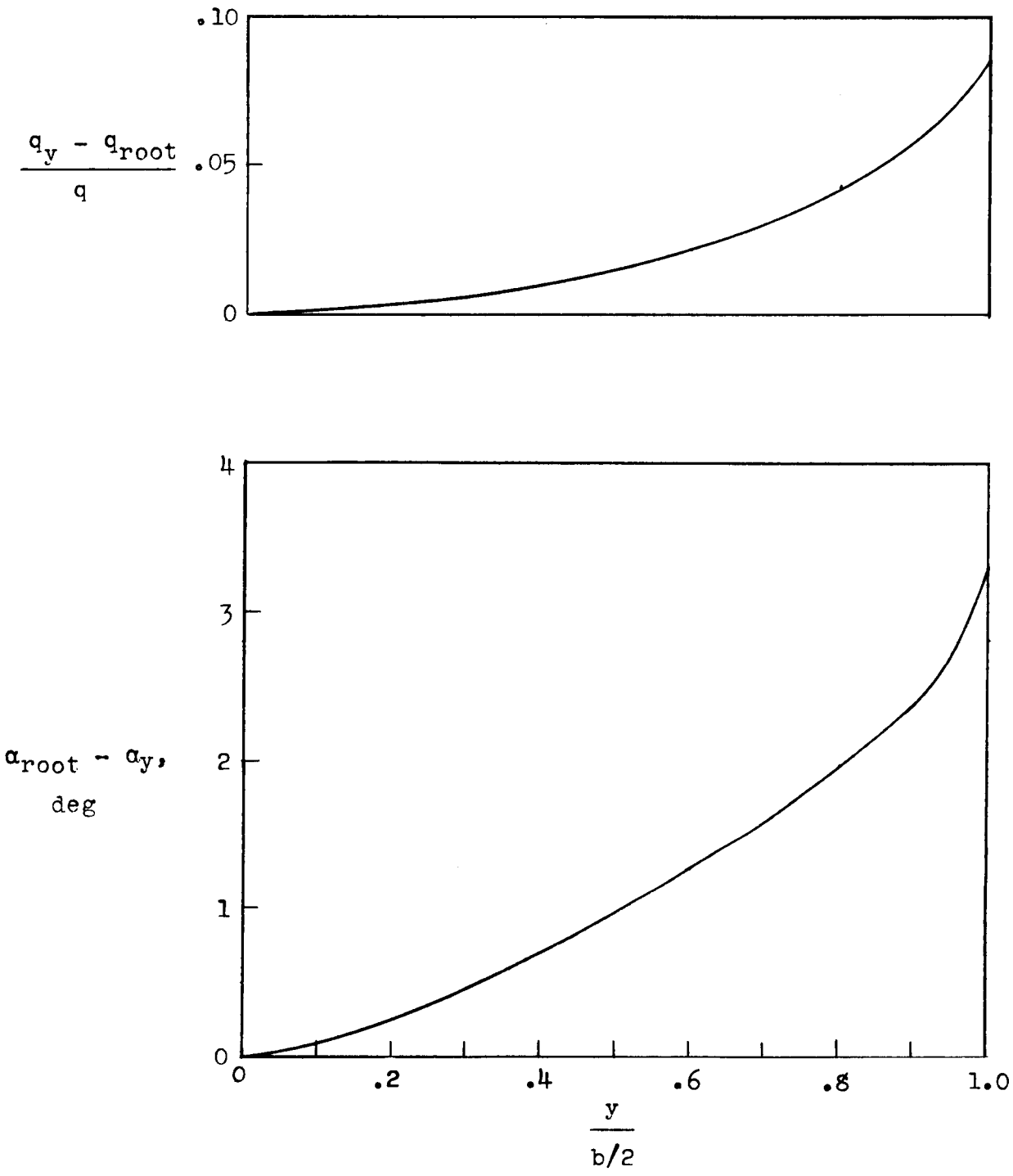

Figure 10.- Typical spanwise variation of jet-boundary induced lateral variation in angle of attack and dynamic pressure. Tilt-wing configuration; $\delta_{f,30} = 0^\circ$; D/L = 0.034; $\alpha = 71.8^\circ$; $C_L = 27.34$.

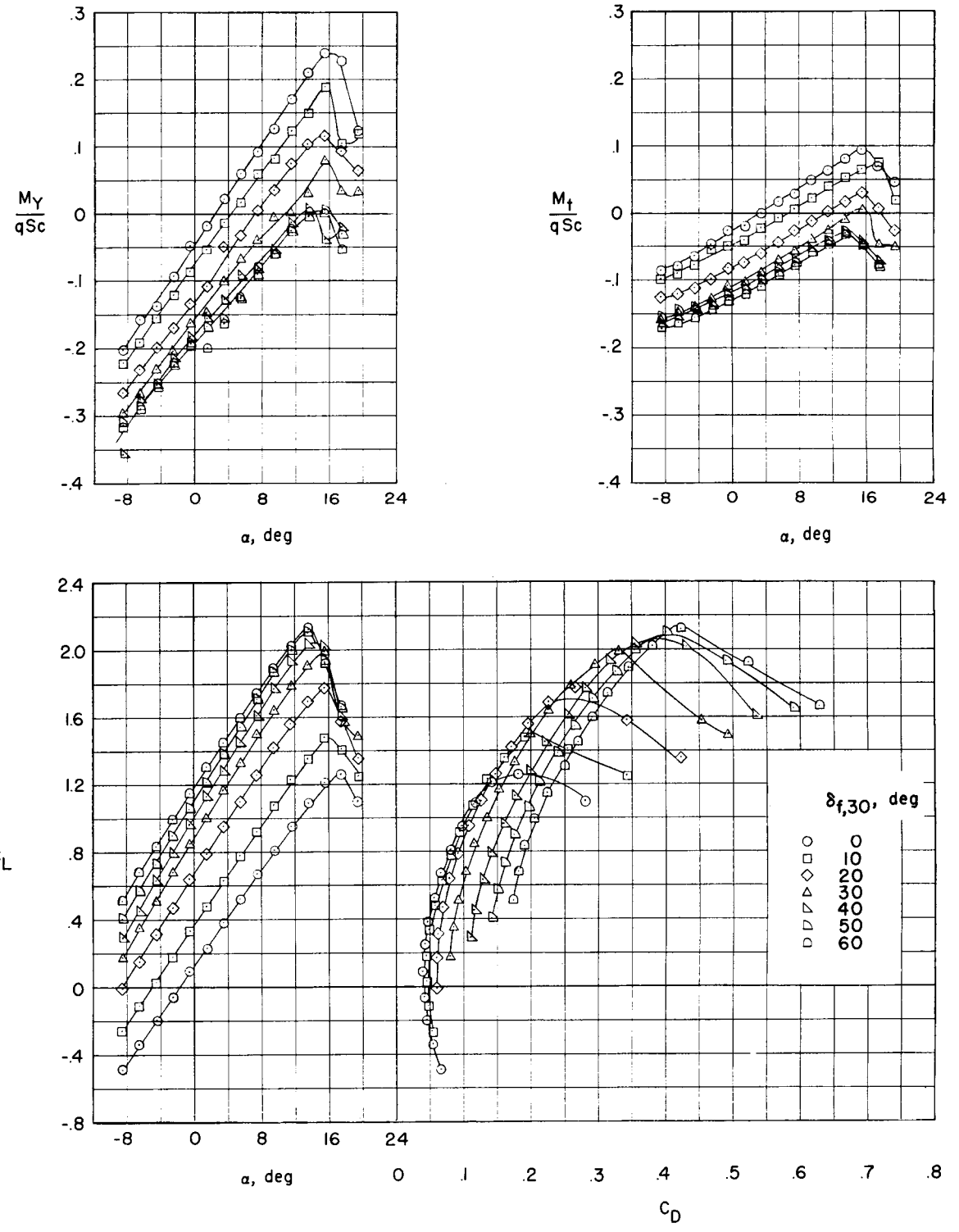

Figure 11.- Aerodynamic characteristics and wing-root loads of basic model. Propellers removed; front flap gap sealed; $i_w = 0^o$.

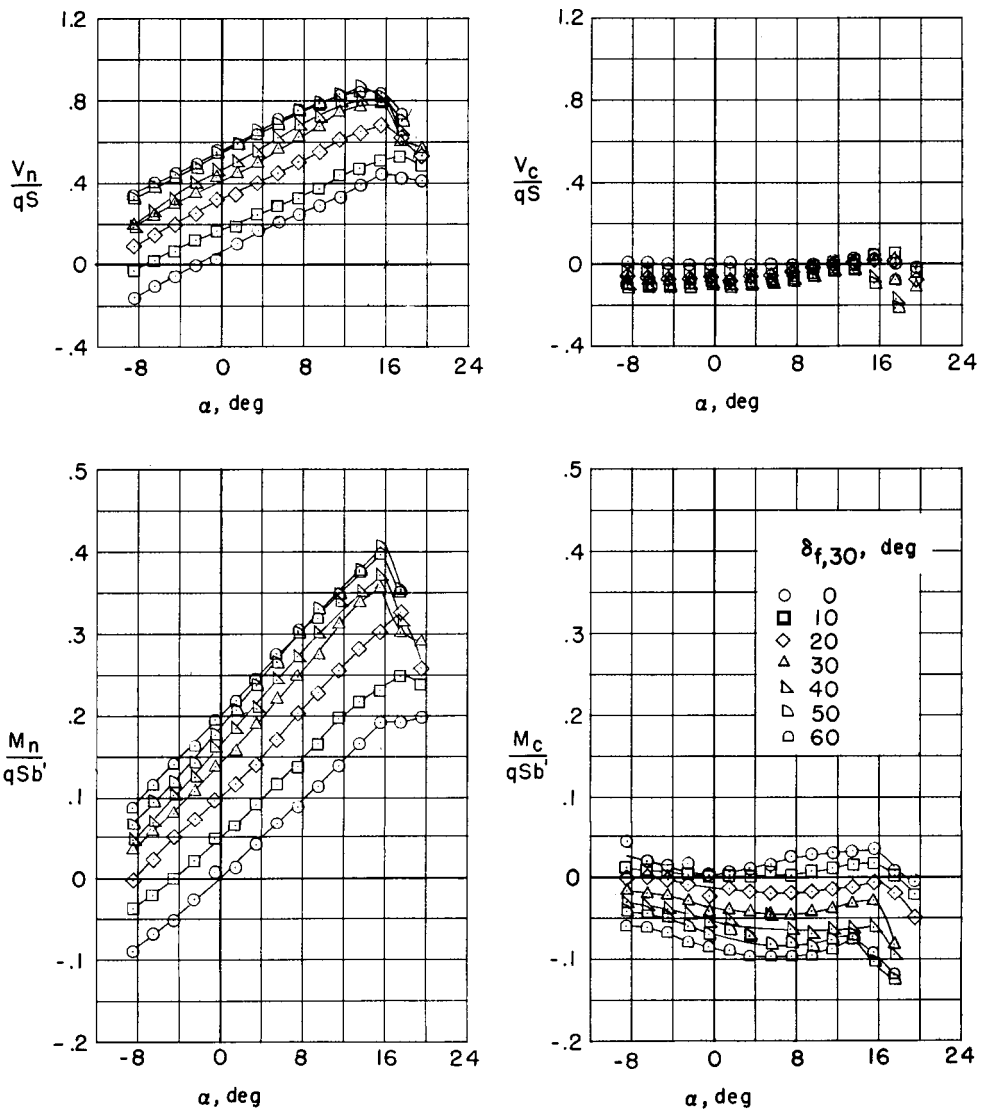

Figure 11.- Concluded.

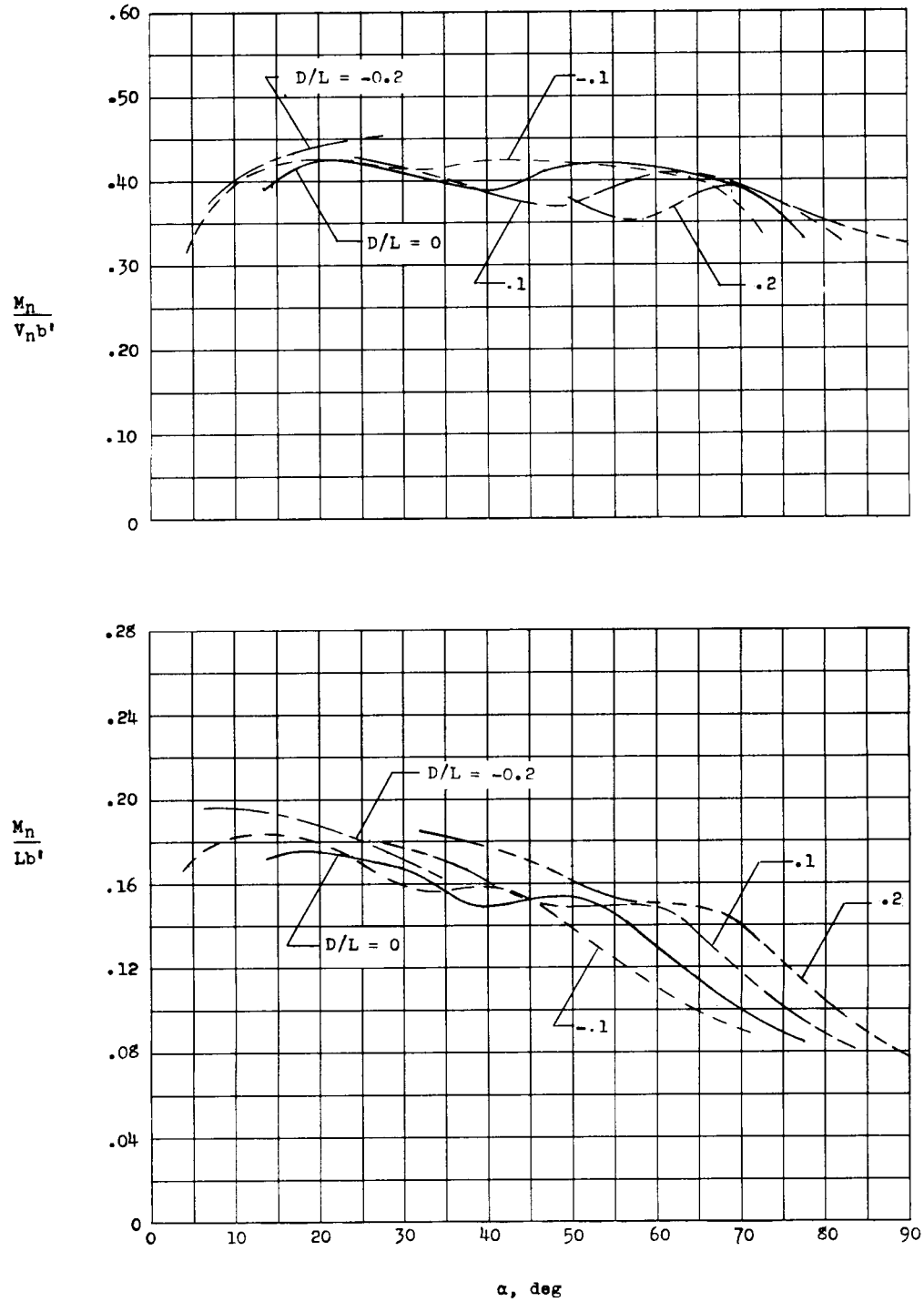

(a) Normal moments and centers of pressure.

Figure 12.- Variation of bending moments, spanwise centers of pressure, and wing torsion with angle of attack and D/L ratio. Tilt-wing configuration; $\delta_{f,30} = 0^{o}$.

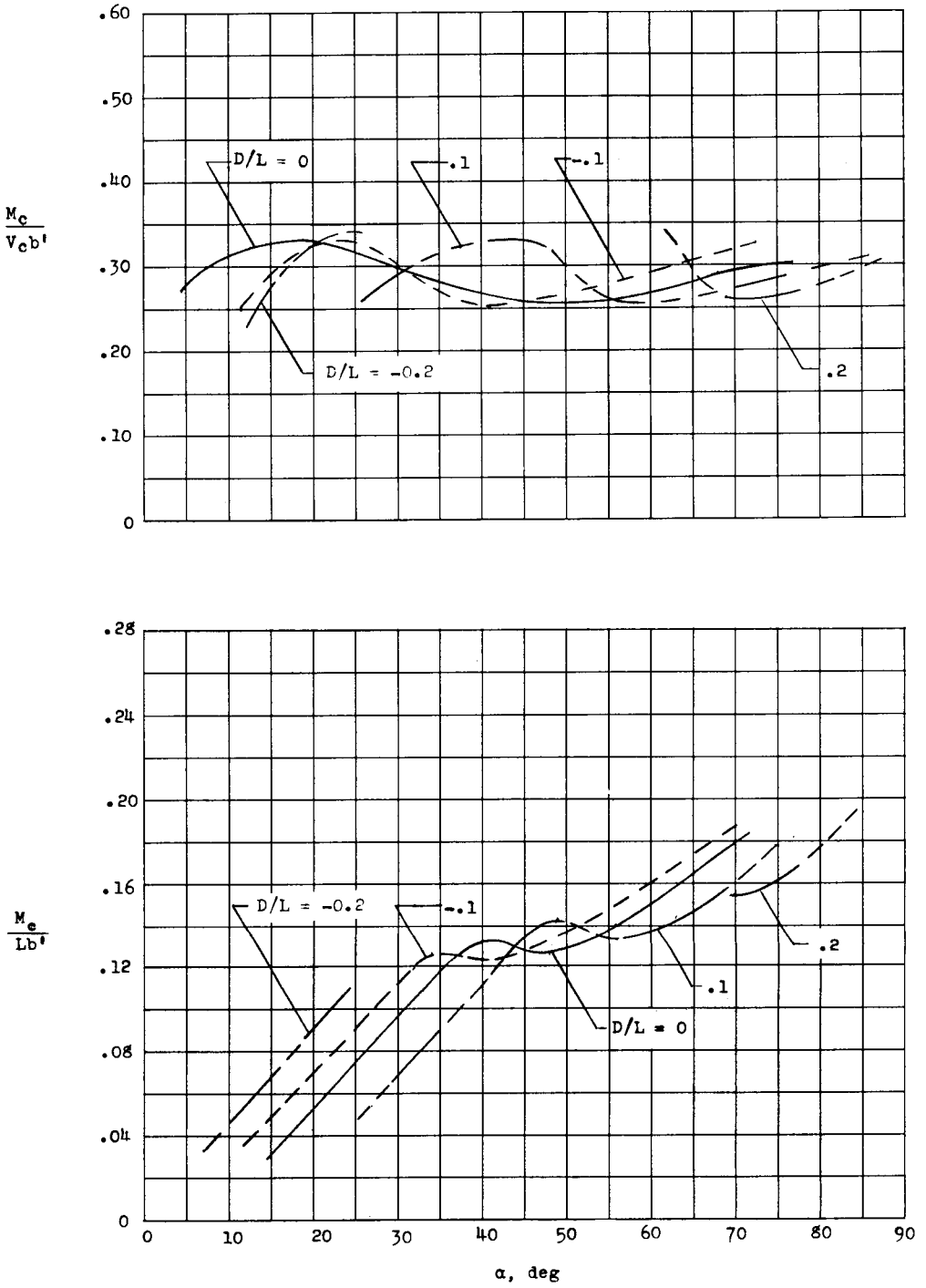

(b) Chordwise moments and centers of pressure.

Figure 12.- Continued.

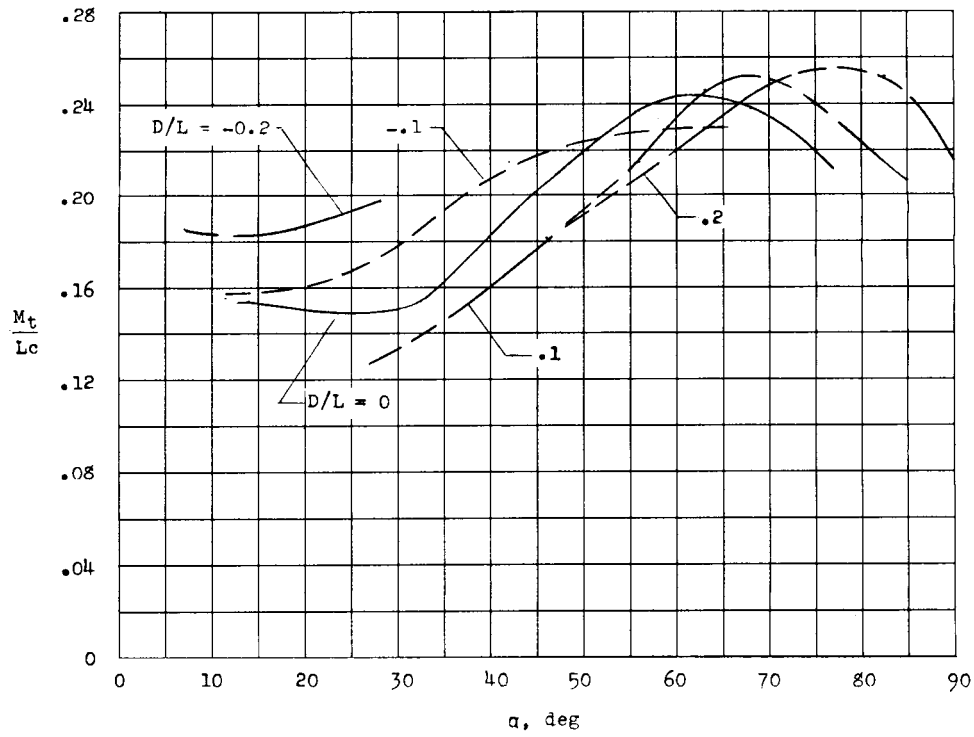

(c) Total wing torsional moment.

Figure 12.- Continued.

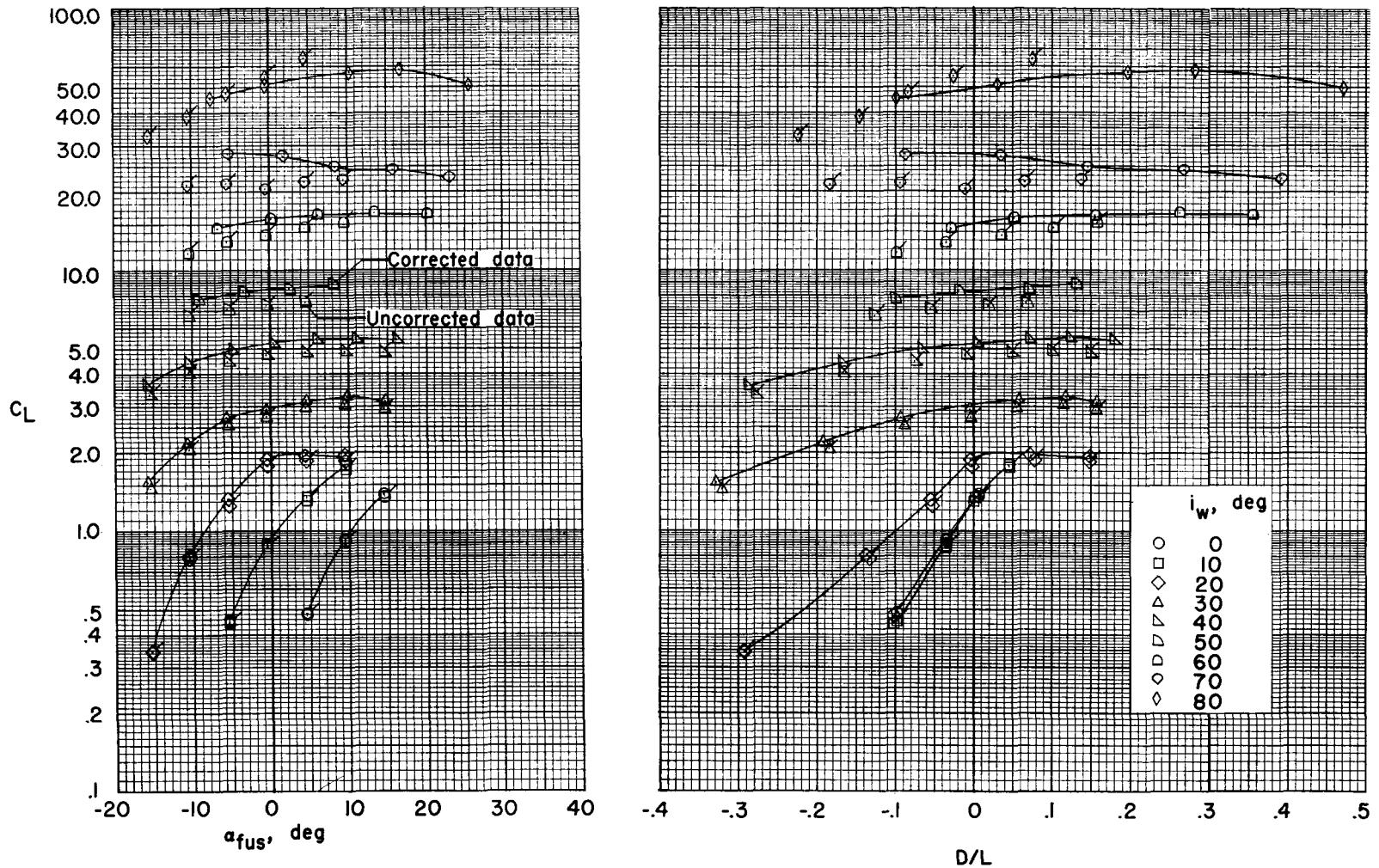

(d) Aerodynamic characteristics (for reference only).

Figure 12.- Concluded.

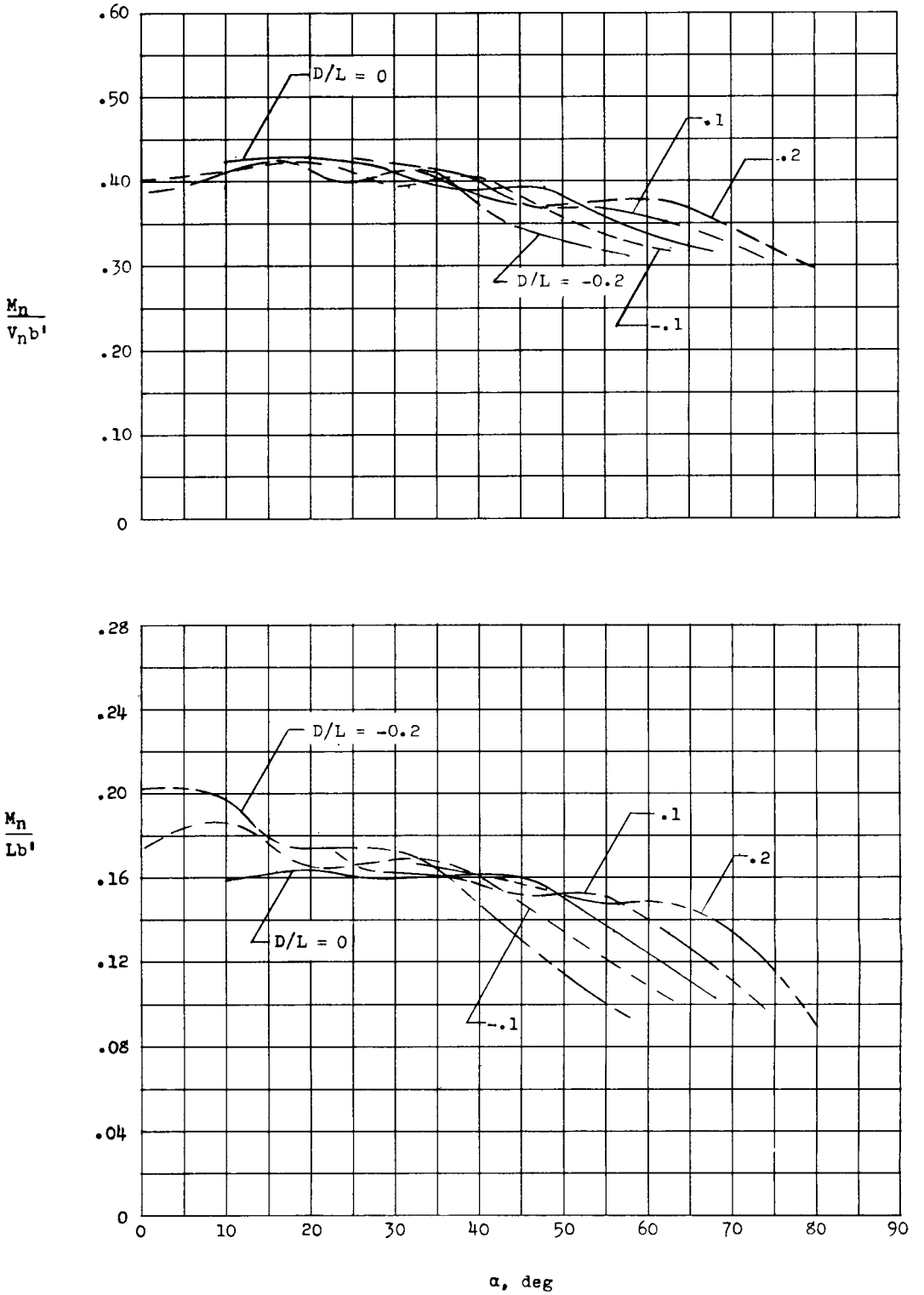

(a) Normal moments and centers of pressure.

Figure 13.- Variation of bending moments, spanwise centers of pressure, and wing torsion with angle of attack and D/L ratio. Tilt wing with flap; $\delta_{f,30} = 10^{\circ}$.

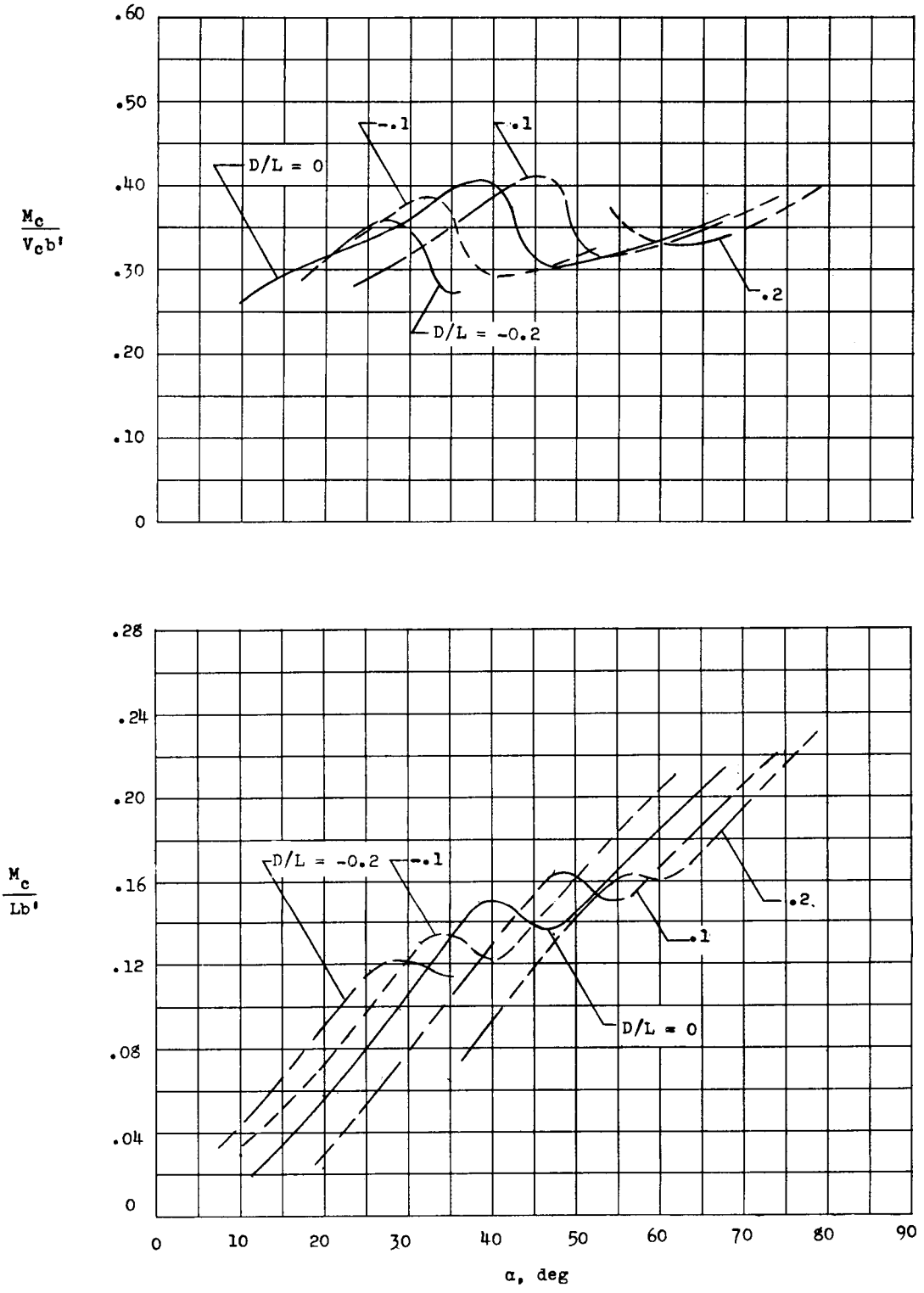

(b) Chordwise moments and centers of pressure.

Figure 13.- Continued.

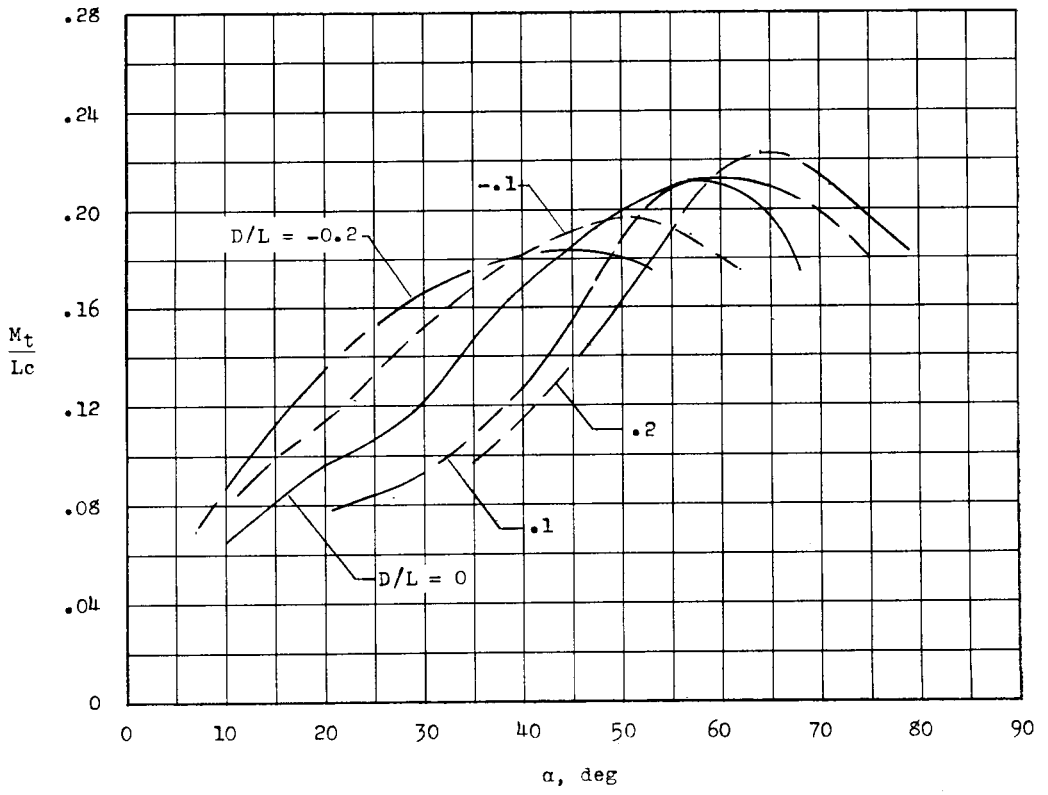

(c) Total wing torsional moment.

Figure 13.- Continued.

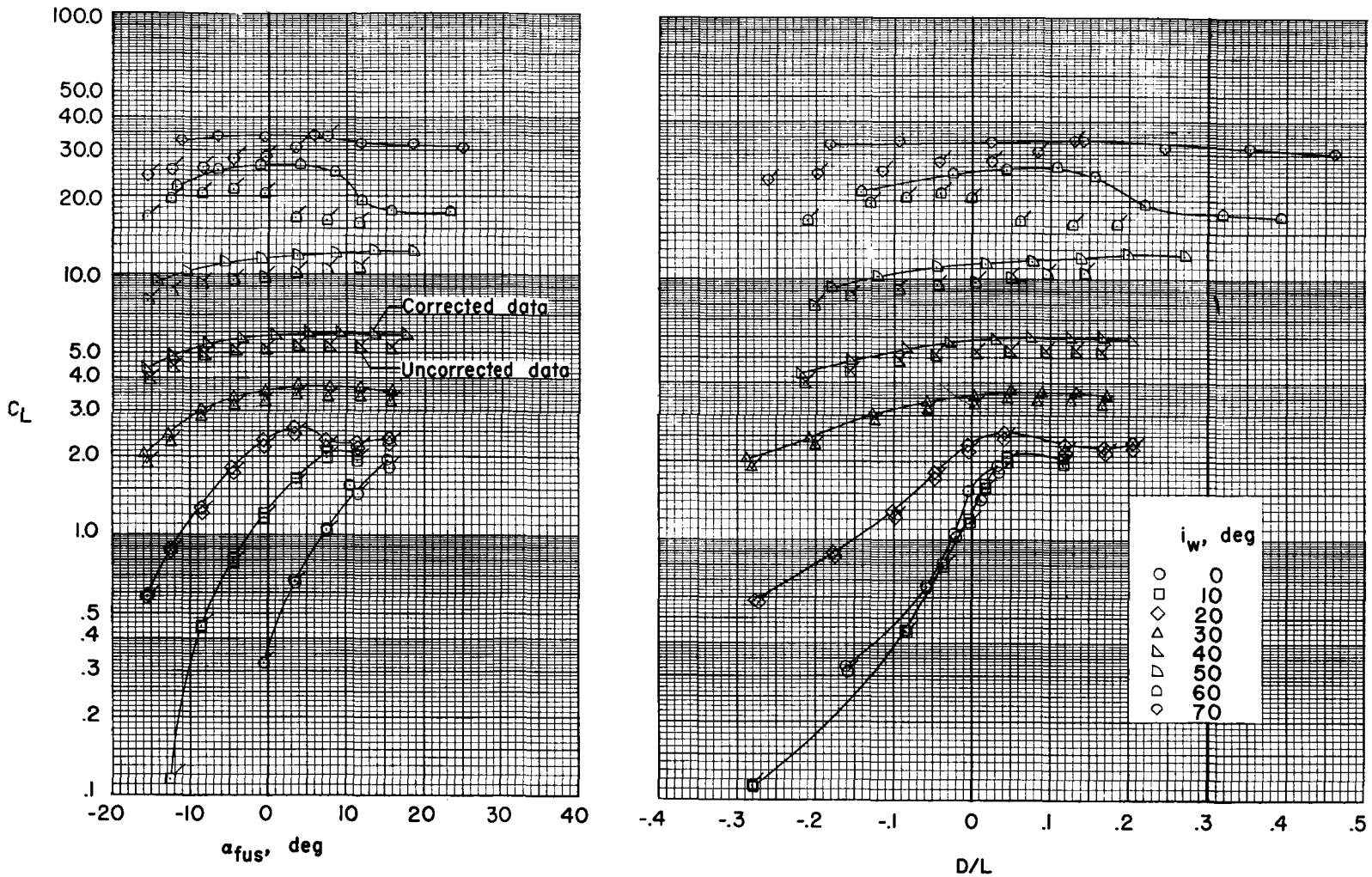

(d) Aerodynamic characteristics (for reference only).

Figure 13.- Concluded.

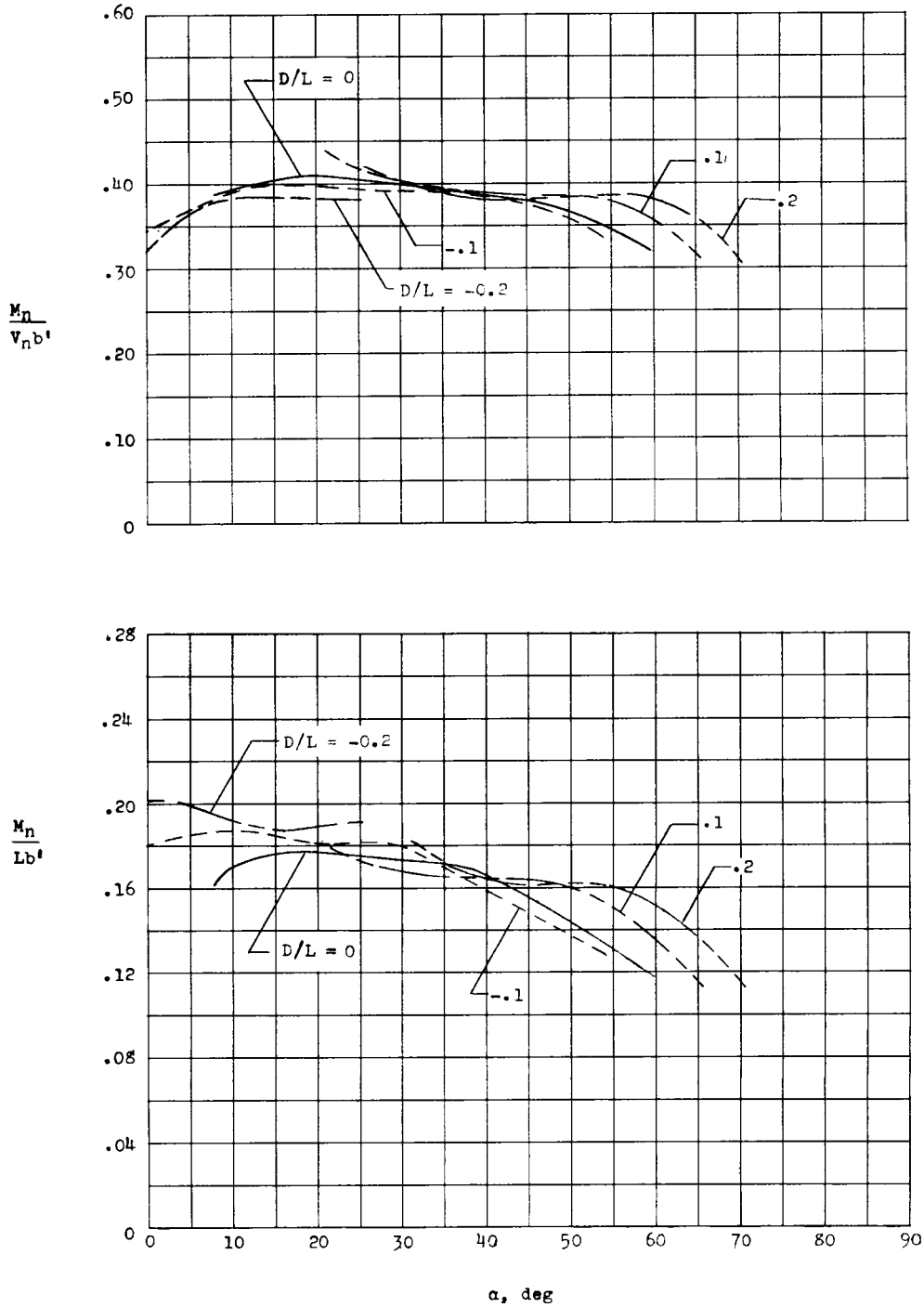

(a) Normal moments and centers of pressure.

Figure 14.- Variation of bending moments, spanwise centers of pressure, and wing torsion with angle of attack and D/L ratio. Tilt wing with flap; $\delta_{f,30} = 20^{\circ}$.

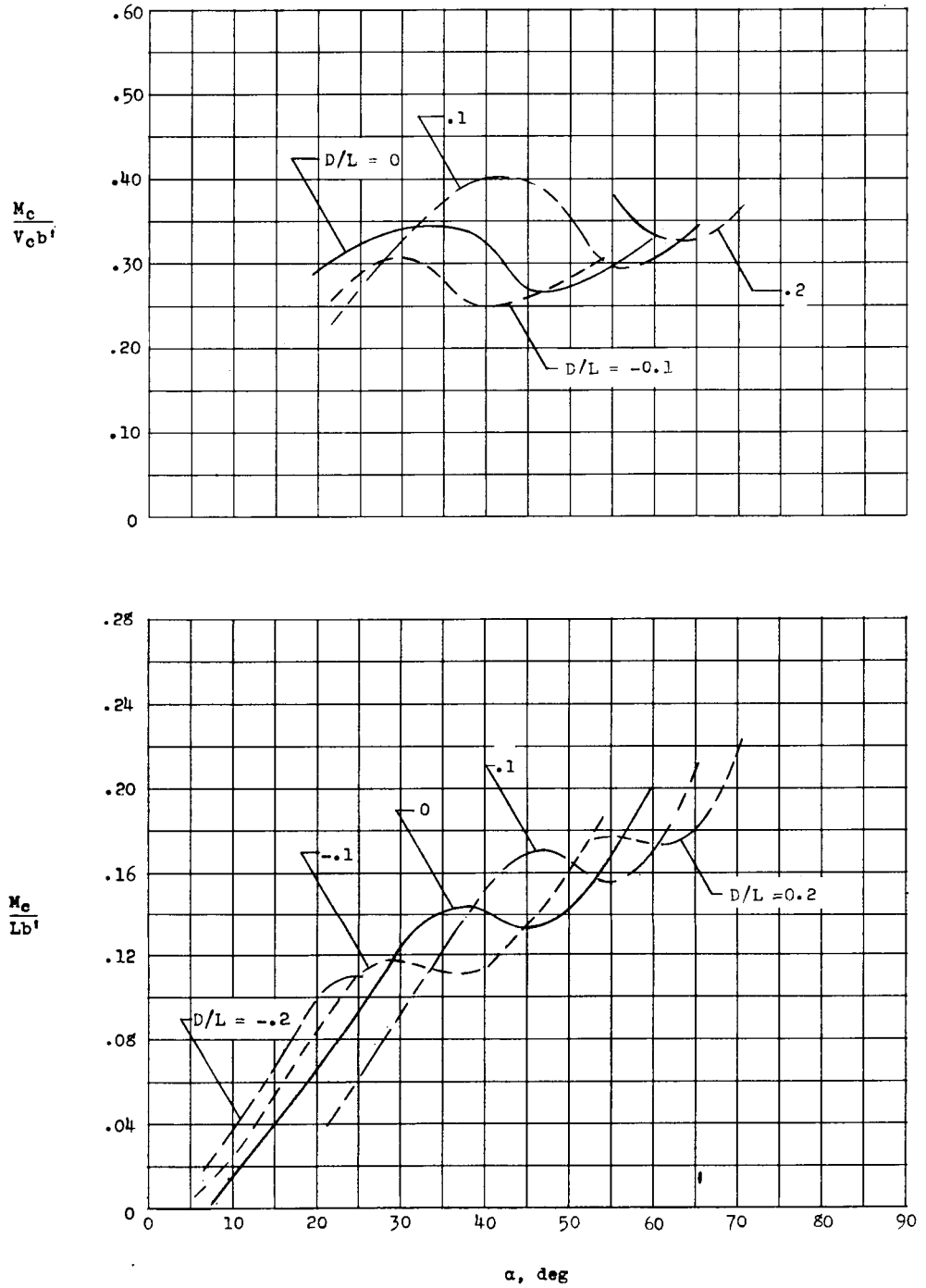

(b) Chordwise moments and centers of pressure.

Figure 14.- Continued.

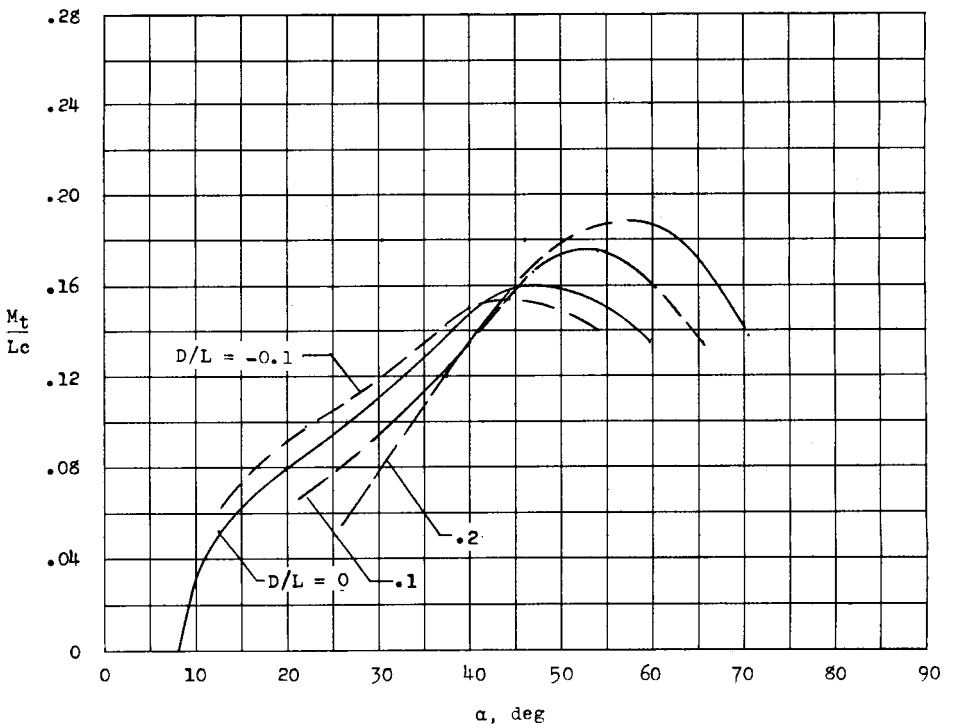

(c) Total wing torsional moment.

Figure 14.- Continued.

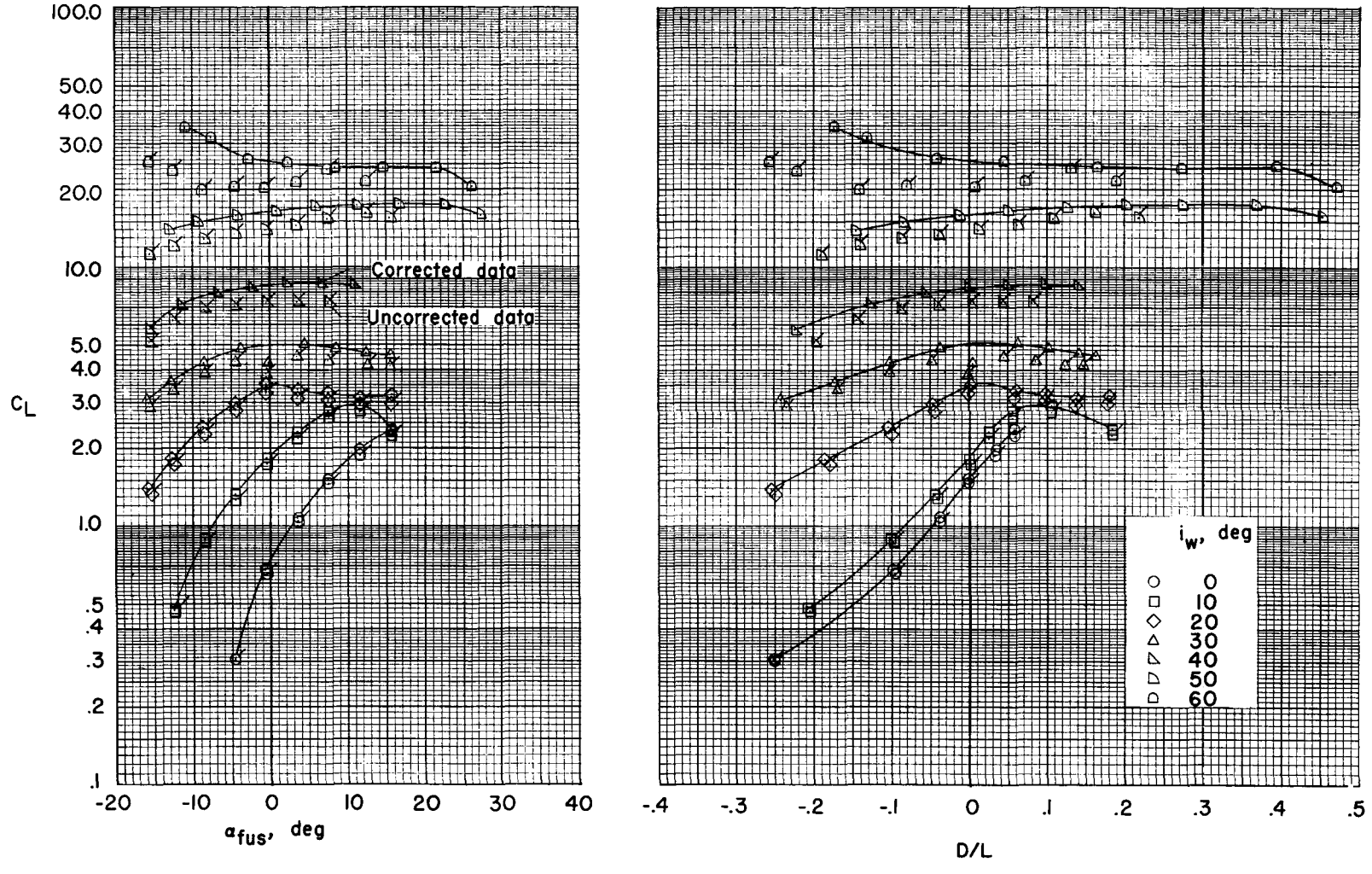

(d) Aerodynamic characteristics (for reference only).

Figure 14.- Concluded.

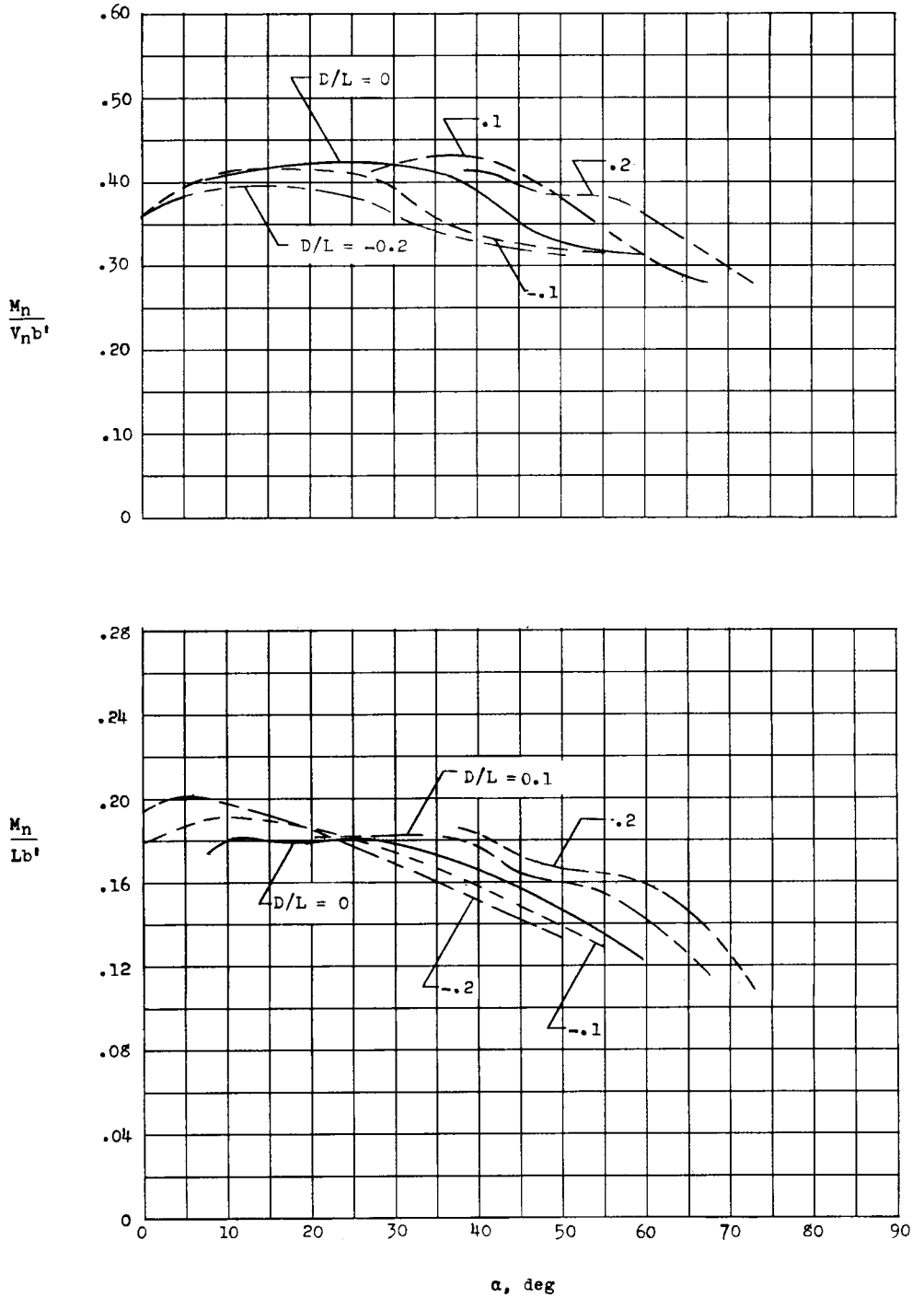

(a) Normal moments and centers of pressure.

Figure 15.- Variation of bending moments, spanwise centers of pressure, and wing torsion with angle of attack and D/L ratio. Tilt wing with flap; $\delta_{f,30} = 30^{\circ}$.

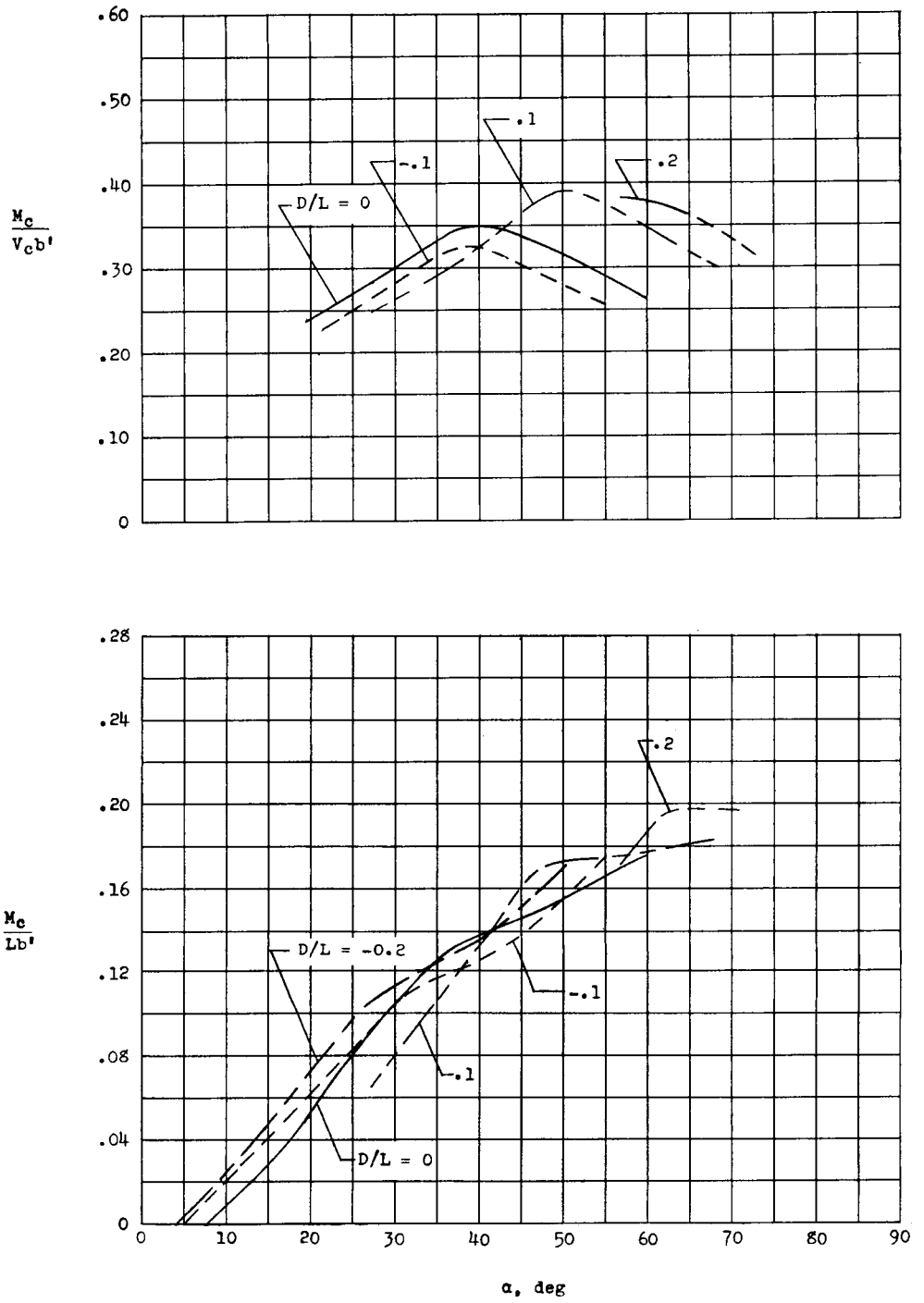

(b) Chordwise moments and centers of pressure.

Figure 15.- Continued.

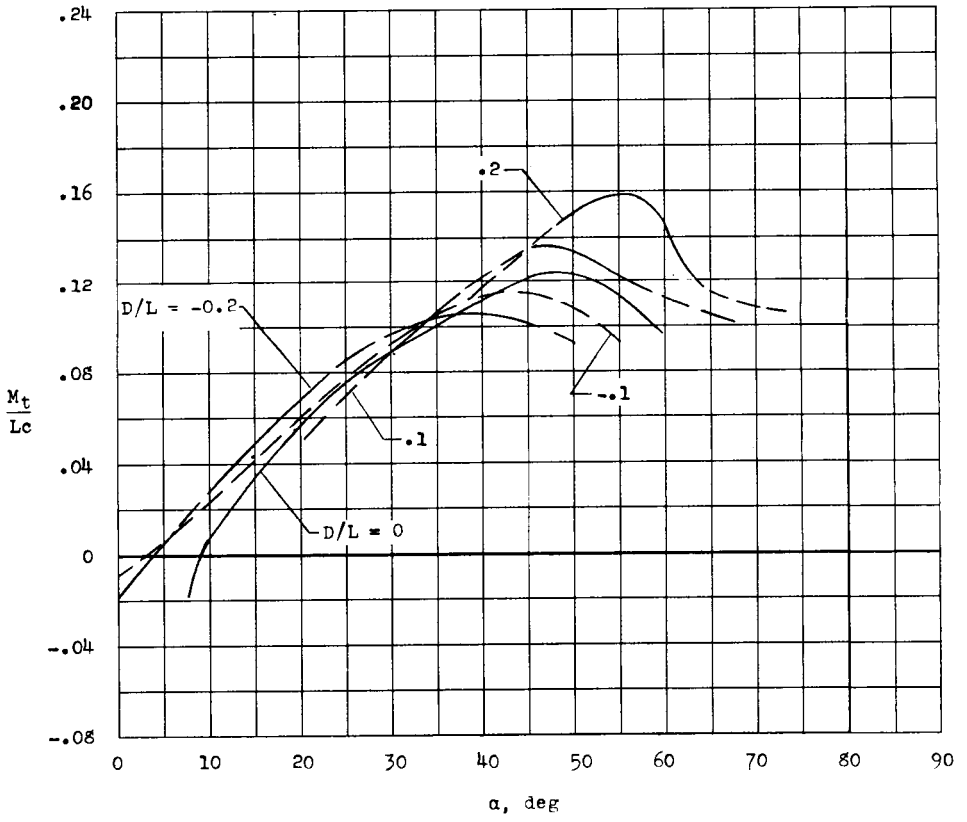

(c) Total wing torsional moment.

Figure 15.- Continued.

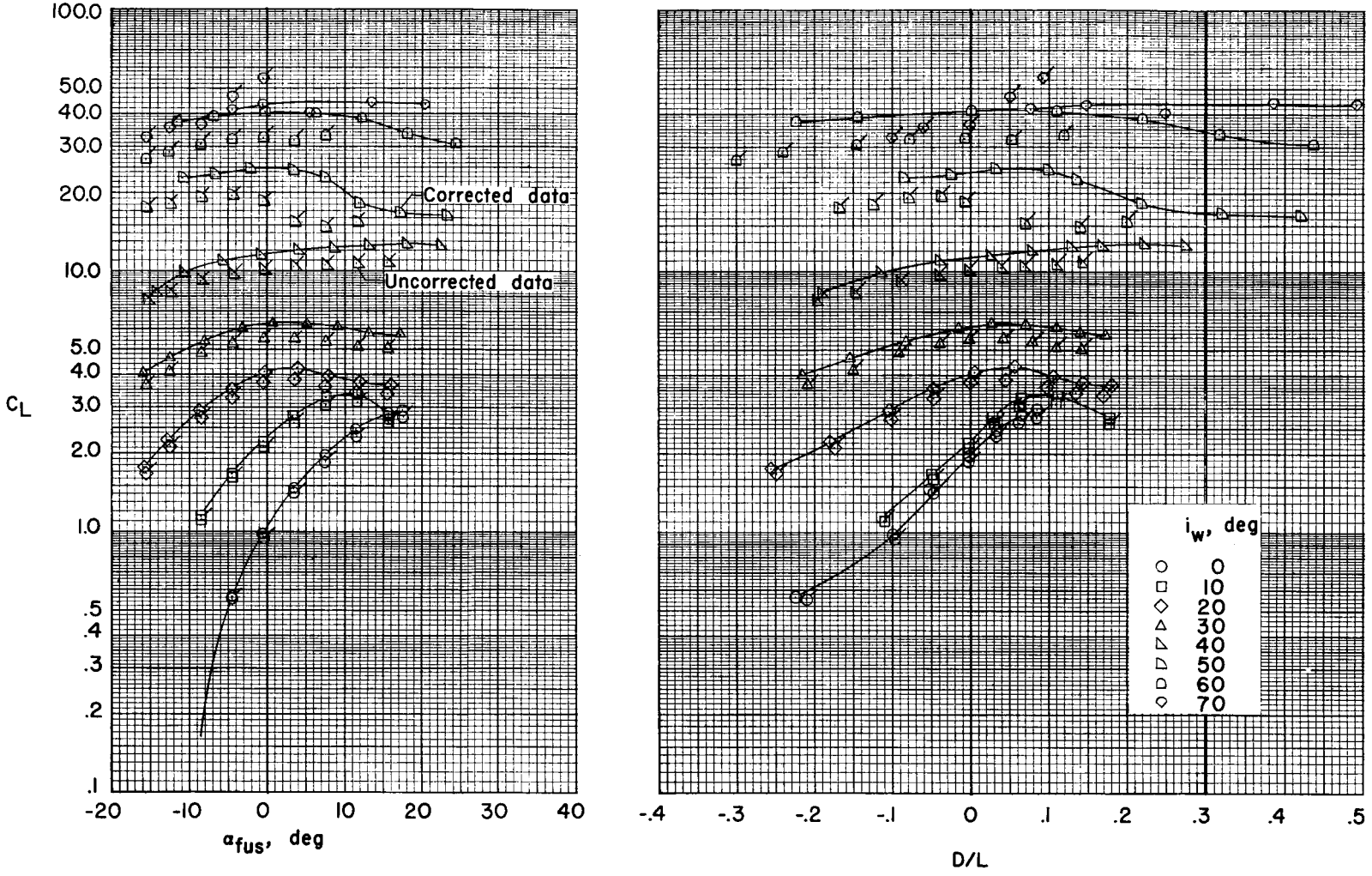

(d) Aerodynamic characteristics (for reference only).

Figure 15.- Concluded.

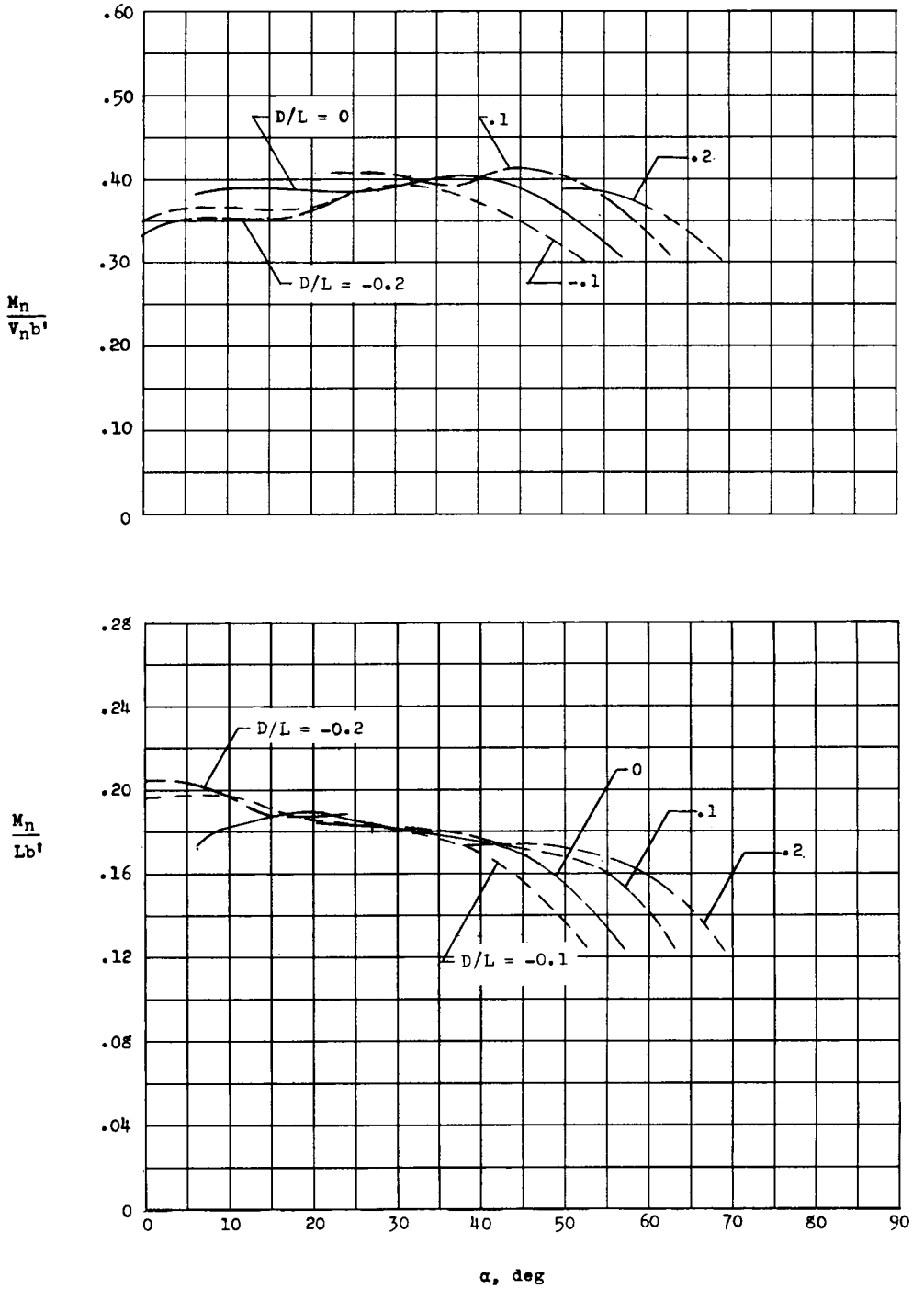

(a) Normal moments and centers of pressure.

Figure 16.- Variation of bending moments, spanwise centers of pressure, and wing torsion with angle of attack and D/L ratio. Tilt wing with flap; $\delta_{f,30} = 40^{\circ}$.

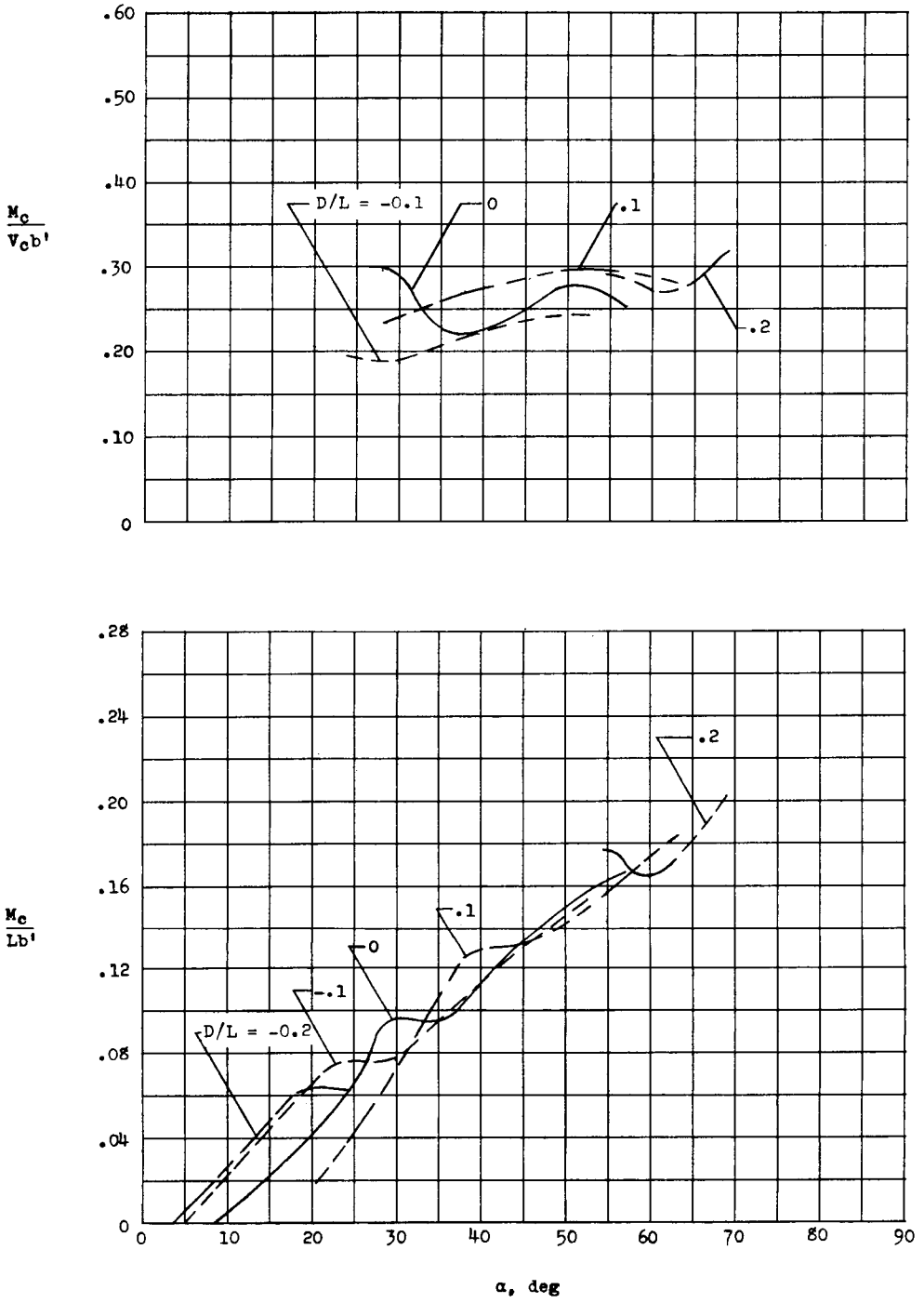

(b) Chordwise moments and centers of pressure.

Figure 16.- Continued.

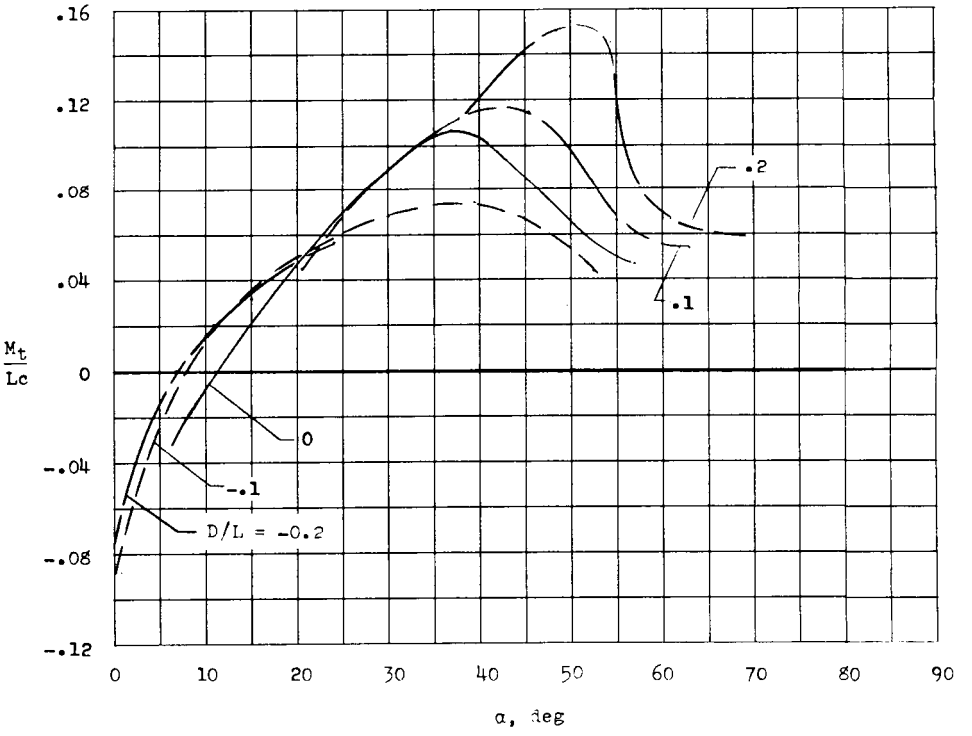

(c) Total wing torsional moment.

Figure 16.- Continued.

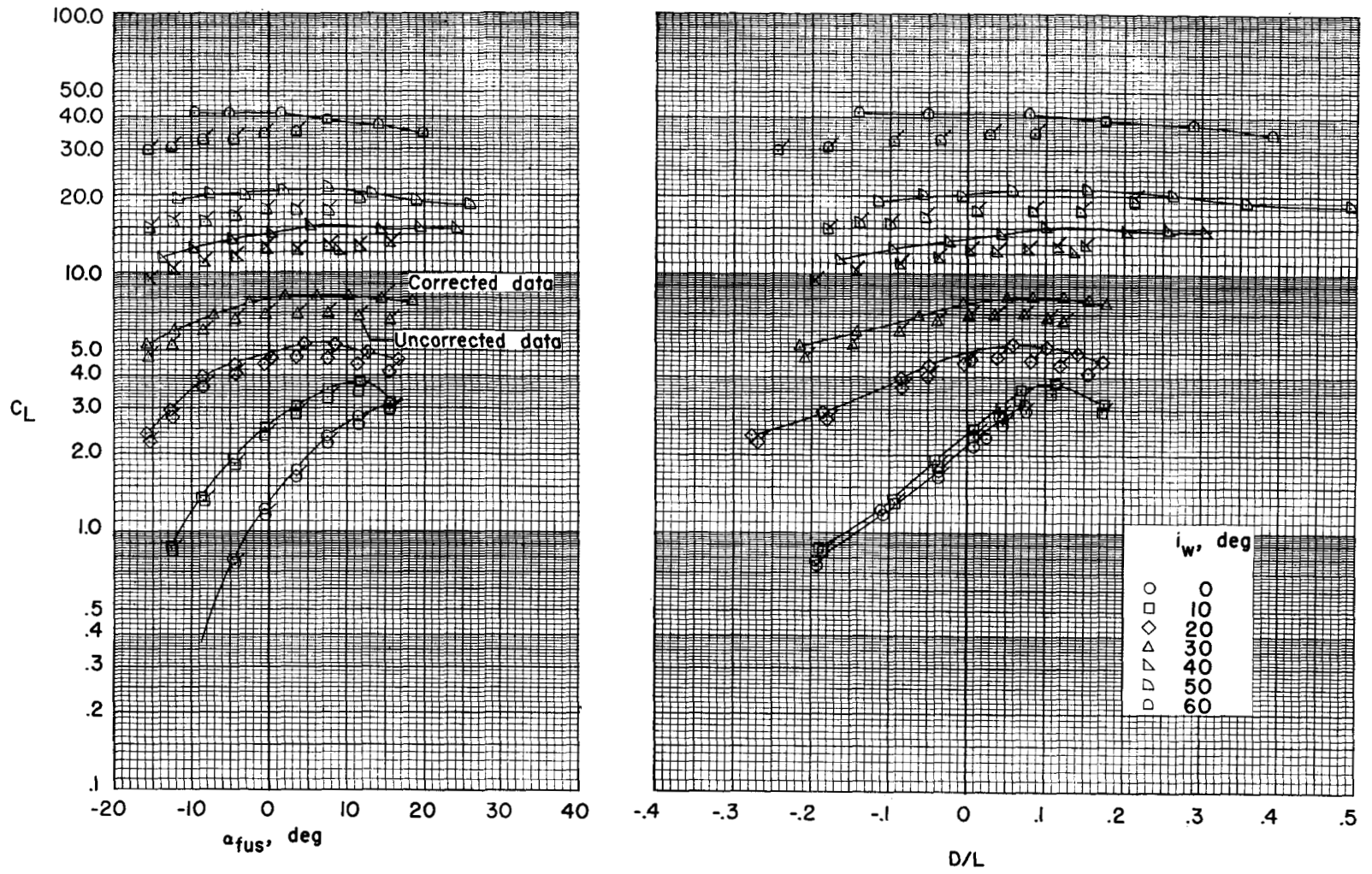

(d) Aerodynamic characteristics (for reference only).

Figure 16.- Concluded.

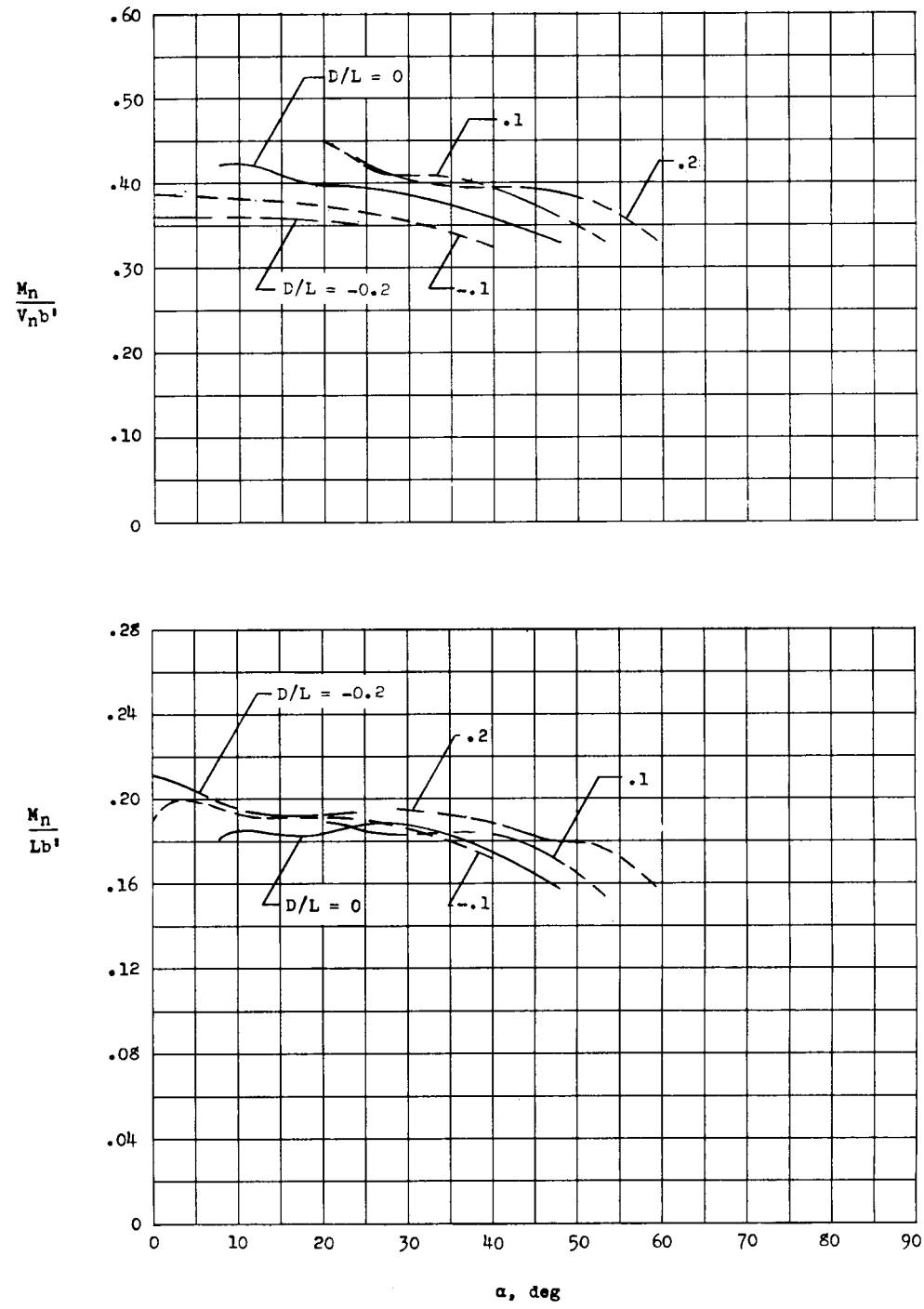

(a) Normal moments and centers of pressure.

Figure 17.- Variation of bending moments, spanwise centers of pressure, and wing torsion with angle of attack and D/L ratio. Tilt wing with flap; $\delta_{f,30} = 50^{\circ}$.

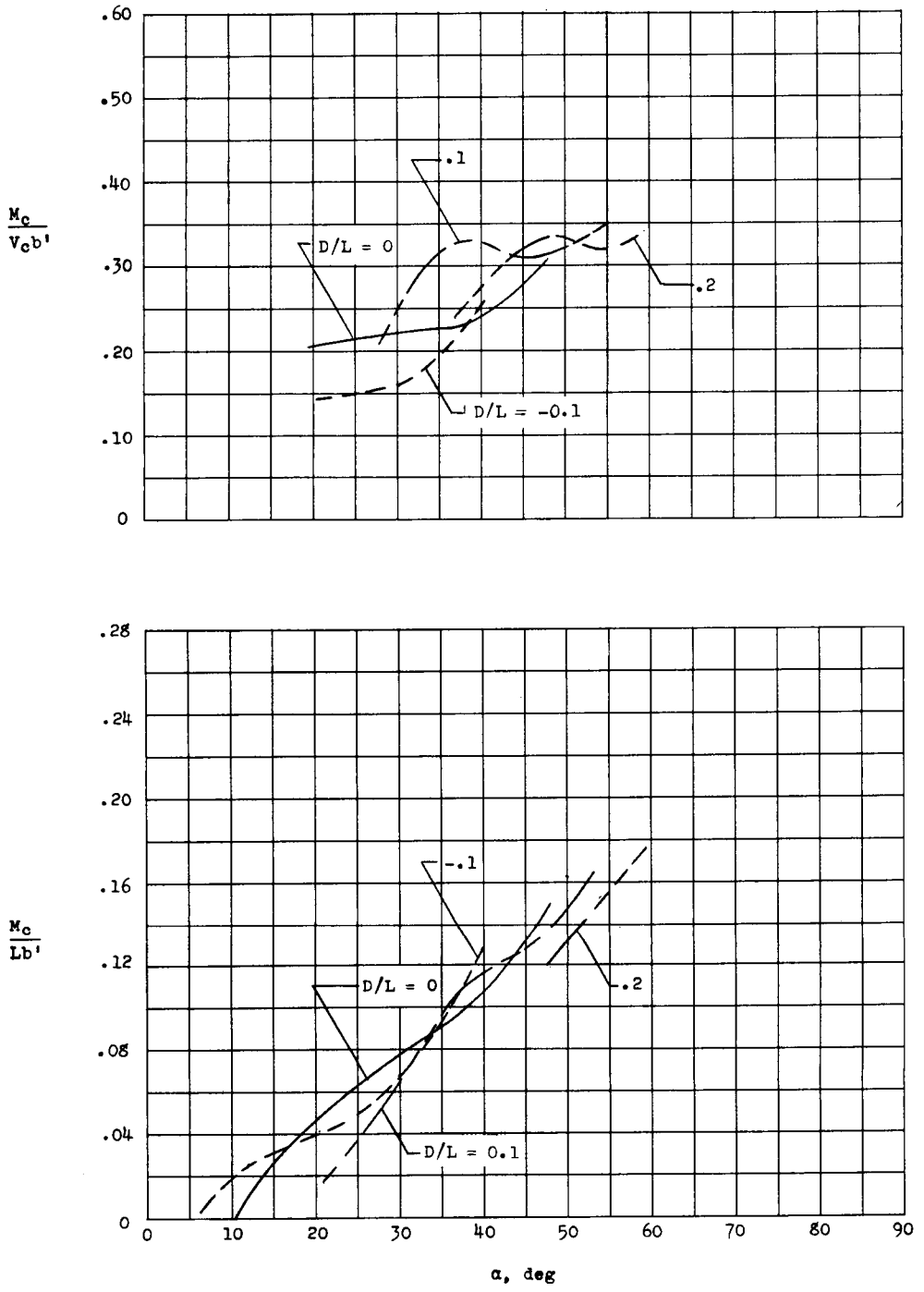

(b) Chordwise moments and centers of pressure.

Figure 17.- Continued.

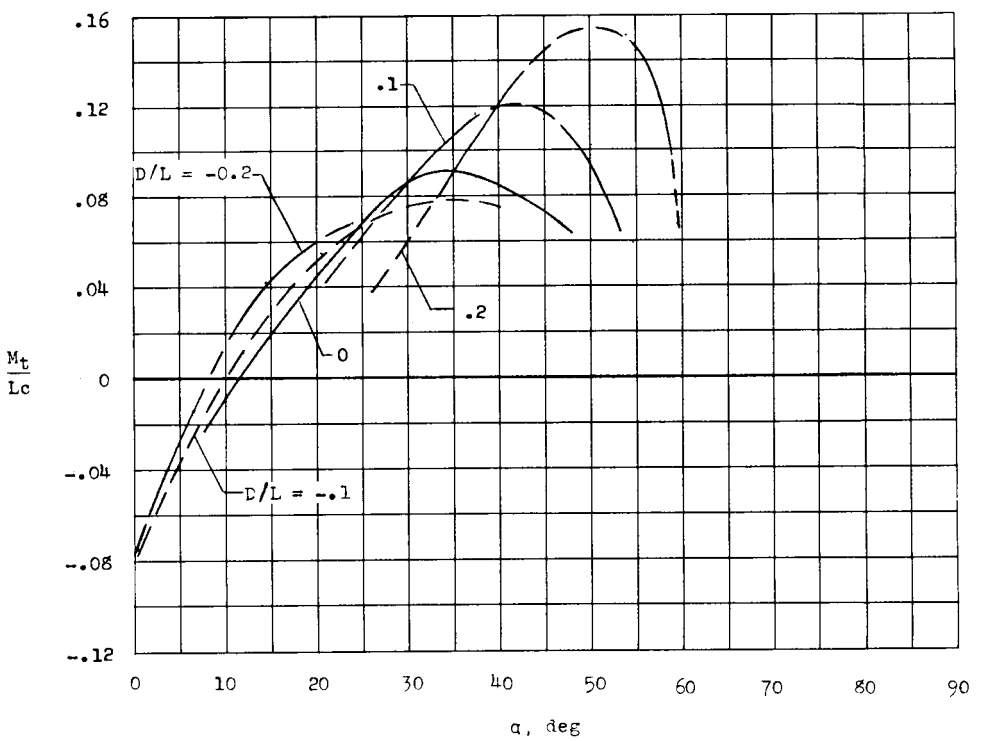

(c) Total wing torsional moment.

Figure 17.- Continued.

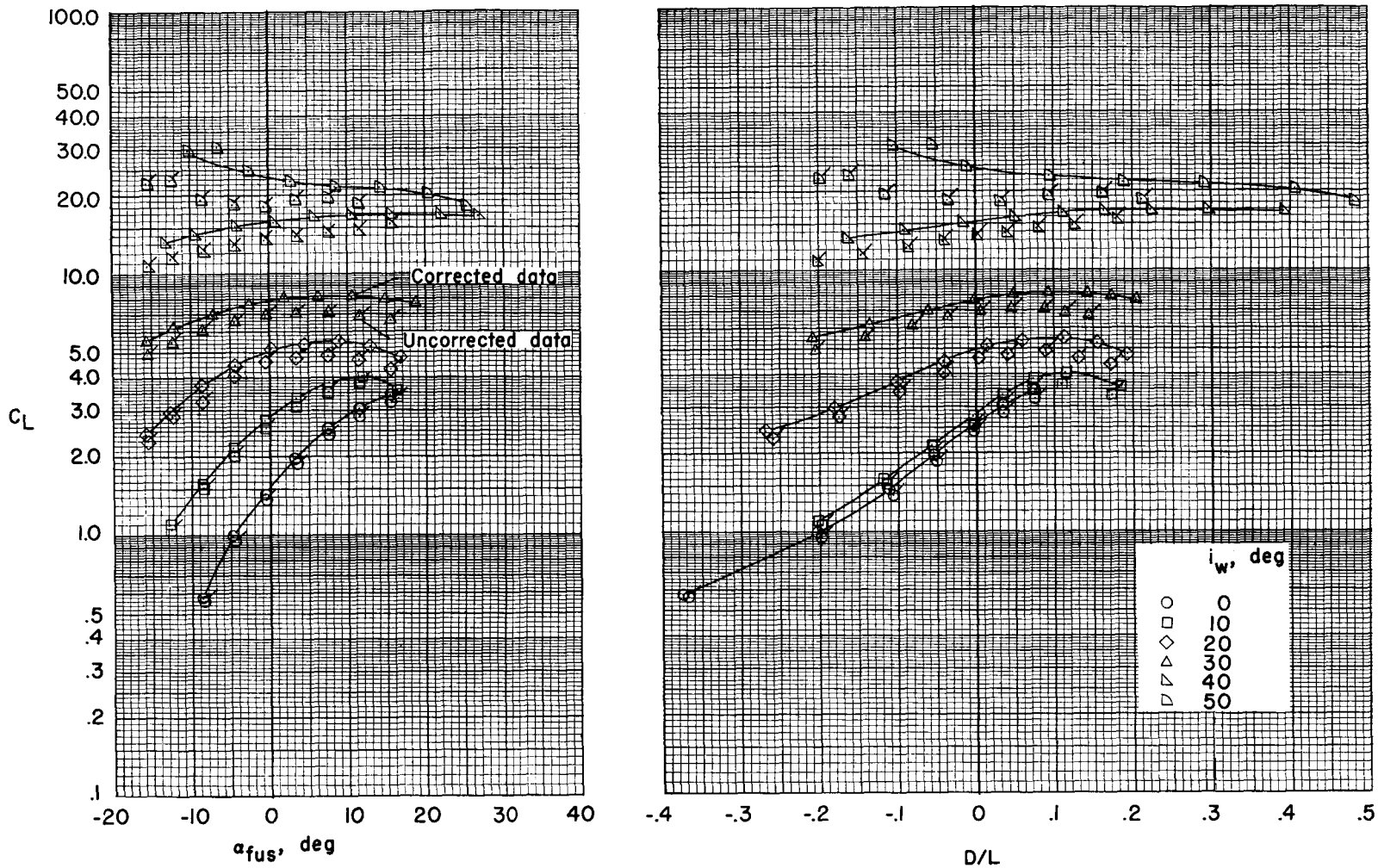

(d) Aerodynamic characteristics (for reference only).

Figure 17.- Concluded.

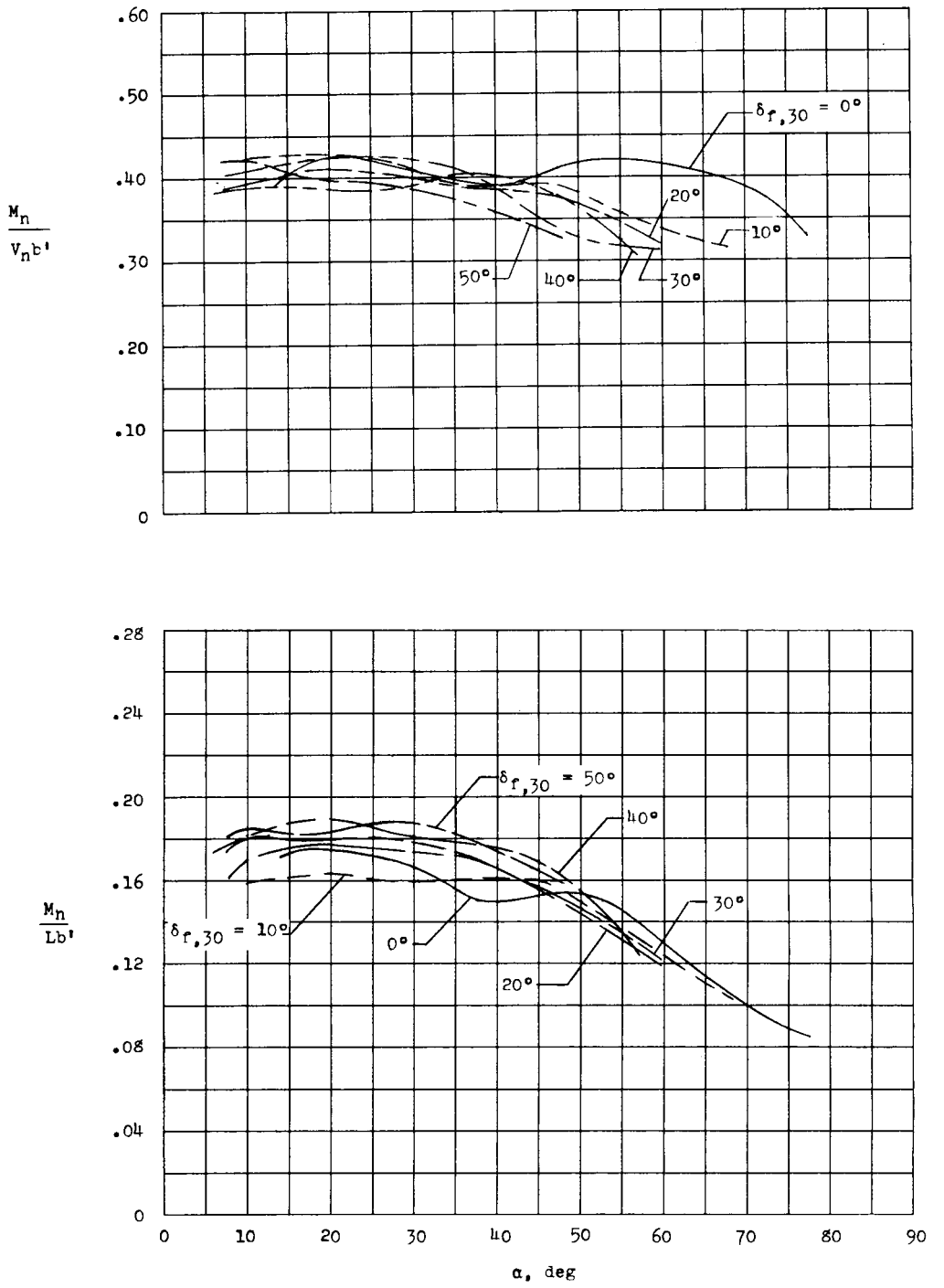

(a) Normal moments and centers of pressure.

Figure 18.- Variation of bending moments, spanwise centers of pressure, and wing torsion with angle of attack and flap deflection. Tilt-wing configuration; D/L = 0.

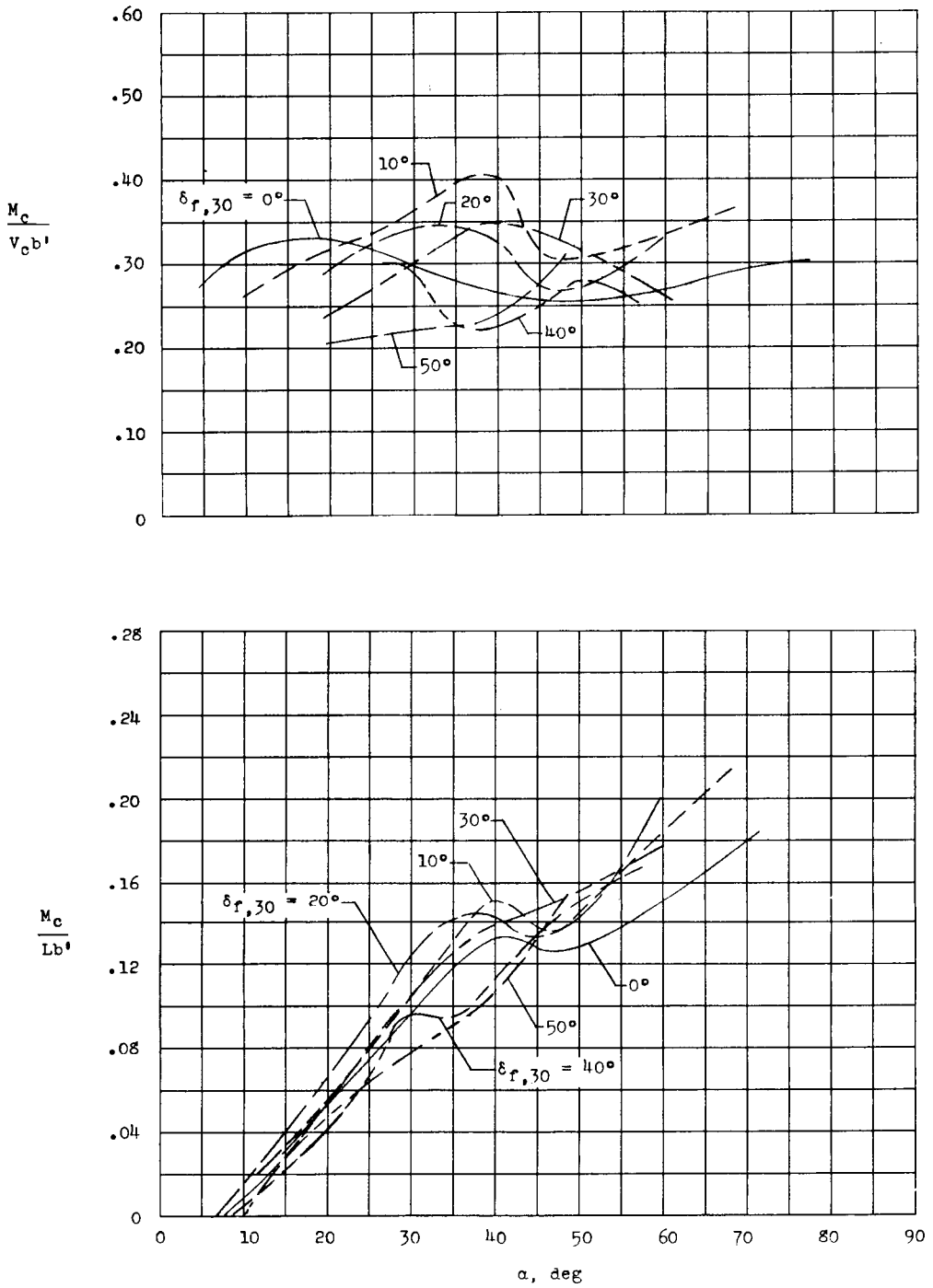

(b) Chordwise moments and centers of pressure.

Figure 18.- Continued.

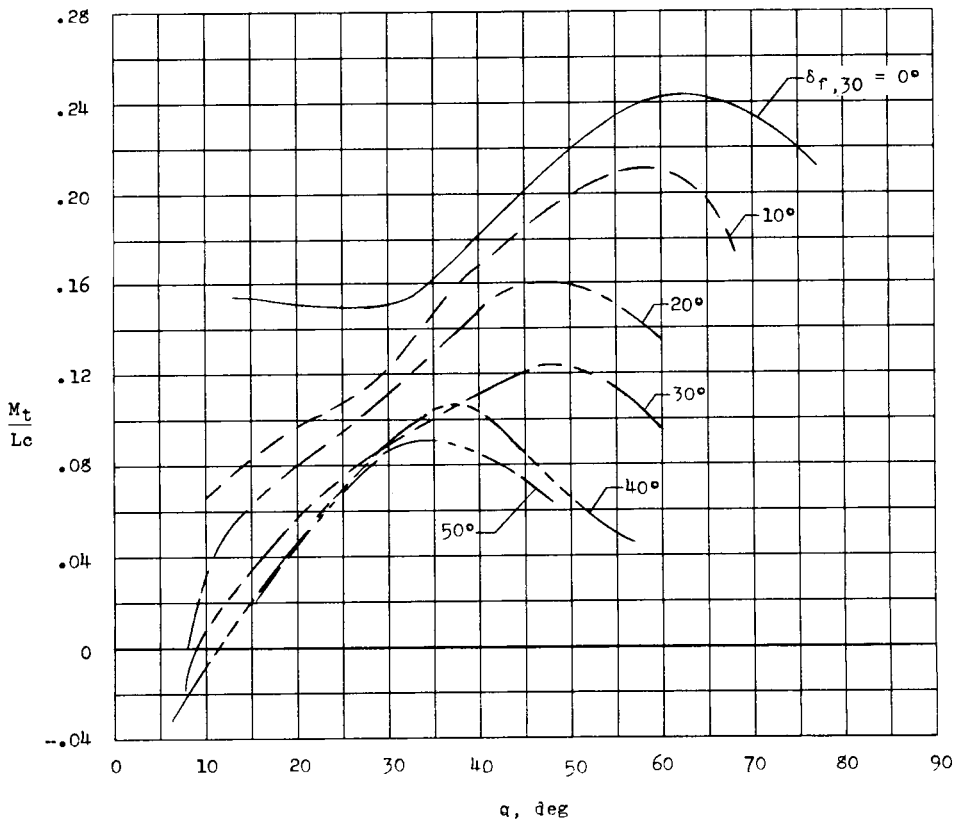

(c) Total wing torsional moment.

Figure 18.- Concluded.

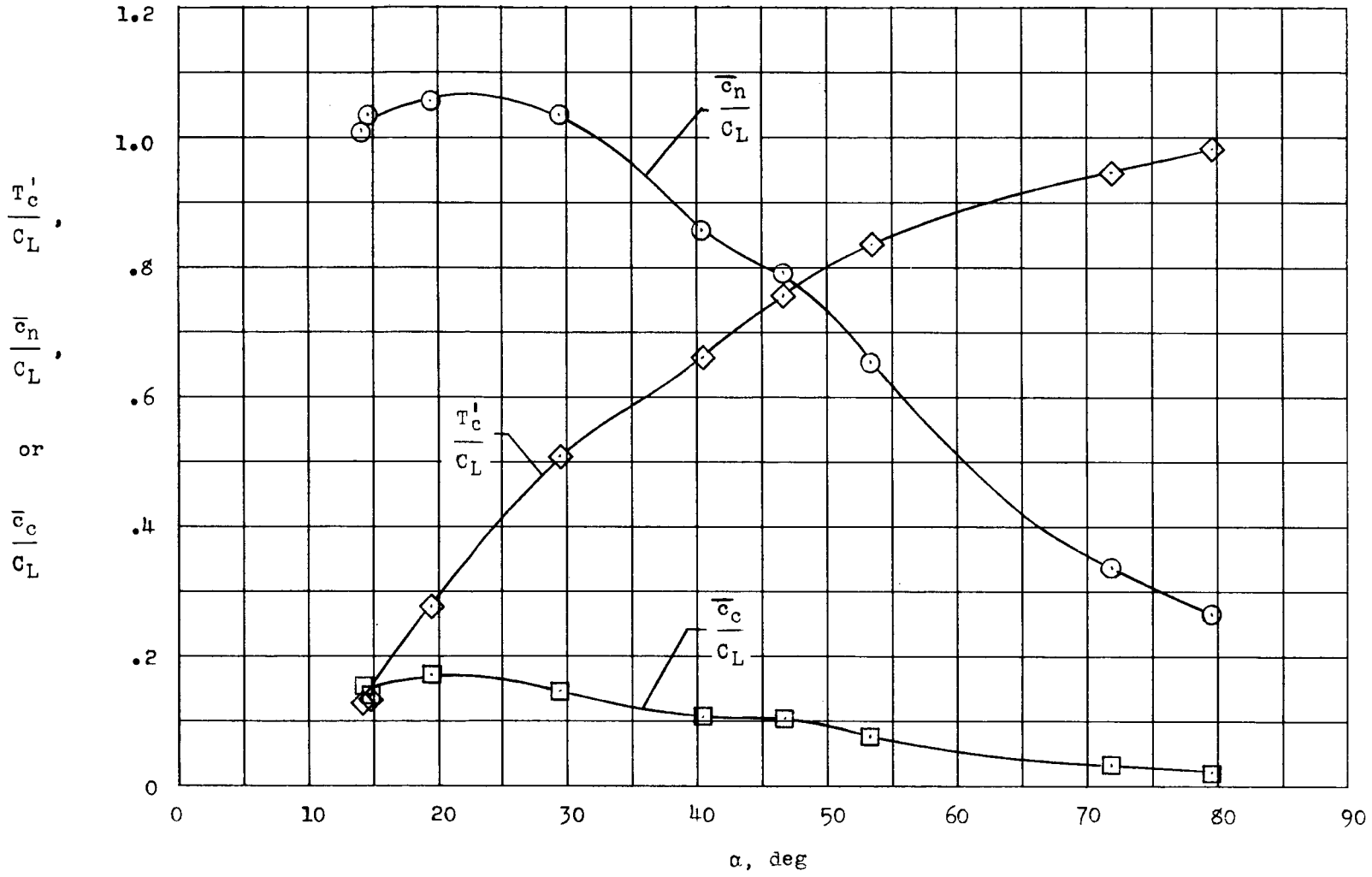

Figure 19.- Typical variation of thrust and wing-segment mean pressure forces with angle of attack. Tilt-wing configuration; $D/L \approx 0$; $\delta_{f,30} = 0$.

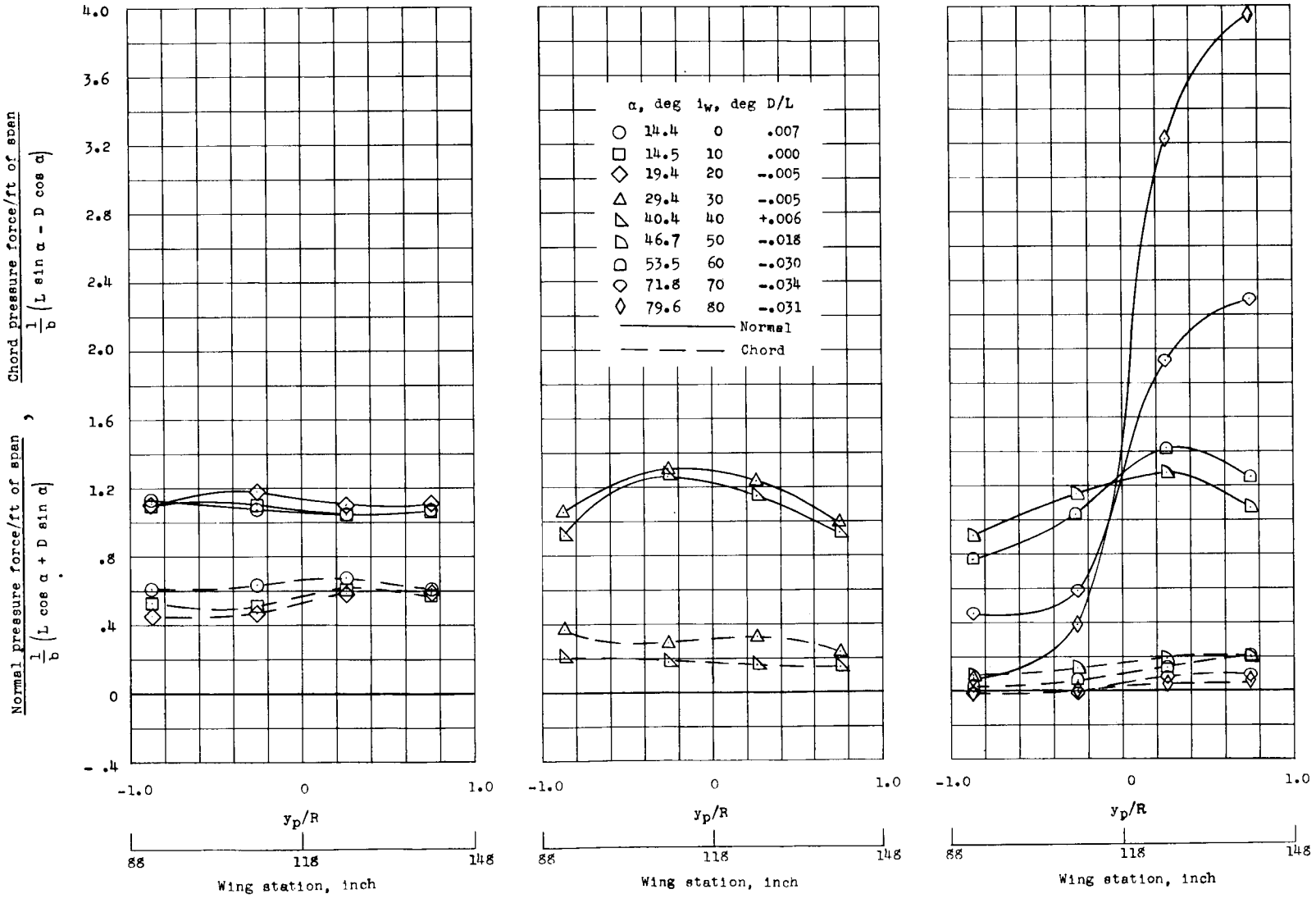

Figure 20.- Variation of normalized loading with angle of attack for tilt-wing configuration. $\delta_{f,30} = 0^{o}$; $D/L \approx 0$.

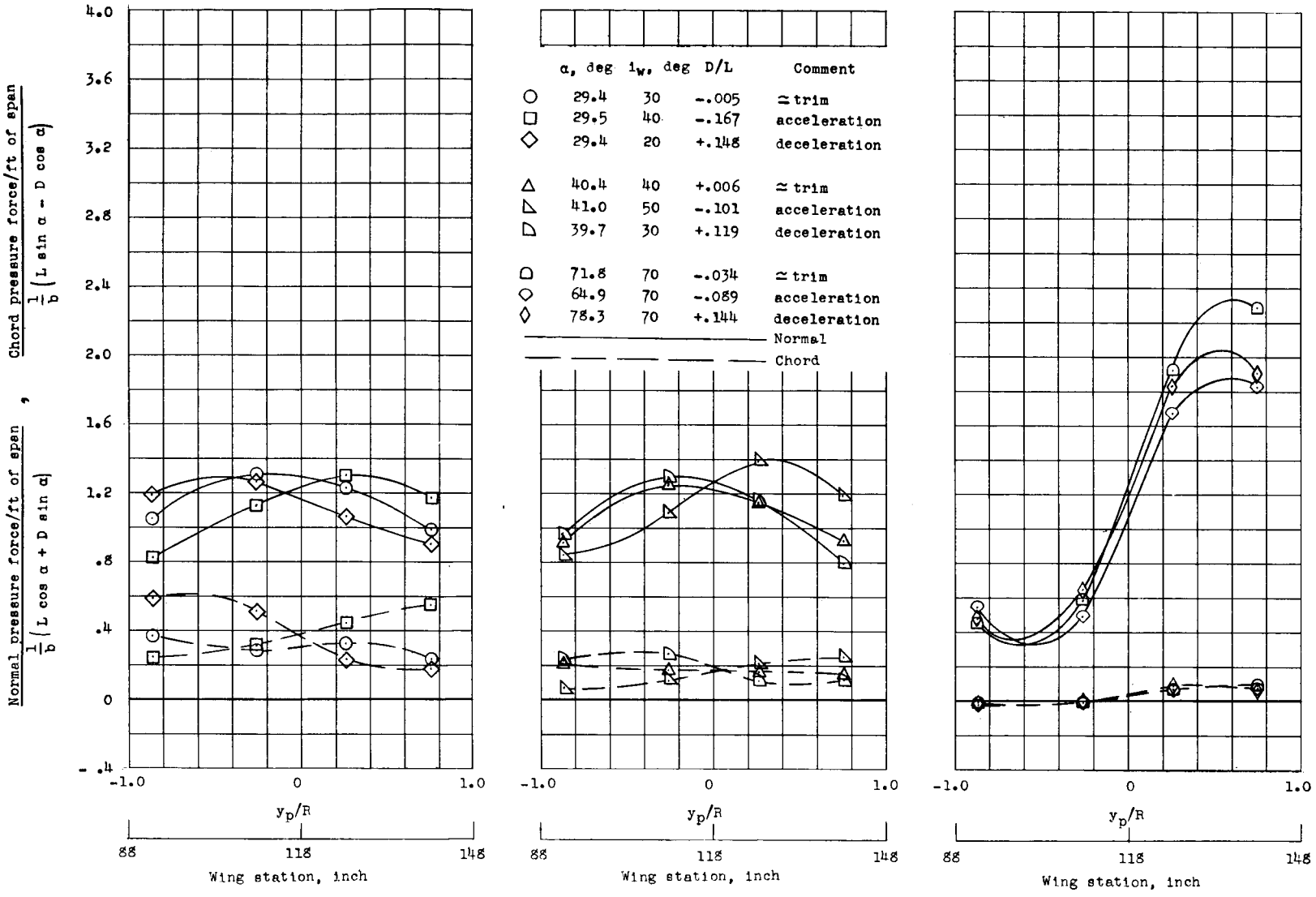

Figure 21.- Variation of normalized loading with D/L for several angles of attack. Tilt-wing configuration; $\delta_{f,30} = 0°$.

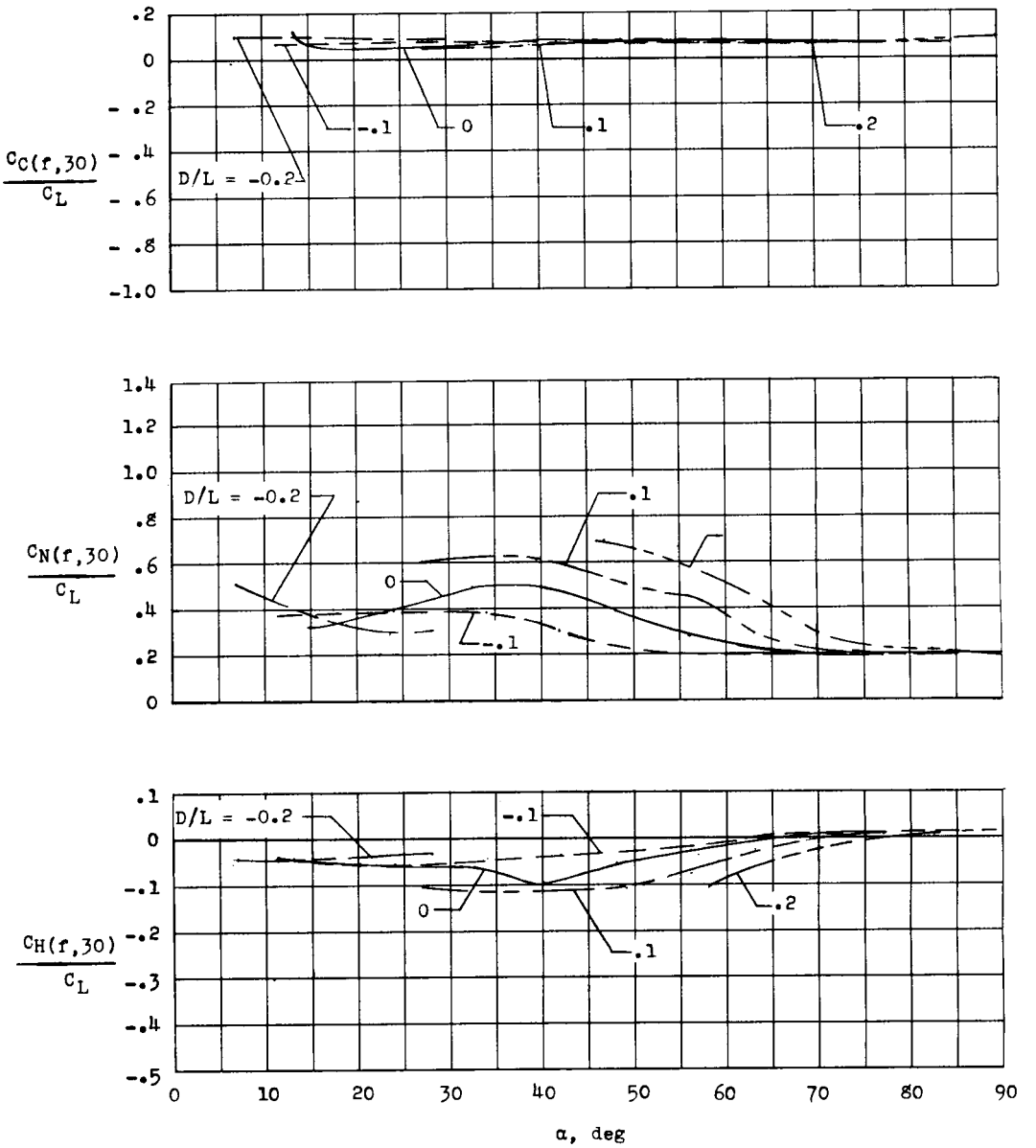

Figure 22.- Variation of flap loads with angle of attack and D/L.
Tilt-wing configuration; $\delta_{f,30} = 0^{o}$.

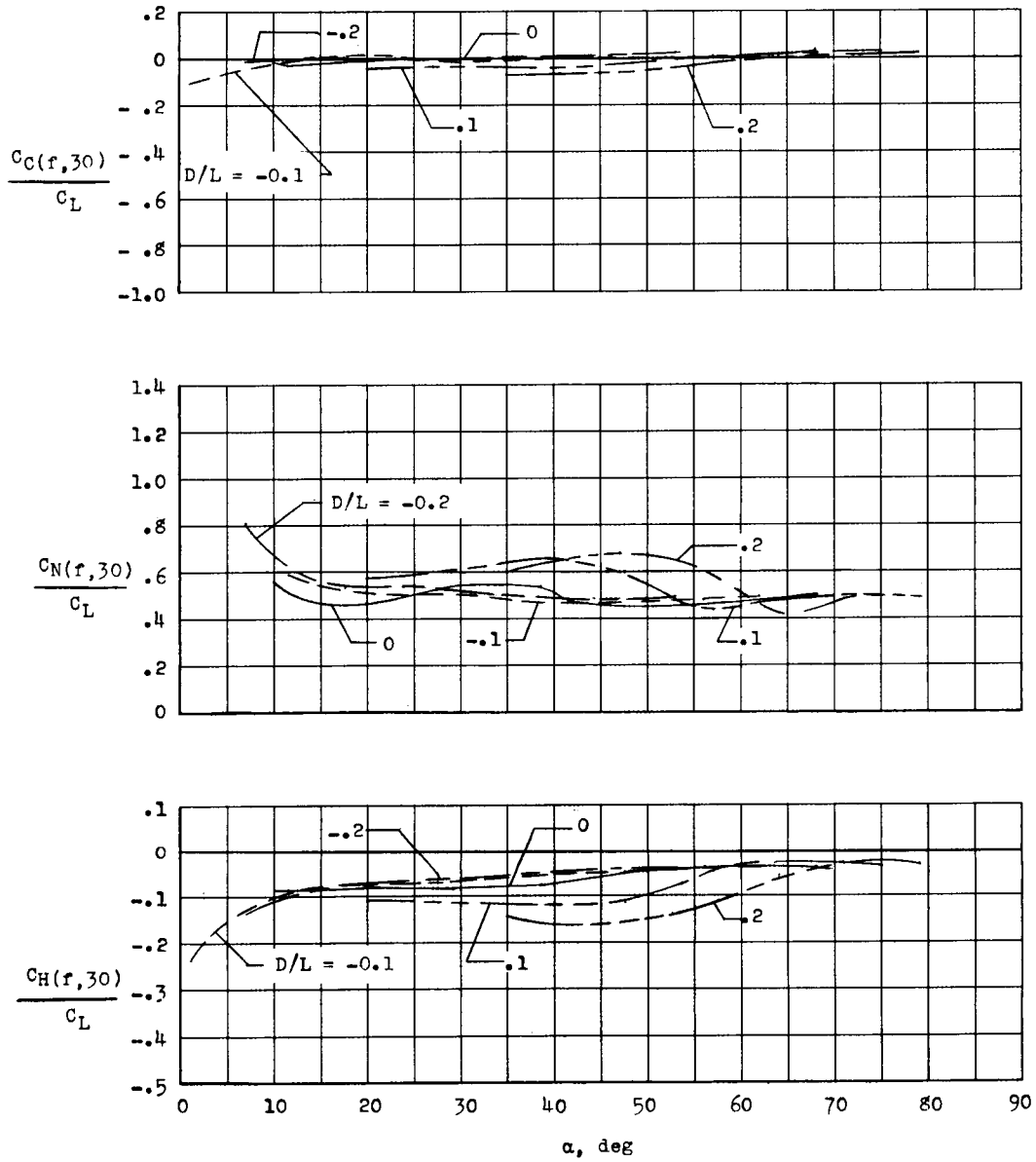

Figure 23.- Variation of flap loads with angle of attack and D/L.
Tilt-wing configuration; $\delta_{f,30} = 10^{o}$.

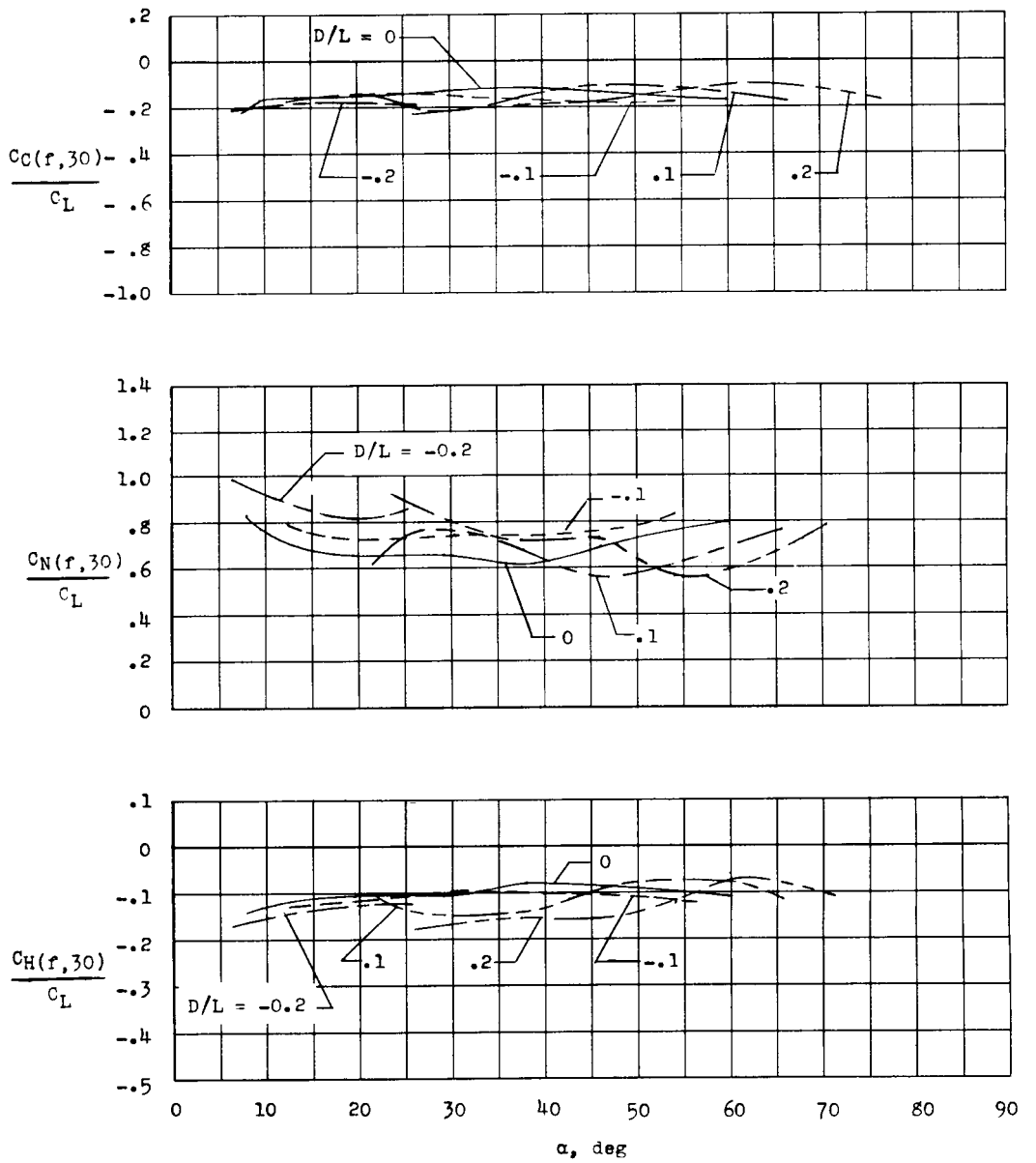

Figure 24.- Variation of flap loads with angle of attack and D/L. Tilt-wing configuration; $\delta_{f,30} = 20^{\circ}$.

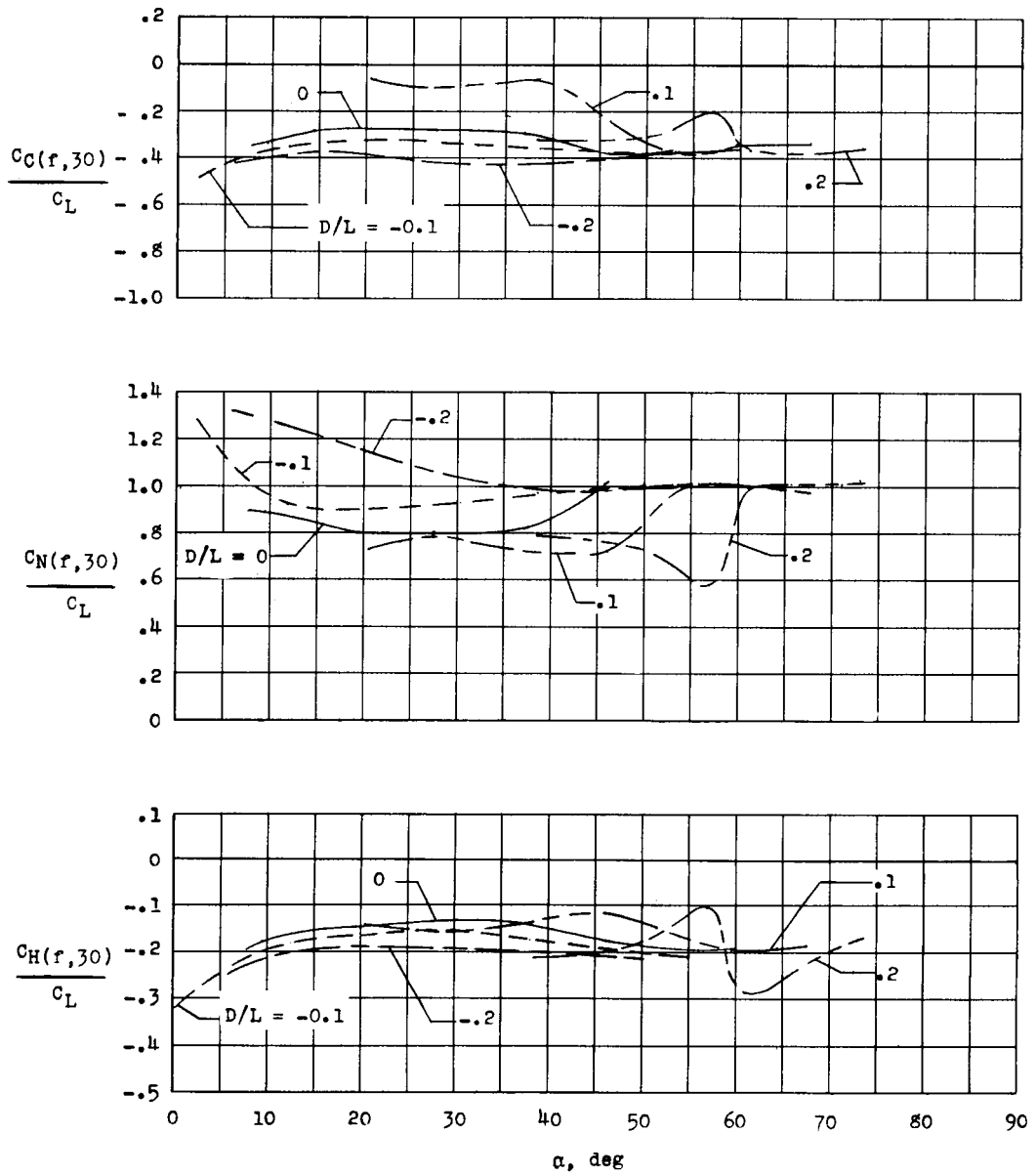

Figure 25.- Variation of flap loads with angle of attack and D/L.
Tilt-wing configuration; $\delta_{f,30} = 30^{\circ}$.

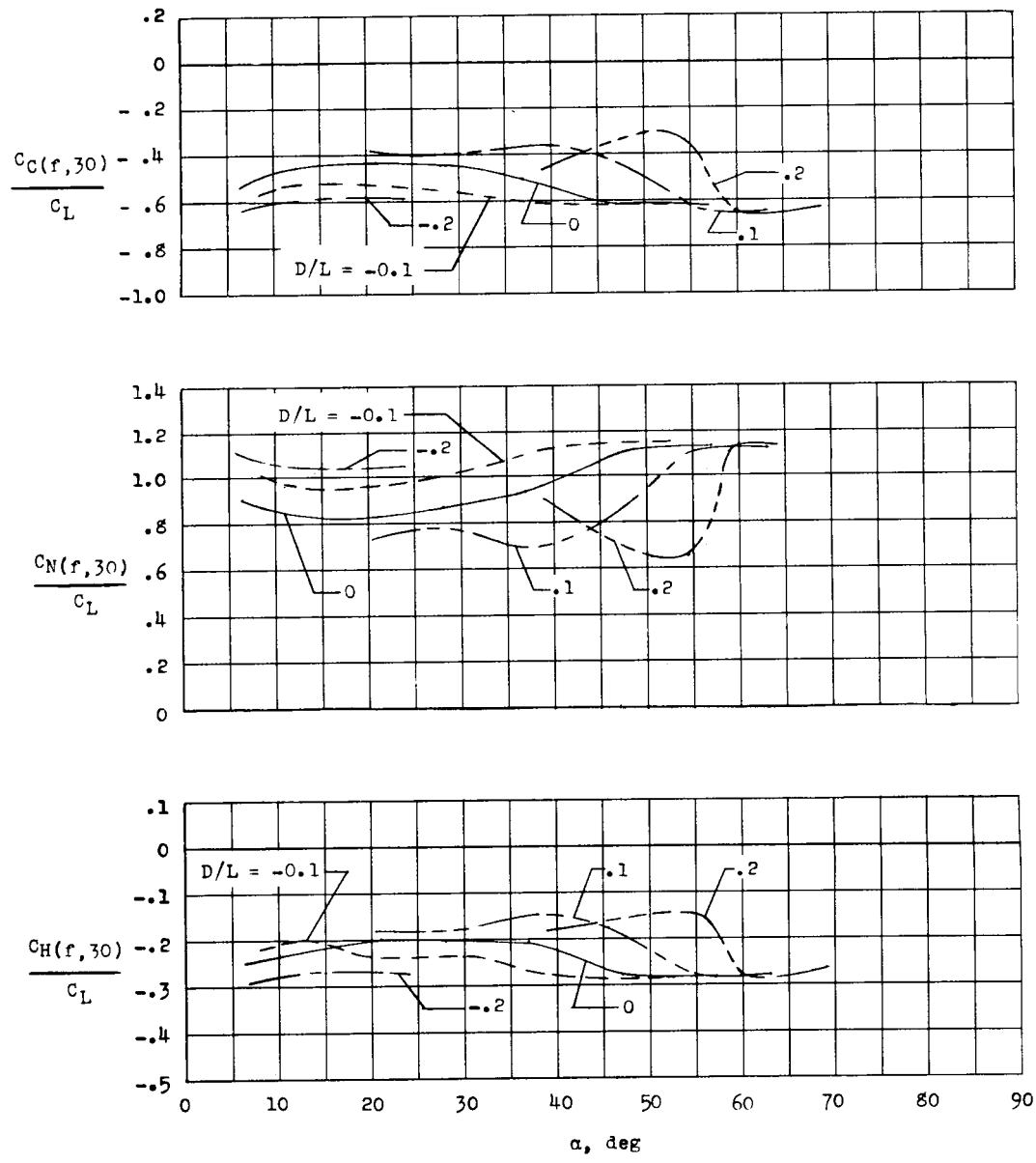

Figure 26.- Variation of flap loads with angle of attack and D/L.
Tilt-wing configuration; $\delta_{f,30} = 40^{\circ}$.

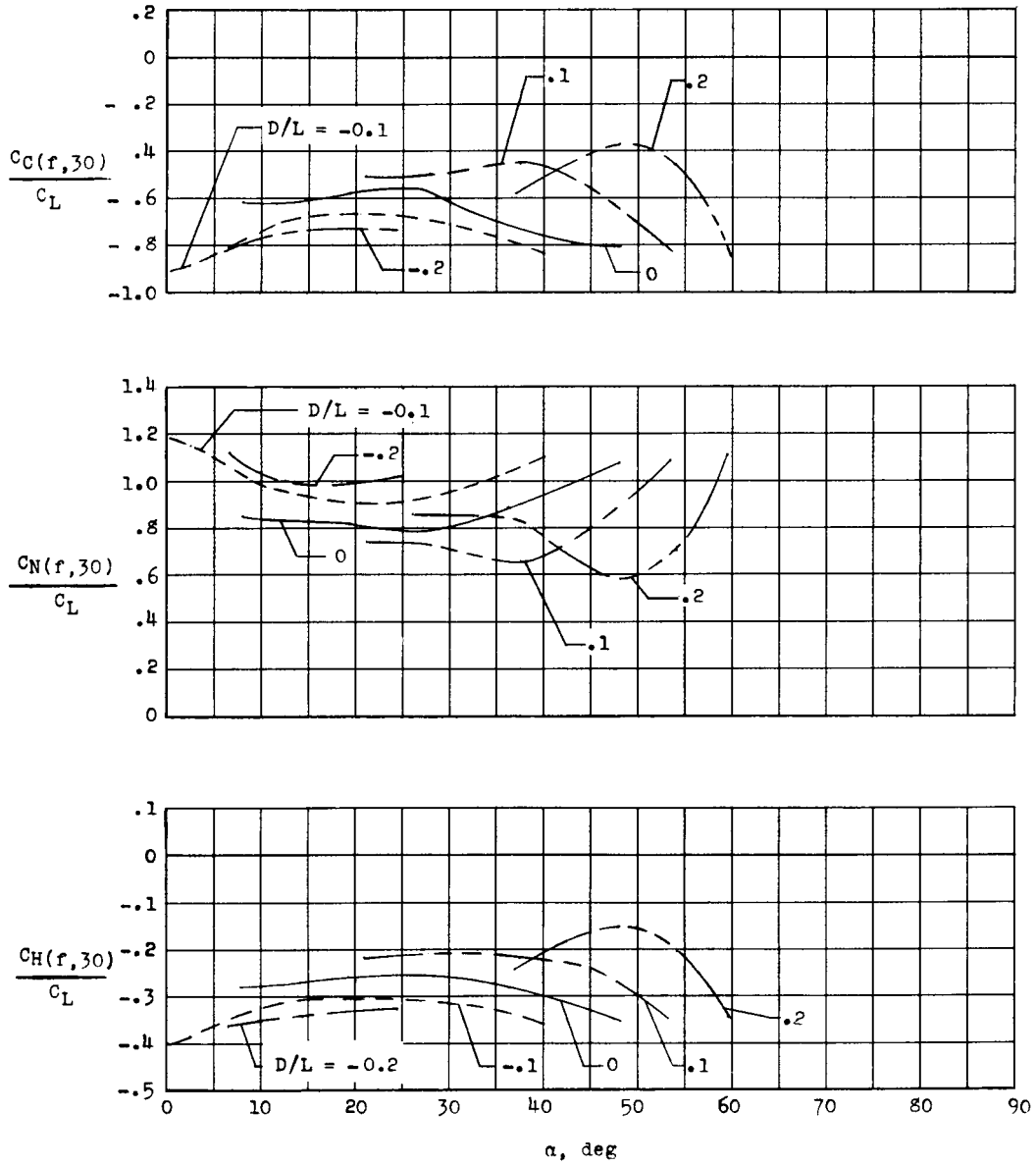

Figure 27.- Variation of flap loads with angle of attack and D/L.
Tilt-wing configuration; $\delta_{f,30} = 50^{\circ}$.

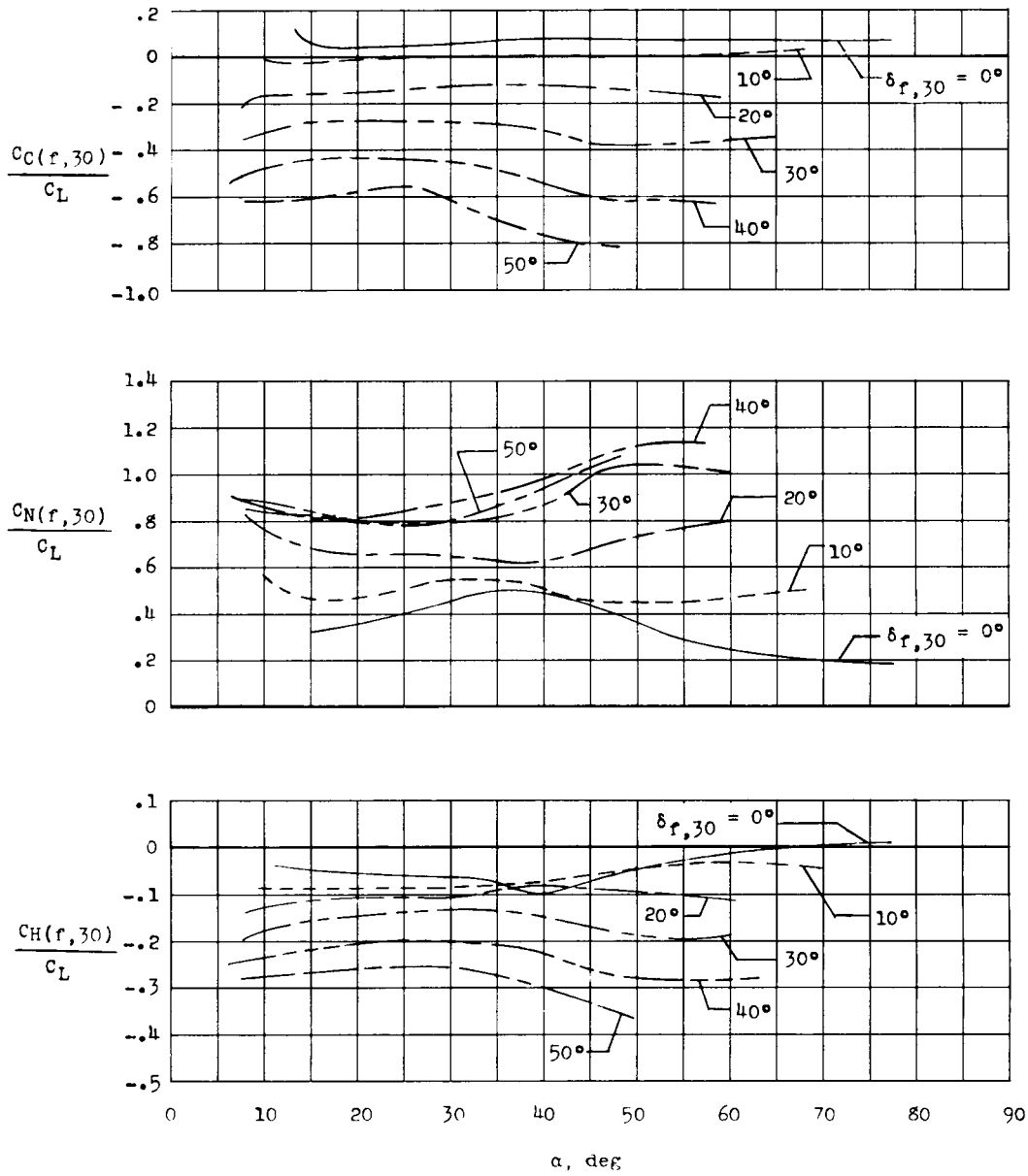

Figure 28.- Variation of flap loads with angle of attack and flap deflection. Tilt-wing configuration; D/L = 0.

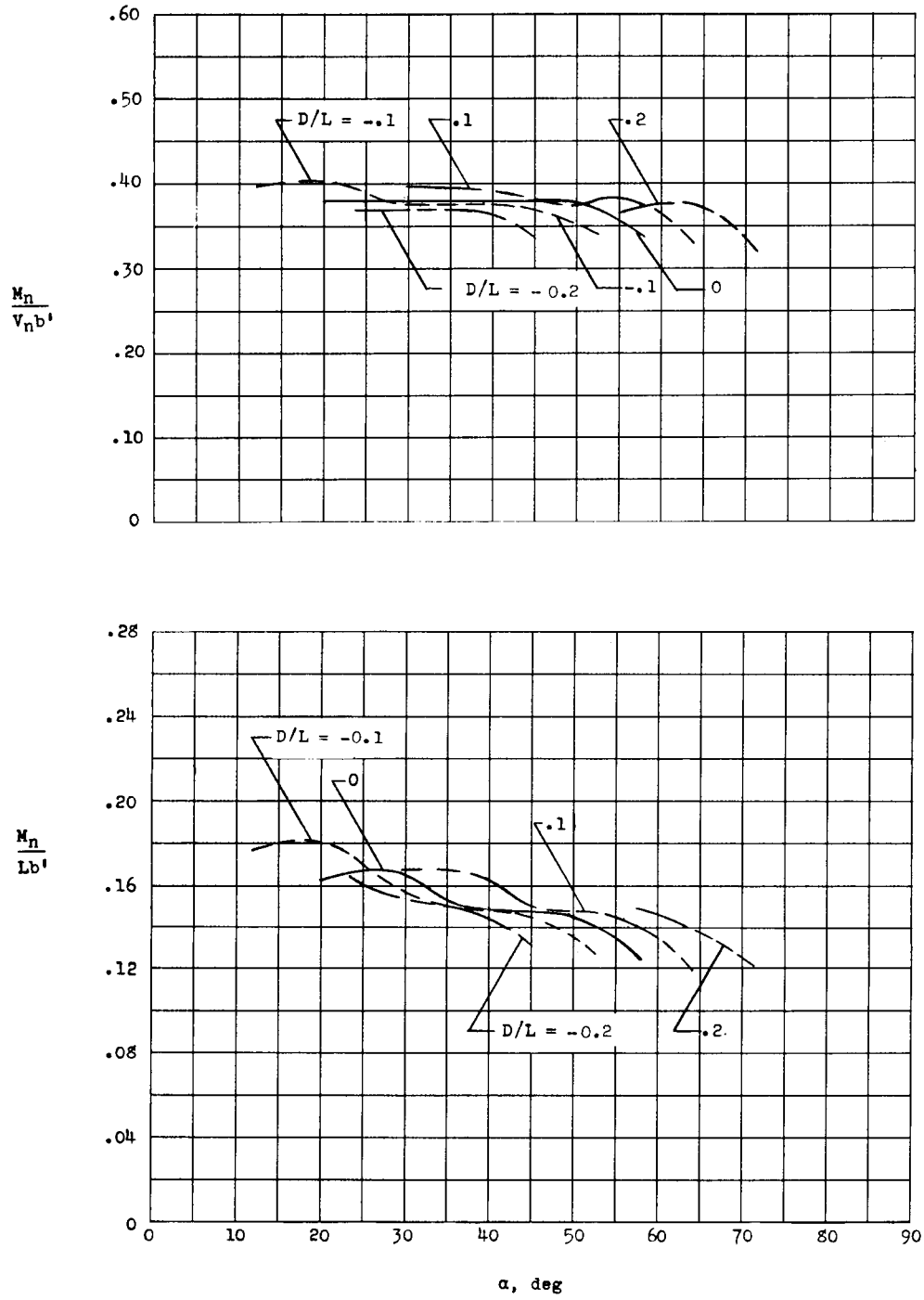

(a) Normal moments and centers of pressure.

Figure 29.- Variation of bending moments, spanwise centers of pressure, and wing torsion with angle of attack and D/L. Tilt wing with flap and slat; $\delta_{f,30} = 0^{\circ}$; $\delta_s = -30^{\circ}$.

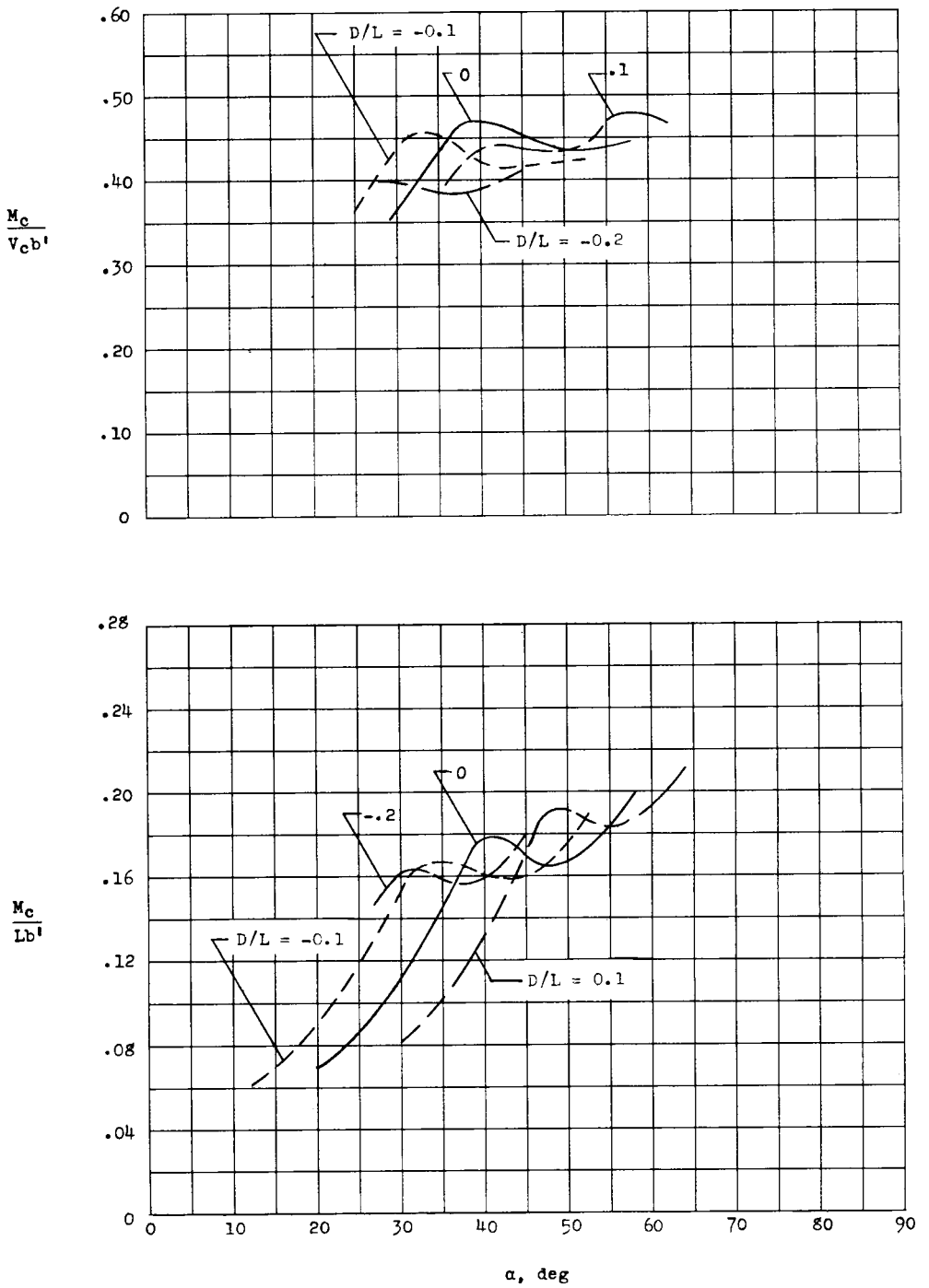

(b) Chordwise moments and centers of pressure.

Figure 29.- Continued.

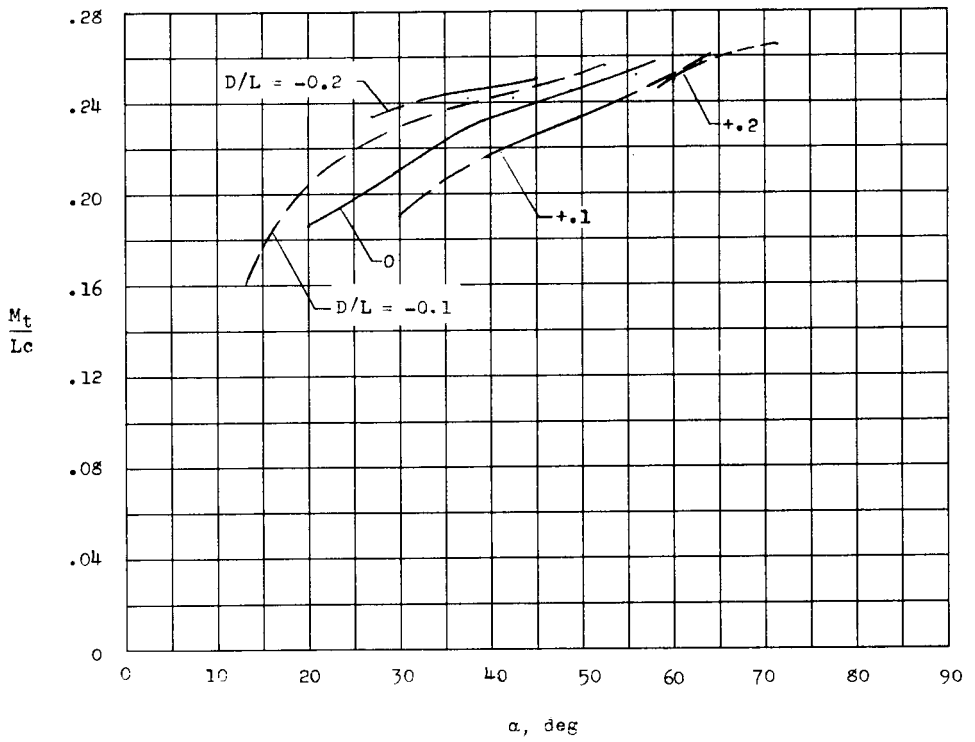

(c) Total wing torsional moment.

Figure 29.- Continued.

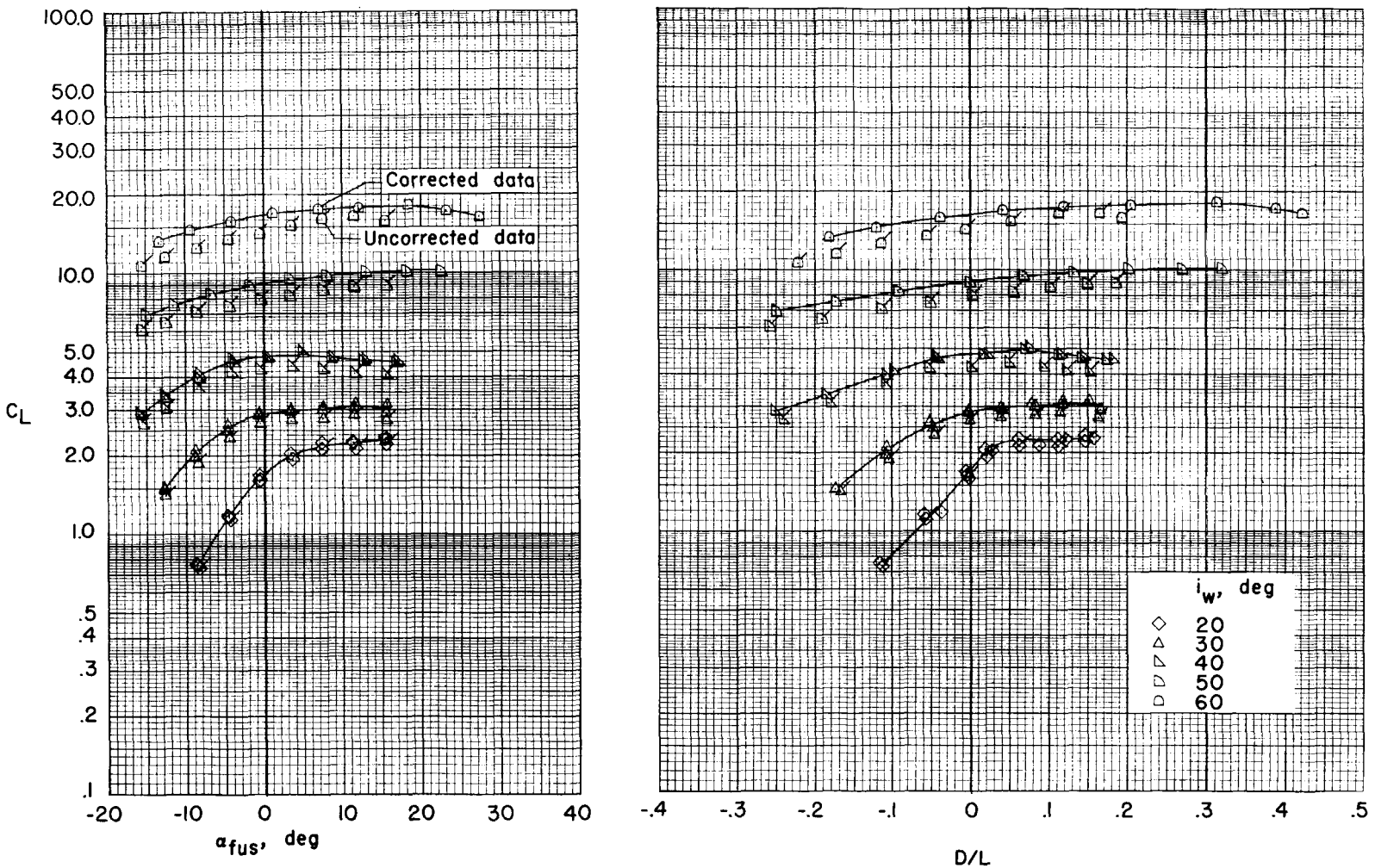

(d) Aerodynamic characteristics (for reference only).

Figure 29.- Concluded.

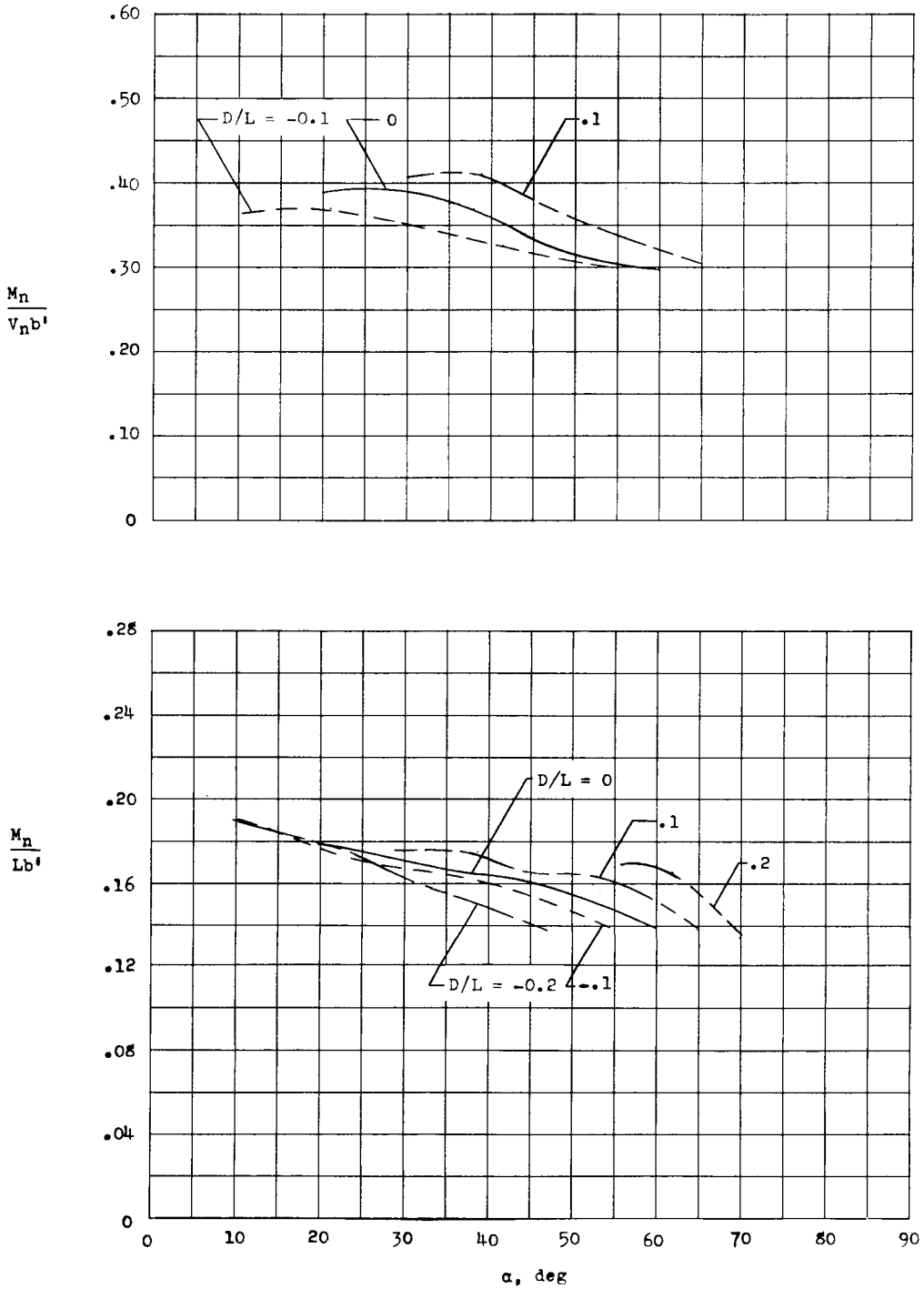

(a) Normal moments and centers of pressure.

Figure 30.- Variation of bending moments, spanwise centers of pressure, and wing torsion with angle of attack and D/L. Tilt wing with flap and slat; $\delta_{f,30} = 30^{\circ}$; $\delta_s = -30^{\circ}$.

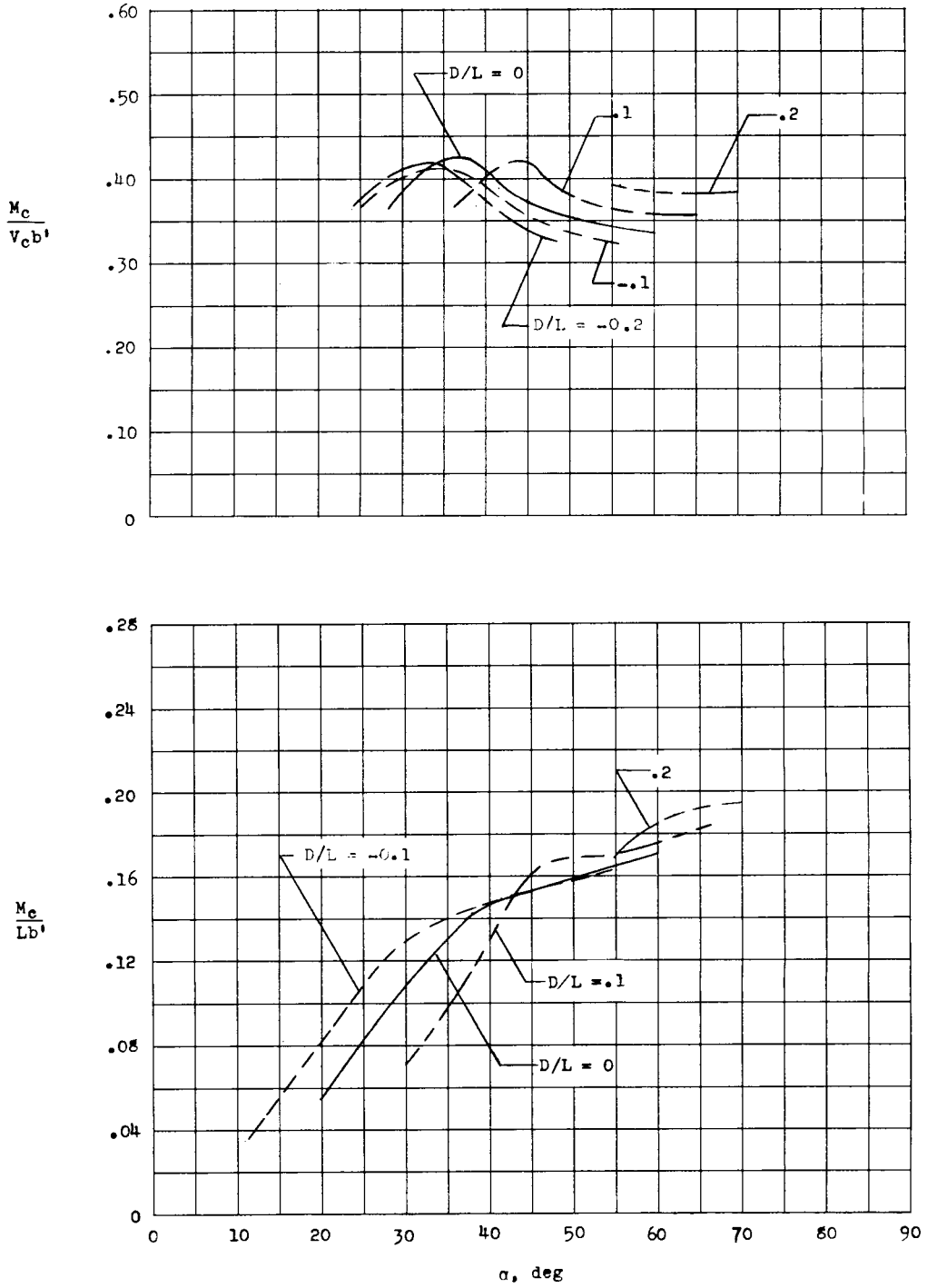

(b) Chordwise moments and centers of pressure.

Figure 30.- Continued.

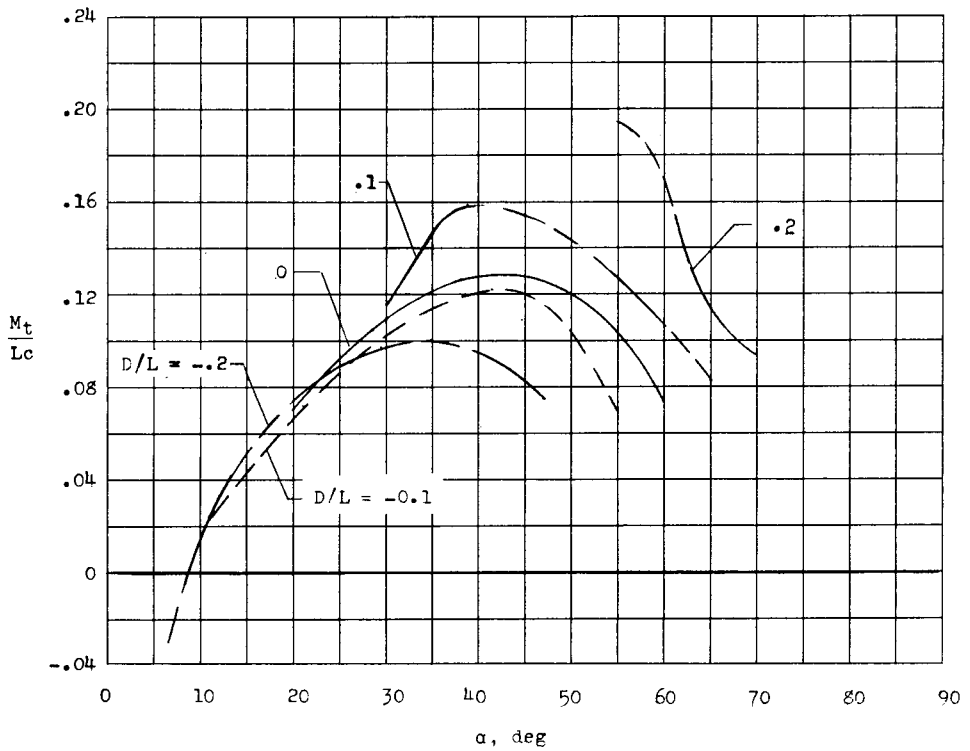

(c) Total wing torsional moment.

Figure 30.- Continued.

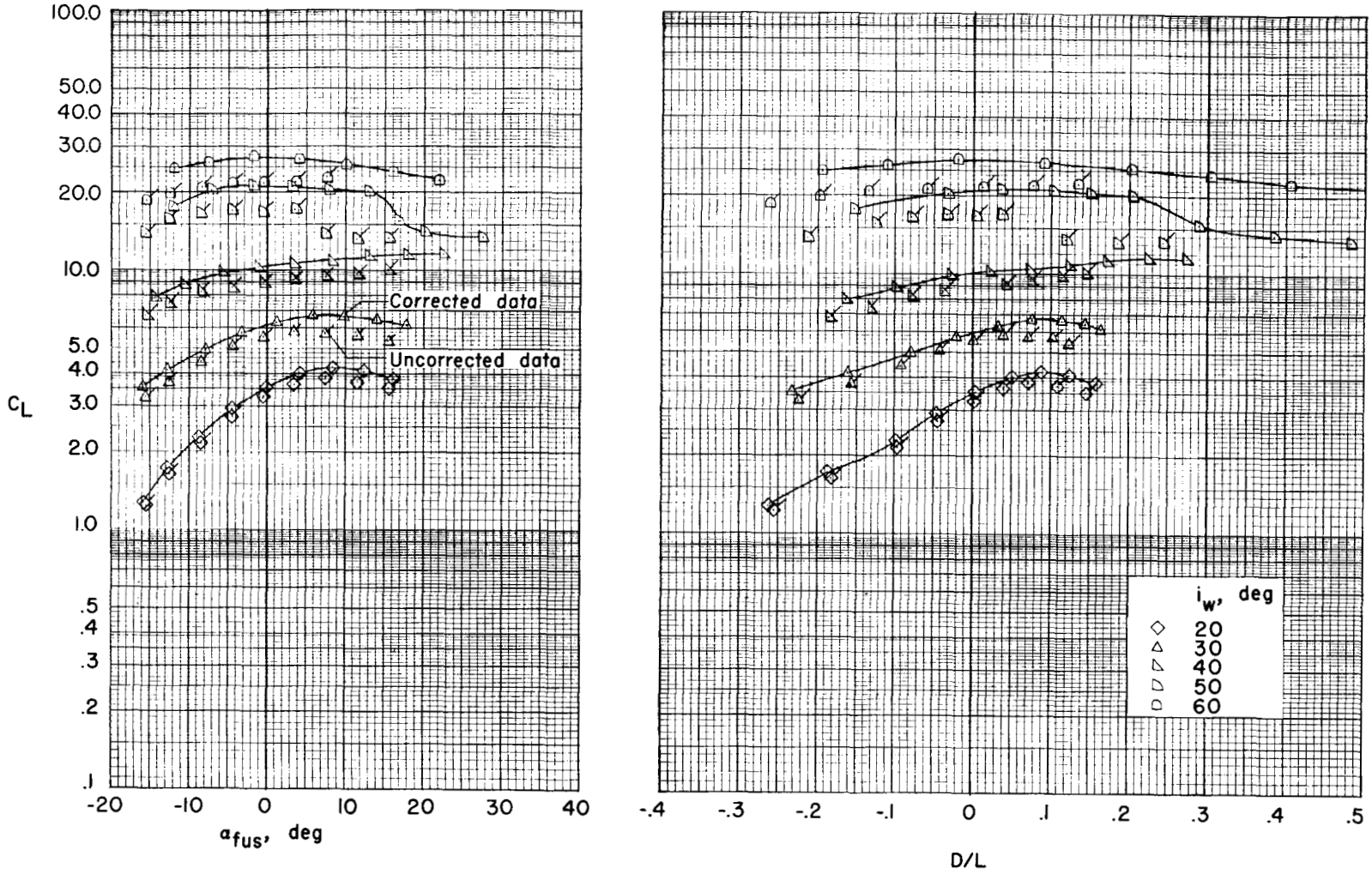

(d) Aerodynamic characteristics (for reference only).

Figure 30.- Concluded.

Component	Steady-state load		Vibratory load (double amplitude as percent of steady state)	
	Slat off	Slat on	Slat off	Slat on
Spanwise center of pressure (normal), M_n/V_nb'	0.43	0.41		
Spanwise center of pressure (chordwise), M_c/V_cb'	.31	.37		
Normal bending moment, M_n/Lb'	.178	.178	26	4
Chordwise bending moment, M_c/Lb'	.127	.125	38	14
Wing torsion, $M_t/L\bar{c}$	.120	.159	48	9

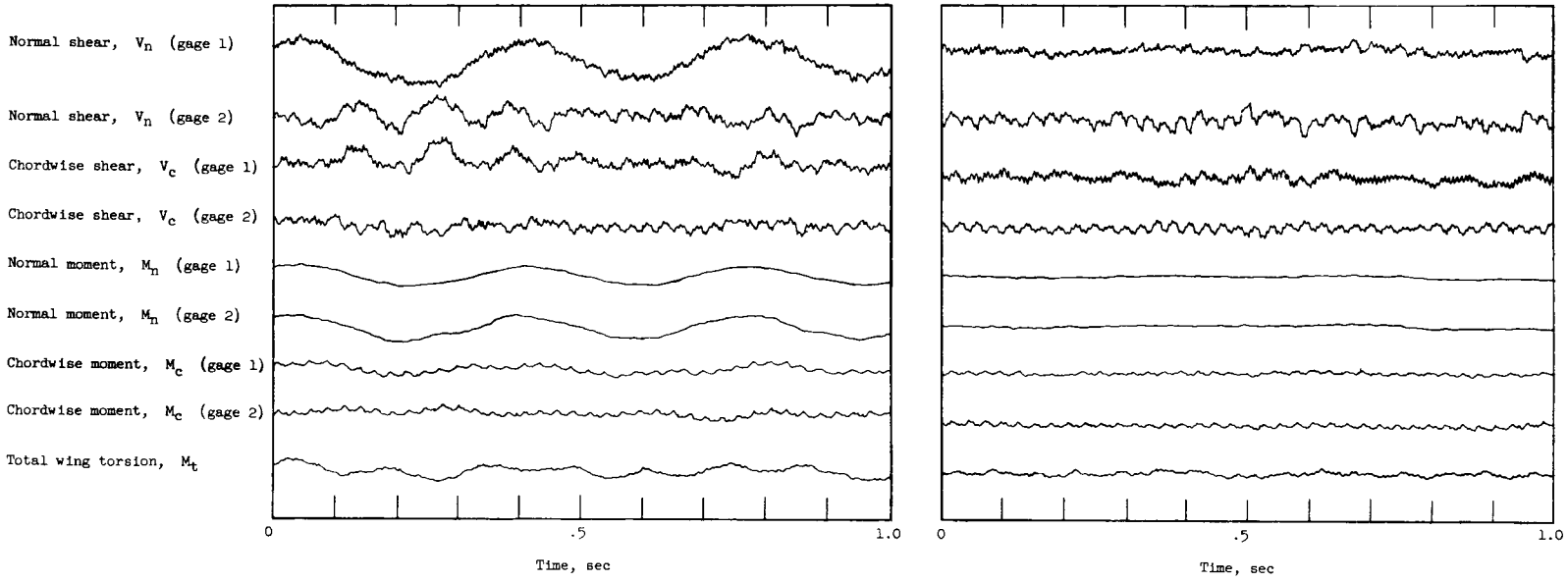

(a) Slat off; $\alpha = 39.3^{\circ}$; $C_L = 6.12$; $D/L = 0.110$; propeller speed = 2,250 rpm.

(b) Slat on; $\alpha = 39.9^{\circ}$; $C_L = 6.61$; $D/L = 0.115$; propeller speed = 2,235 rpm.

Figure 31.- Typical vibratory loads during transition. $\delta_{f,30} = 30^{\circ}$.

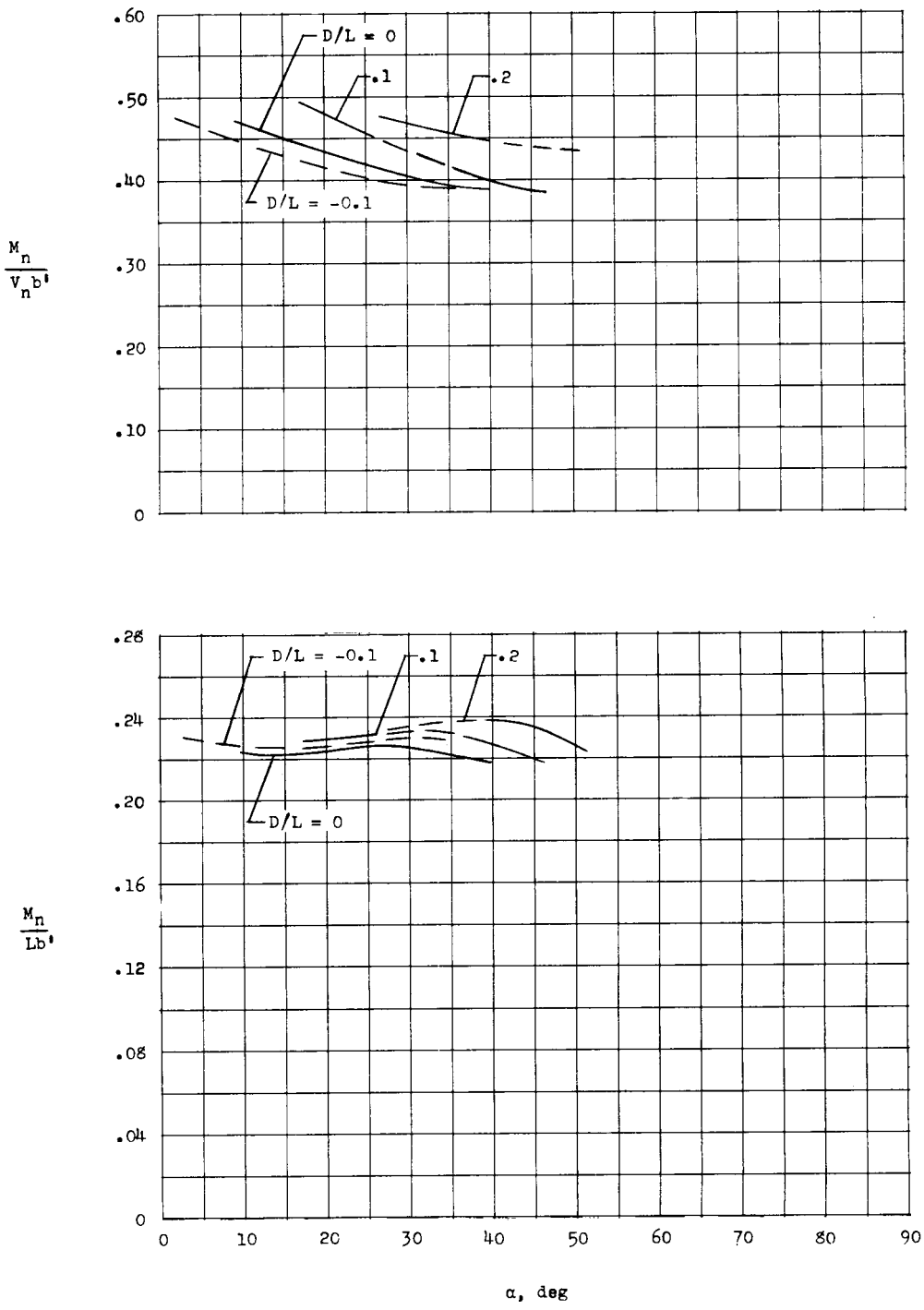

(a) Normal moments and centers of pressure.

Figure 32.- Variation of bending moments, spanwise centers of pressure, and wing torsion with angle of attack and D/L. Deflected slipstream configuration; $\delta_{f,55} = 20^{\circ}$; $\delta_{f,30} = 40^{\circ}$.

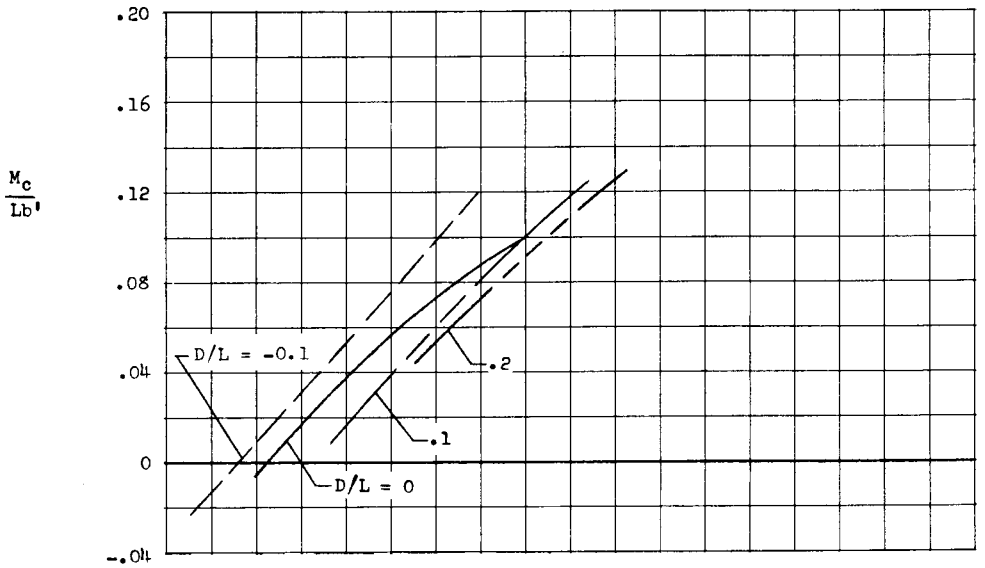

(b) Chordwise moments.

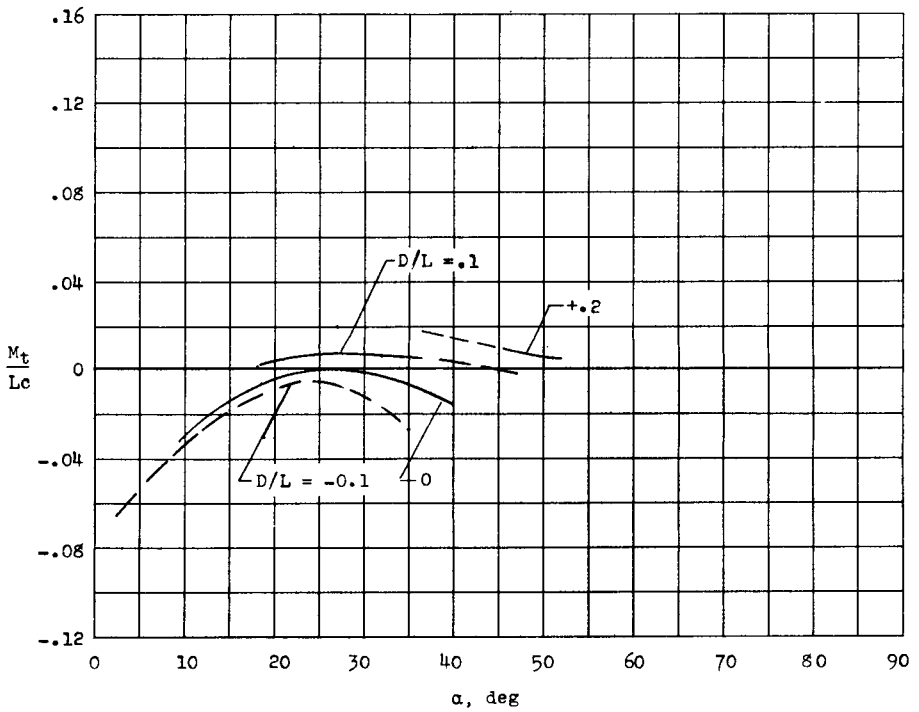

(c) Total wing torsional moment.

Figure 32.- Continued.

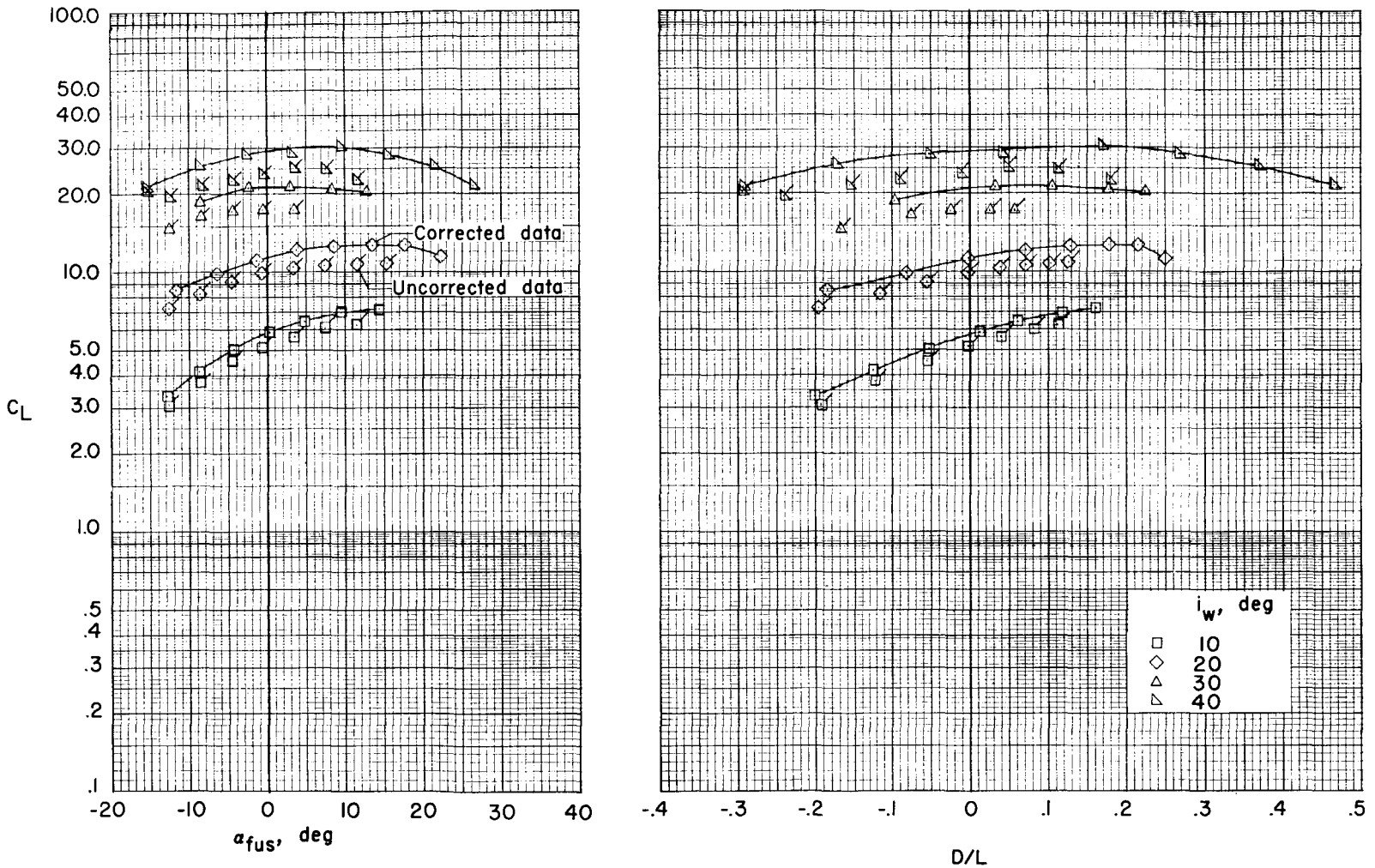

(d) Aerodynamic characteristics (for reference only).

Figure 32.- Concluded.

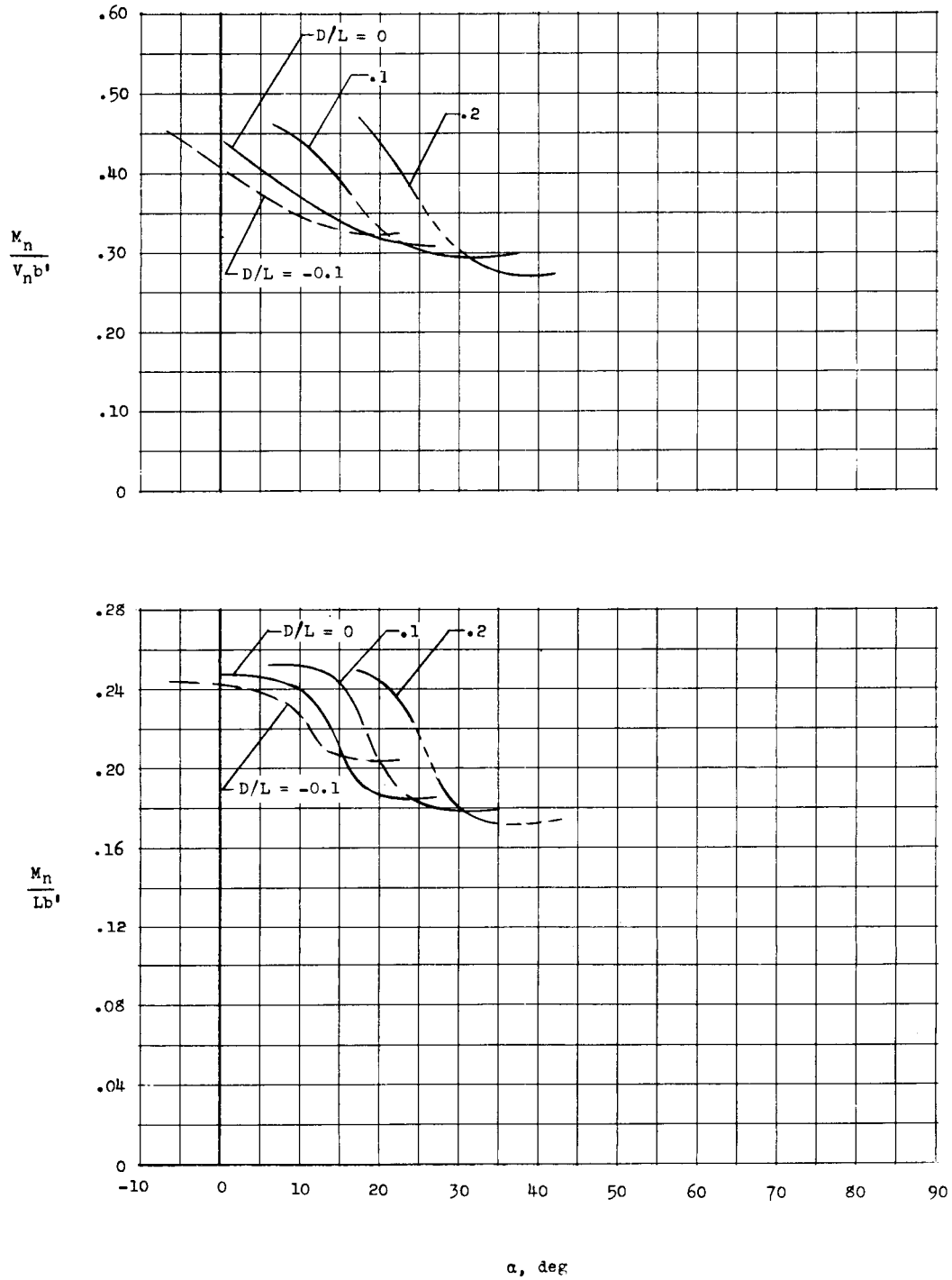

(a) Normal moments and centers of pressure.

Figure 33.- Variation of bending moments, spanwise centers of pressure, and wing torsion with angle of attack and D/L. Deflected slipstream configuration. $\delta_{f,55} = 40^\circ$; $\delta_{f,30} = 50^\circ$.

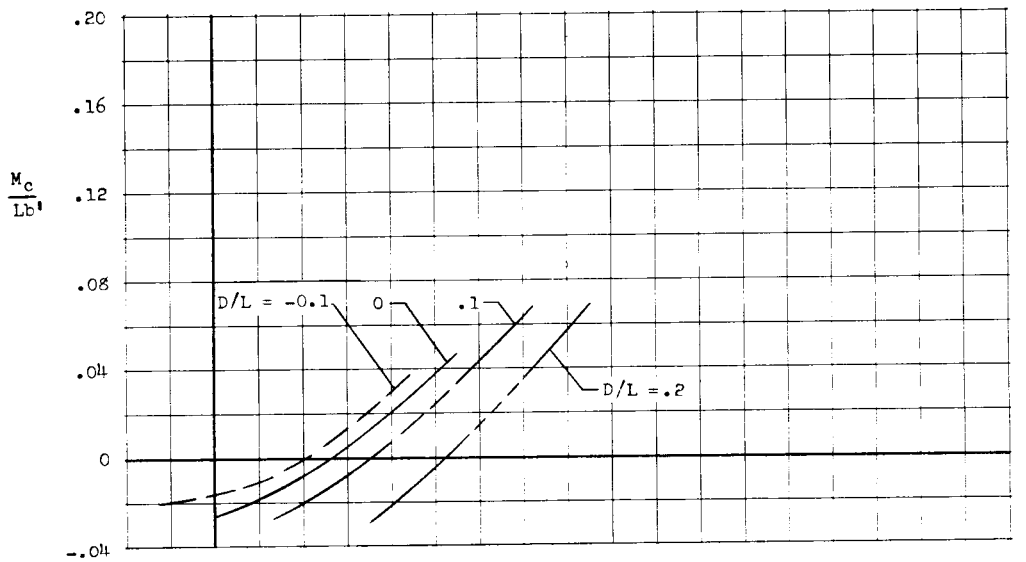

(b) Chordwise moments.

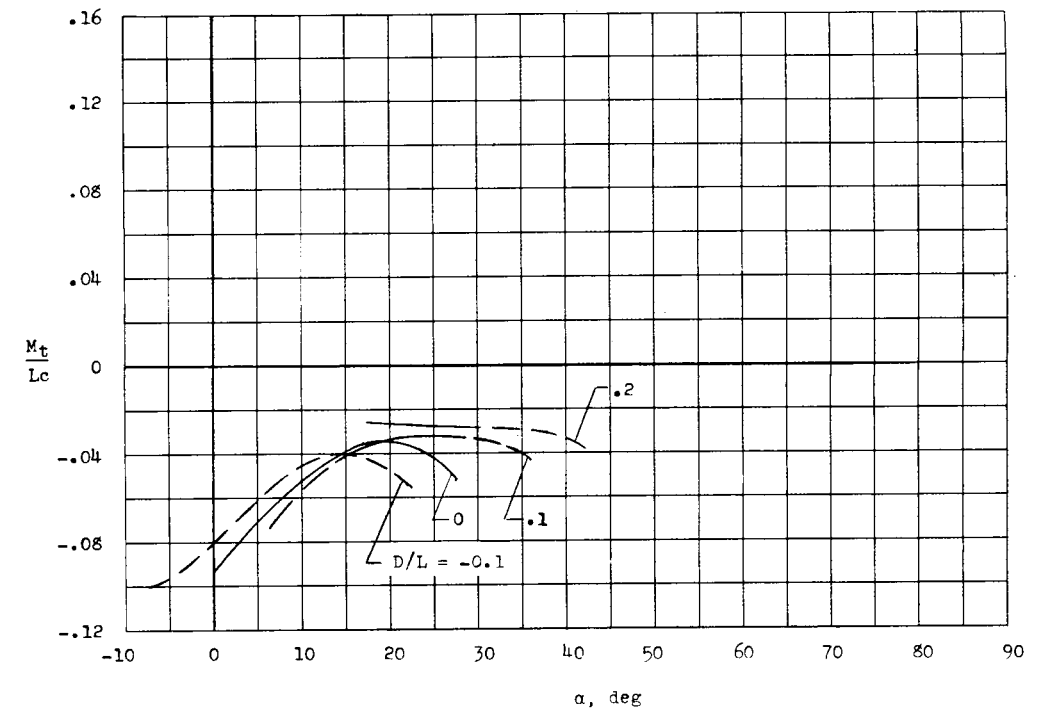

(c) Total wing torsional moment.

Figure 33.- Continued.

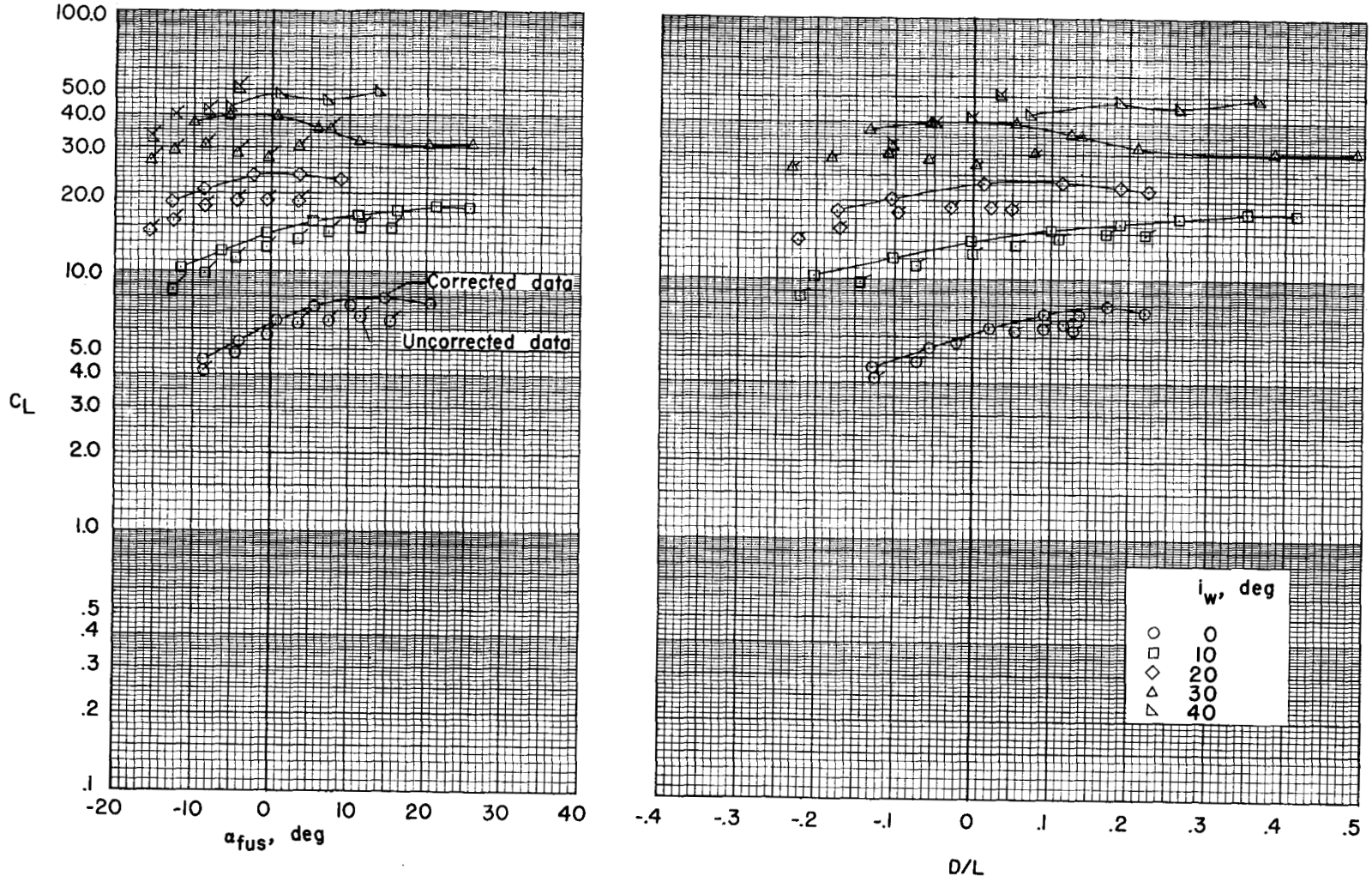

(d) Aerodynamic characteristics (for reference only).

Figure 33.- Concluded.

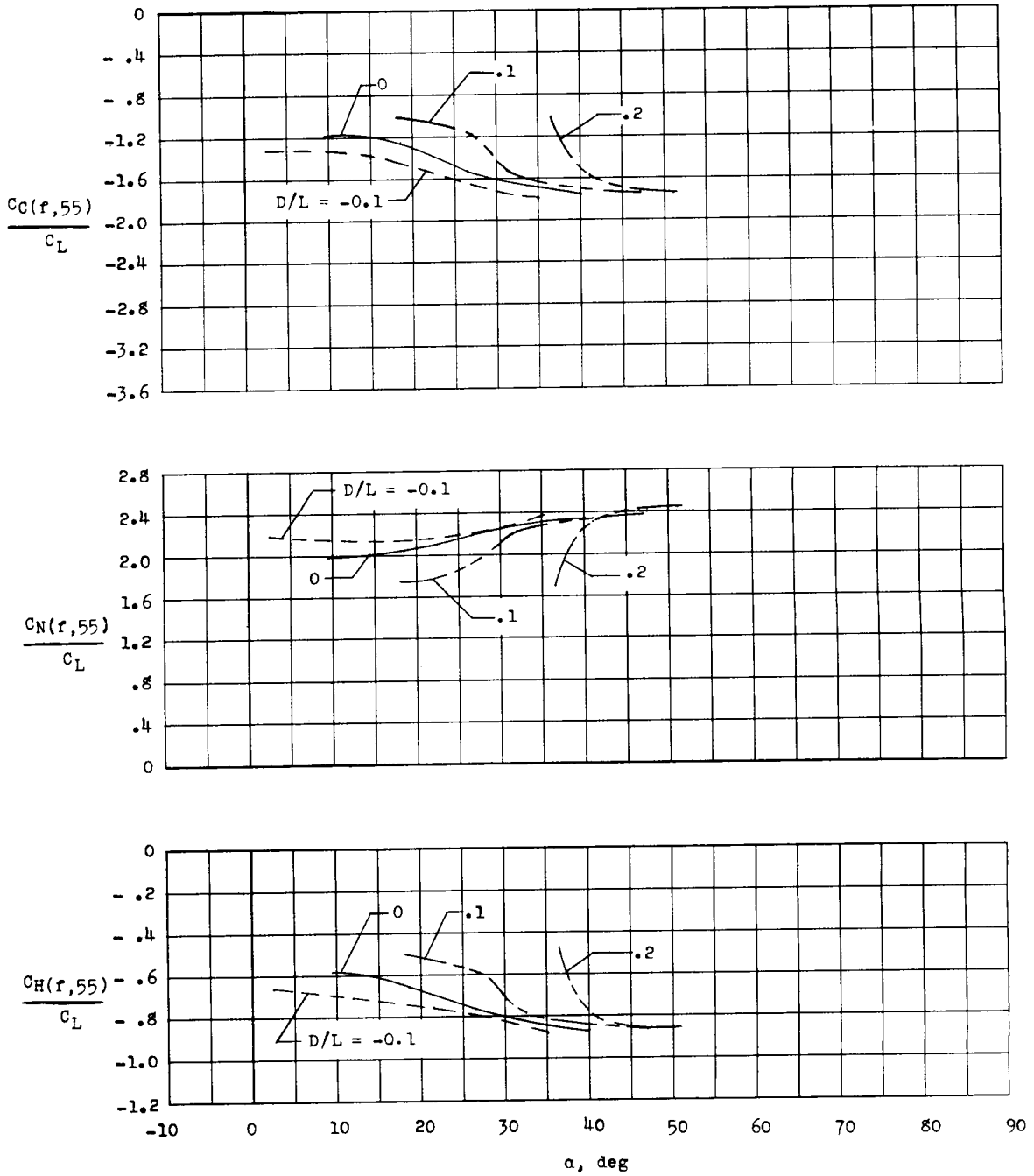

(a) Total flap loads.

Figure 34.- Variation of flap loads with angle of attack and D/L. Deflected slipstream configuration; $\delta_{f,55} = 20^{\circ}$; $\delta_{f,30} = 40^{\circ}$.

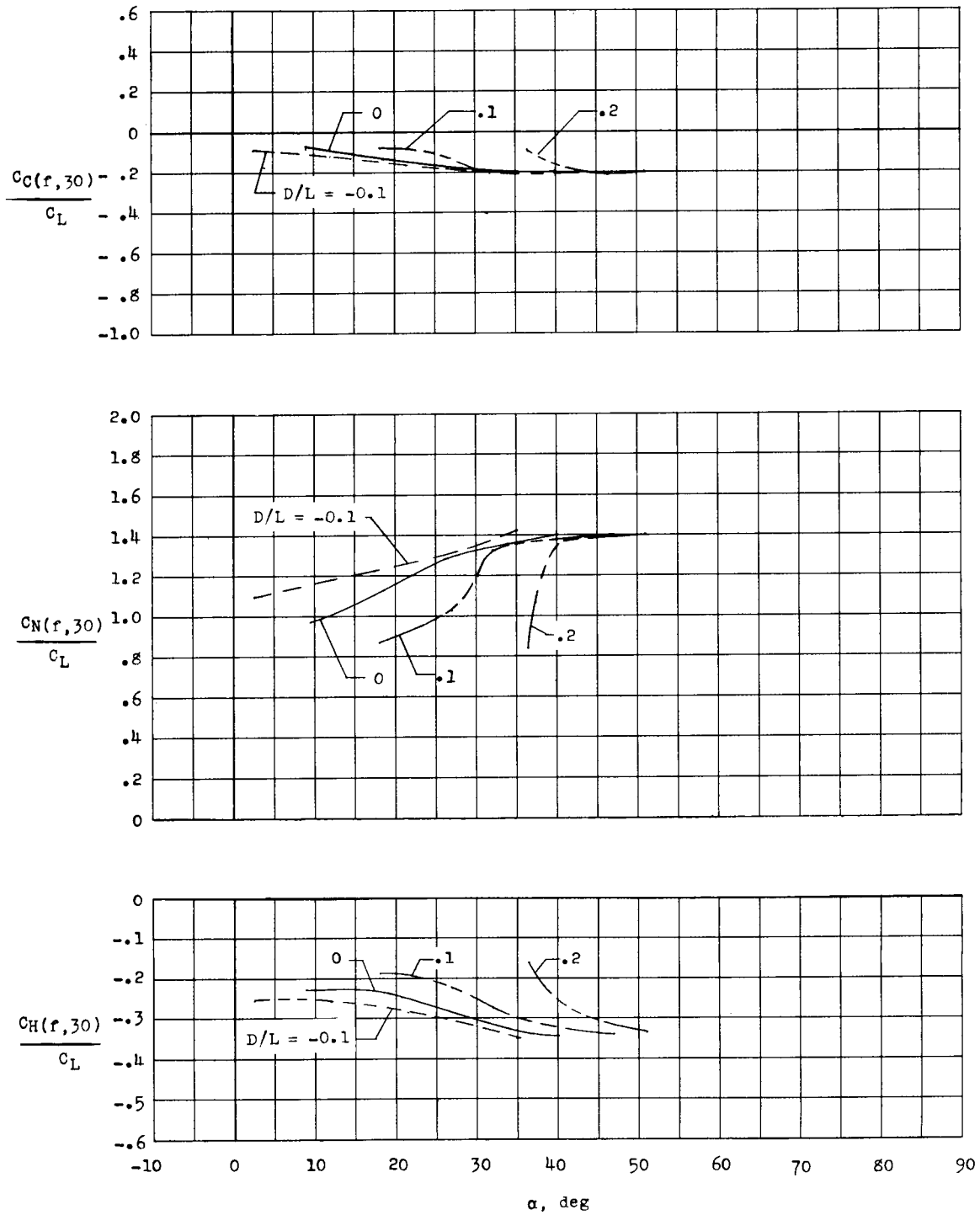

(b) Rear flap loads.

Figure 34.- Concluded.

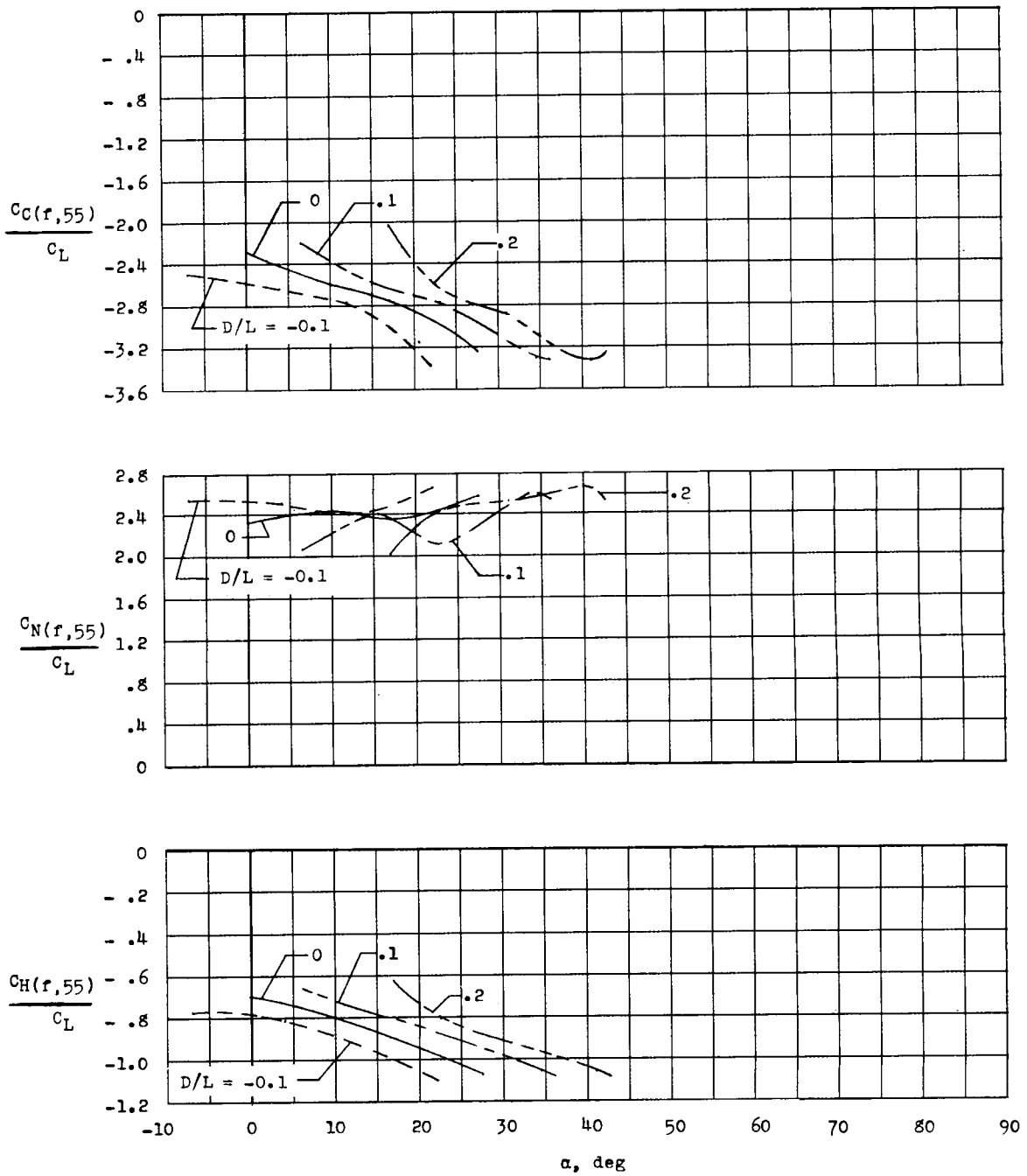

(a) Total flap loads.

Figure 35.- Variation of flap loads with angle of attack and D/L. Deflected-slipstream configuration; $\delta_{f,55} = 40^\circ$; $\delta_{f,30} = 50^\circ$.

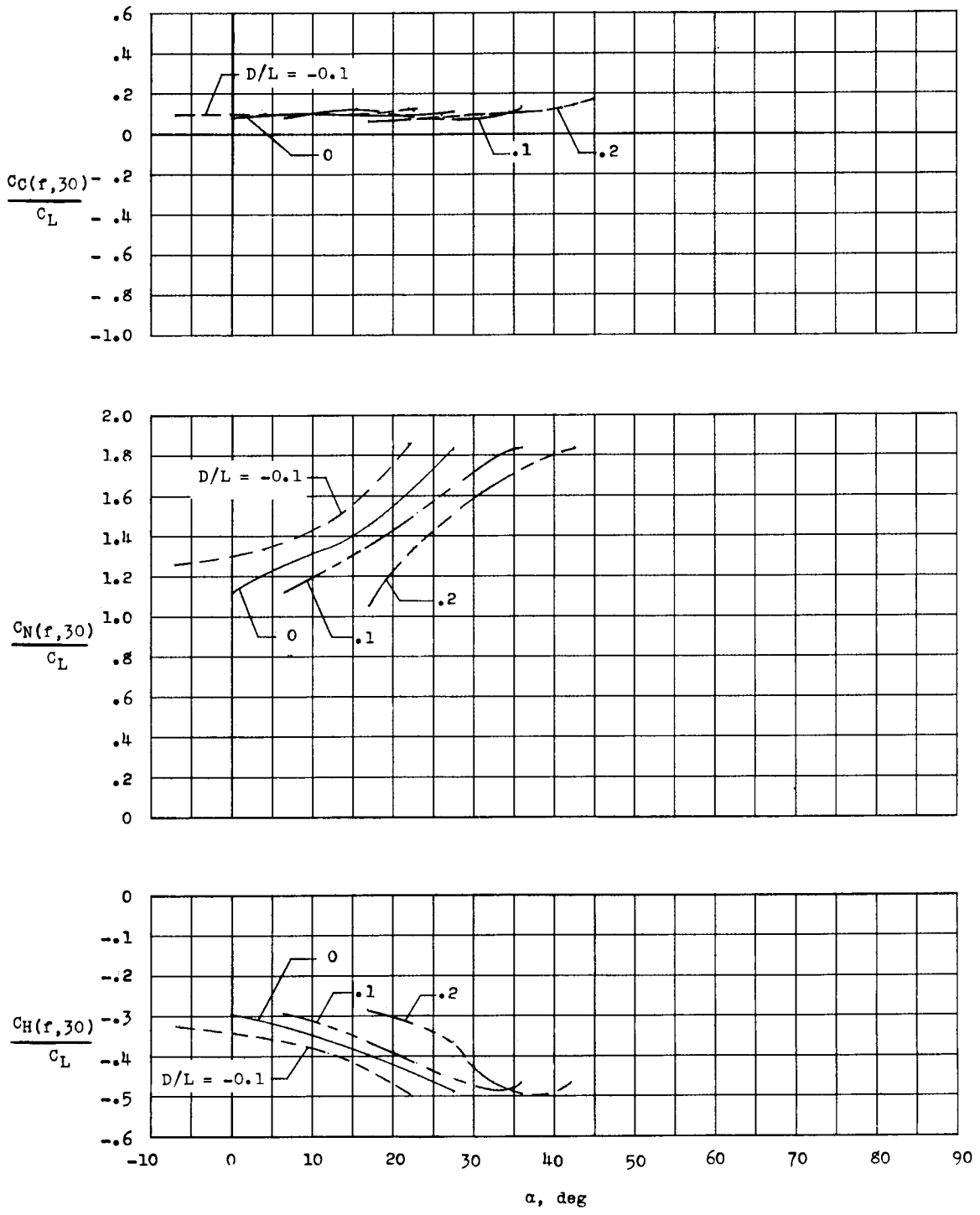

(b) Rear flap loads.

Figure 35.- Concluded.